5-2013

An Investigation of the Electronic Coupling in Some Dimeric Ruthenium (II) Polypyridine Complexes

Roland Ngebichie Njabon
University of Arkansas, Fayetteville

AN INVESTIGATION OF THE ELECTRONIC COUPLING IN SOME DIMERIC RUTHENIUM (II) POLYPYRIDINE COMPLEXES

AN INVESTIGATION OF THE ELECTRONIC COUPLING IN SOME DIMERIC RUTHENIUM (II) POLYPYRIDINE COMPLEXES

A dissertation submitted in partial fulfillment
of the requirements for the degree of
Doctor of Philosophy in Chemistry

By

Roland Ngebichie Njabon
University of Buea
Bachelor of Science in Chemistry, 2001
Universitaet GesamtHochschule Siegen
Master of Science in Chemistry, 2005

May 2013
University of Arkansas

ABSTRACT

A detailed understanding of respiration at the molecular level requires an understanding of the many electron transfer steps involved in the process. These electron transfer processes are extremely fast and are impossible to measure by simple rapid mixing techniques. In order to get around this problem, scientists have used laser flash photolysis. This technique relies on the fact that under proper conditions, a reactant can be generated by a very short laser pulse. Once generated, the course of the reaction can be monitored by various techniques capable of very rapid time response. Many applications of this methodology rely on the use of ruthenium (II) polypyridine complexes to initiate the reactions of interest. This approach has been used to study the rates of electron transfer between cytochrome c, and cytochrome b_5, cytochrome peroxidase and cytochrome oxidase and the bc_1 complex. The latter are key components in the respiration process. In these investigations special emphasis was placed on the design of ruthenium complexes that were efficient and compatible with the biological components. A thorough understanding of the design parameters are critical to continued success in this area.

Dimeric ruthenium complexes at the current time appear to be among the best candidates for photochemical initiators. The photophysical properties of these complexes, however, have not yet been examined. In particular the excited-state lifetime of some of the monomers of interest appears to be comparable or even longer than the corresponding dimers. This observation is inconsistent with the single covalent bond that links the two monomeric units which would provide strong electronic coupling and rapid excited state decay. Preliminary observations suggest a very weak electronic coupling. The underlying basis of this inconsistency is important in future design endeavors and may provide useful information for the use of these complexes in other areas such as solar energy conversion.

In order to investigate the magnitude of the electronic coupling, both symmetric and asymmetric ruthenium (II) dimeric complexes were synthesized. The ligands used in the synthesis of these dimers were limited to either those commercially available or those that could be easily synthesized. The symmetric ruthenium (II) bipyridine dimer ($[Ru(bpy)_2diphen(bpy)_2](PF_6)_4$)and ($[Ru(TAP)_2diphen(TAP)_2](PF_6)_4$ were synthesized through a nickel catalyzed coupling reaction . The asymmetric dimer ($[Ru(bpy)_2diphen(dmbpy)_2](PF_6)_4$) on the other hand was synthesized by decarbonylating $[Ru(dmbpy)_2(CO)_2](PF_6)_2$ with three fold of excess trimethylamine N-oxide in the presence of 2-methoxy ethanol and reacting it with $[Ru(bpy)_2diphen](PF_6)_2$.

Emission measurements confirmed that there is no significant difference in the excited state lifetime of the monomers and the dimers (both symmetric and asymmetric) used in this study. The result from our electrochemical studies showed that the mixed dimer complex was made up of two metal centers with different redox potentials. The symmetric dimer on the other hand has the same redox potential for each of the two metal centers and they do not interact with each other thus giving a single two electron oxidation at the same potential. Finally, our result from the emission study of the mixed dimer showed that the emission energy of the mixed dimer was equal to the average of the bpy and dmbpy dimers.

From the photochemical studies, one can conclude that the mixed dimer and the symmetric dimers behaved as the monomers because there was no significant change in the excited state life time This indicates that the metal center of both the mixed dimer and the symmetric dimers are weakly coupled by the bridging ligand and there is no significant coupling between the two metal centers.

This dissertation is approved for recommendation
to the Graduate Council.

Dissertation Director

Dr. Bill Durham

Dissertation Committee

Dr. David Paul

Dr. Jim Hinton

Dr. Ryan Tian

DISSERTATION DUPLICATION RELEASE

I hereby authorize the University of Arkansas Libraries to duplicate this dissertation when needed for research and / or scholarship.

Agreed_____
ROLAND NGEBICHIE NJABON

Refused_____
ROLAND NGEBICHIE NJABON

ACKNOWLEDGEMENTS

I would begin by acknowledging my parents Mr. Njabon John and Mrs. Njabon Emilia for their relentless support and encouragement in every aspect of my life. They brought me up in a Christian home and in the fear of the Lord and have made me to understand that with God everything is possible. This has help build up my character and made me the man I am today. Without these attributes, I wouldn't have been able to survive the challenges that are posed by graduate studies. I would also like to acknowledge my uncle Dr. Njameni Jacob whose financial and moral support has made me realized my dreams of obtaining a doctorate in chemistry. I also want to extend my gratitude to all of my siblings: Dr. Njabon Eric, Njabon Jacob, Njabon William, Njabon Francis Lawrence, Njamen Lilian, Njabon Carine and Njabon Diane for all their love, support and encouragement in everything I have done in my life. I want to also extend my regards to all of my uncles and aunts and my entire family for being with me through the good times and the tough times of my life.

I want to extend my sincere gratitude and appreciation to Dr. Durham for giving me the opportunity to do research in his lab and for his mentoring and guidance in every step of the way in my scientific career. You cannot imagine how grateful I am for all the things you have done for me. I also want to extend my gratitude to every member on my committee, Drs: Ryan Tian, David Paul and Jim Hinton for their scientific guidance and critique which has helped me become a better scientist. I would also use this opportunity to thank all the past and present members of the Durham's research group and also Dr Raman Subbu for his invaluable help in electrochemistry.

My achievement today won’t be possible without the help of my local church, Association of Baptist Students (ABS) and the International Student Christian Organization (ISCA). Mr. Warren Dugas and Mr. Kevin Smith of ABS and ISCA respectively have been instrumental in shaping up my life spiritually. Warren, I especially cherished the moments we spent together in the coffee shop once every week talking about God, politics and every aspect of life. Pastor Phil Heppner, Jim Craven, Dave Anderson, Jeff warren, Mr and Mrs Terry Warren and all the folks at Calvary chapel, Fayetteville, you have been like a family to me and I want to express my gratitude for your love and spiritual support in my life. I would also use this opportunity to acknowledge all of my friends both here in the US and in Cameroon.

Last but not least, I want to extend my gratitude to my God fearing wife Eliotte-Diane Ngebichie for her love and support in everything I do.

TABLE OF CONTENTS

ABBREVIATIONS

MLCT	Metal-to-Ligand Charge Transfer
LMCT	Ligand-to-Metal Charge Transfer
MC	Metal-center
ESI	Electrospray ionization
NMR	Nuclear Magnetic Resonance Spectrotroscopy
UV-VIS	Ultraviolet-Visible spectroscopy
MALDI-TOF	Matrix Assisted Laser Desorption Ionization Time of Flight
HPLC	high pressure liquid chromatography
Bpy	2,2'-bipyridine
$[Ru(bpy)_3]^{2+}$	ruthenium (II) tris 2,2'-bipyridine
Cl-phen	5-Chloro-1,10-phenanthroline
Diphen	5,5'-bi-1,10-phenanthroline
RBF	round bottom flask
hr	hour
TAP	1,4,5,8-tetraazaphenanthrene
PPh_3	triphenyl phosphine
Me_3NO	trimethyl amine N oxide
Dmbpy	4,4'-dimethyl 2,2'-bipyridine
DmF	dimethyl formamide
THF	tetrahydrofuran
Bpz	2,2'-bipyrazine
EtOH	ethanol
MeOH	methanol
DCM	1,2-dichloromethane
v/v	volume to volume
Fc/Fc+	ferrocene / ferrocenium ion
Ip	peak current
Ep	peak voltage
CV	cyclic voltammetry
CD_3CN	deuterated acetonitrile
$CDCl_3$	deuterated chloroform
nm	nanometer
min	minutes
mL	milliliter
NH_4PF_6	ammonium hexafluorophosphate
Cyt c	cytochrome c
s	second
NADH	Nicotinamide Adenosine dinucleotide
ADP	Adenosine dinucleotide
ATP	Adenosine triphosphate
CCO	Cytochrome c oxidase

CHAPTER 1: INTRODUCTION

1.1 Introduction

Ruthenium (II) polypyridine complexes such as $Ru(bpy)_3^{2+}$ have been extensively investigated over the past four decades.

The intense interest in these complexes derives from the fact that they show significant promise as solar energy conversion catalysts. The properties that make these complexes of interest in this area also make them candidates in a number of other areas. For example a variety of oxygen and pH sensors have been developed with ruthenium polypyridine complexes as the key component. This family of complexes has also been extensively used in fundamental studies of electron transfer, especially reactions of biological interest. In this application, the photoredox chemistry is used to initiate electron-transfer processes of interest which are then monitored by a technique called laser flash photolysis.

The basis of all of these applications is a long-lived excited state that is both a strong oxidant and a strong reductant. The excited-state lifetime is approximately 300 n sec in air saturated aqueous solution. While this is a very short amount of time, it is adequate for redox reactions of the excited state to proceed in high yield. This characteristic is not unique to this family of compounds. However, ruthenium complexes offer the added advantage that they are thermally stable in multiple oxidation states. The combination makes them ideal candidates for the applications described above.

This dissertation will focus on the photochemical and electrochemical characterization of some dimeric complexes that have been successfully applied to an exploration of the redox reactions involved in respiration. In this context, a specific group of complexes will be examined in an effort to understand what determines the excited state lifetime and how this information can

be used to design more efficient photoredox complexes. The discussion will begin with an introduction to the basic biological system of interest. This will be followed by a brief description of laser flash photolysis. The overall photoredox reactions used to address specific questions and the design criteria used in selecting ruthenium complexes will be described. Finally the properties of dinuclear complexes will be discussed and compared to the monomeric analogues.

The question of interest is whether or not the dimeric molecules of interest behave as two independent monomers with photochemical properties similar to the monomeric subunits. Alternatively the dimeric molecules may have new properties as a result of the interaction of the two metal centers. A final option is a compromise between these two extremes; the molecule is similar to the monomeric complexes but has some new features. The appearance of these features may be temperature dependent. In the terms used in the literature in the first case the metal centers have weak electronic coupling, the second case strong coupling and in the third case the coupling is intermediate in magnitude.

1.2 Oxidative Phosphorylation

The mitochondria inner membrane is one of the most complex of all biological membranes. It is a highly specialized system for oxidative phosphorylation. The enzymes of the electron transport and oxidative phosphorylation are found in a fluid lipid bilayer that acts both as a permeability barrier to polar molecules and as a framework capable of accommodating a variety of proteins [1]. The plant respiratory chain like its animal counterpart consist of only four protein complexes namely: complex I, complex II, complex III (also known as cytochrome bc_1

complex) and complex IV (or cytochrome c oxidase). These complexes (except for cytochrome c) are very hydrophobic and are soluble in the fluid lipid bilayer membrane of the mitochondria inner membrane.

Complex I is responsible for electron transfer from NADH to ubiquinone and pumps four protons into the membrane space starting to build up the proton gradient in the inter membrane space. Complex II generates $FADH_2$ by the oxidation of succinate to fumarate in the krebb's cycle. The $FADH_2$ is then used to generate ubiquinol from ubiquinone. In this process however, there are no protons pumped into the inner membrane.

Complex III (cytochrome bc_1 complex) was discovered and purified from bovine heart mitochondria in 1961 [2, 3]. This enzyme catalyzes electron transfer from dihydroubiquinone (QH_2) to cytochrome c and this reaction is coupled to a trans membrane proton translocation [4]. Complex III is only functional in a dimeric form with each monomer consisting of eleven subunits. The mechanism of oxidation and reduction of ubiquinone in the mitochondrial respiratory chain at complex III is currently described by a process known as the Q cycle. The electrons enter the protein by way of oxidation of dihydro ubiquinone at the Qo site. The initial electron is transferred to the Rieske iron-sulfur center. The Riske center then rotates to transfer its electron to cytochrome c_1. The electron is then transferred to an oxidized cytochrome c that is electrostatically bound to bc1 complex close to cytochrome c1. The second electron from ubiquinol is then transferred to cytochrome b_L (low affinity) followed by the electron being transferred to cytochrome b_H (high affinity). This electron is then transferred to a quinone that is docked at the Qi site. At the end of the cycle, two QH_2 molecules are reduced to two cytochrome c molecules generating one ubiquinol. Two protons are removed from the matrix to form new

QH_2 and four protons are pumped across the inner membrane. These protons contribute to the protein gradient used to drive ATP synthesis.

Complex IV (cytochrome c oxidase) is the terminal complex of the electron transport chain. It is a multi-subunit enzyme complex that catalyzes the terminal act of respiration by transporting electrons derived from the step wise oxidation of foodstuff to molecular oxygen [5] Cytochrome c oxidase catalyzes four electron reduction of molecular oxygen and the electrons are provided by ferrocytochrome c.[6].

During the course of this oxidation, cytochrome c shuttles rapidly between cytochrome c_1 and cytochrome c oxidase. The enzyme (cytochrome c oxidase) is made up of four redox centers. The first center is Cu_a which is the recipient of electrons from ferrocytochrome c and the second redox center is cytochrome a_1, cytochrome a_3 and Cu_b which is the site for oxygen reduction form the overall redox chain.

Numerous investigators have contributed to the current state of understanding of oxidative phosphorylation. Measurement of the rate constants of the reactions is a central theme in these investigations and laser flash photolysis using ruthenium polypyridine complexes as photochemical initiators has played a major role in these measurements. It remains for many reactions to be the only means currently available for the accurate determination of the rate constants. Many of these measurements have been recently reviewed.[7-11]

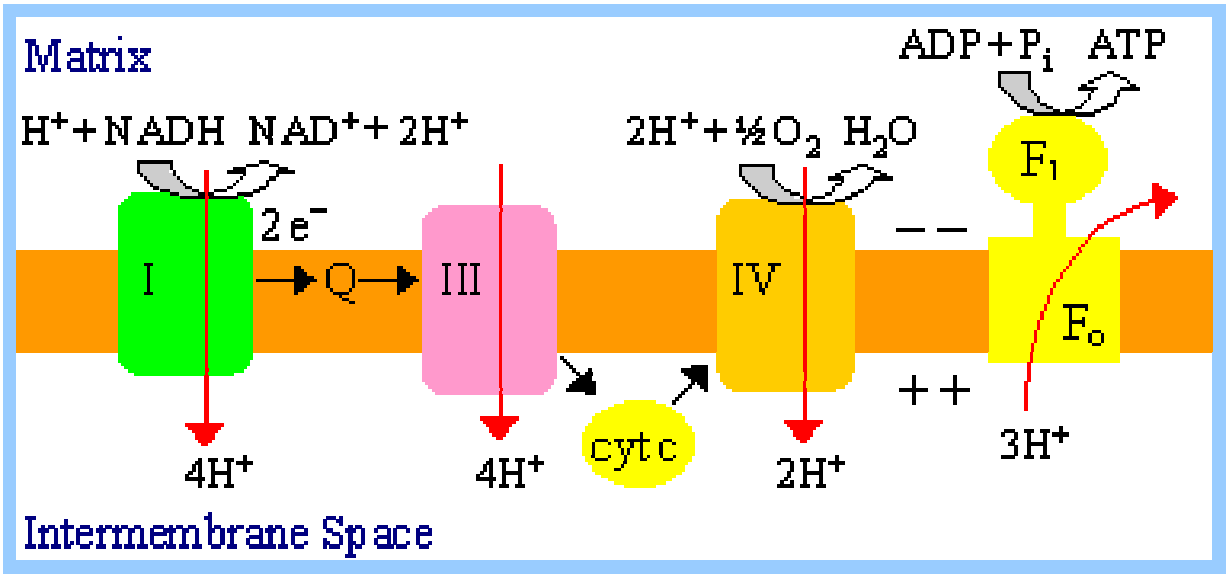
Matrix
ADP+Pi ATP
H+ + NADH NAD+ + 2H+
2H+ + ½O2 H2O
F1
2 e-
I
Q
III
IV
Fo
cyt c
4H+
4H+
2H+
3H+
Intermembrane Space

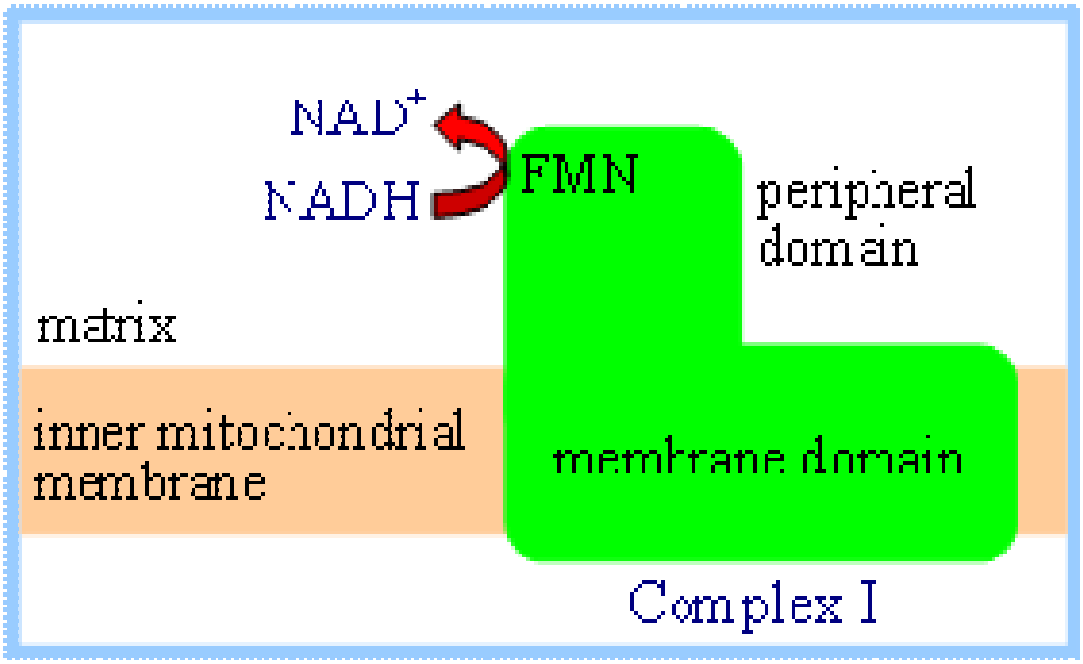
NAD+
NADH
FMN
peripheral domain
matrix
inner mitochondrial membrane
membrane domain
Complex I

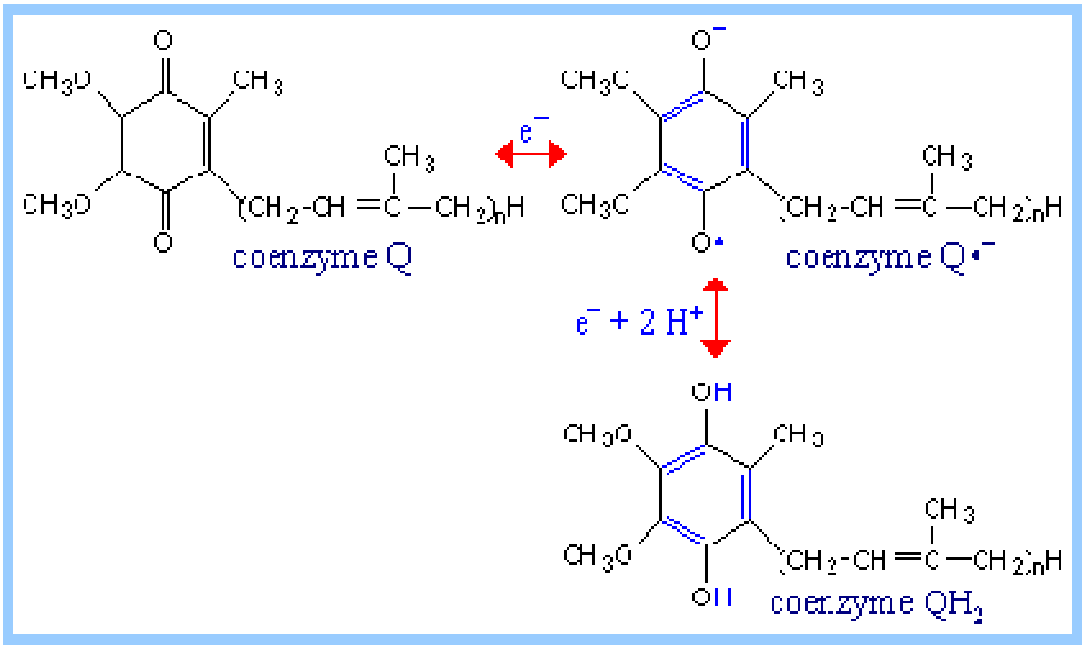
coenzyme Q
coenzyme Q•⁻
e⁻ + 2 H⁺
coenzyme QH₂

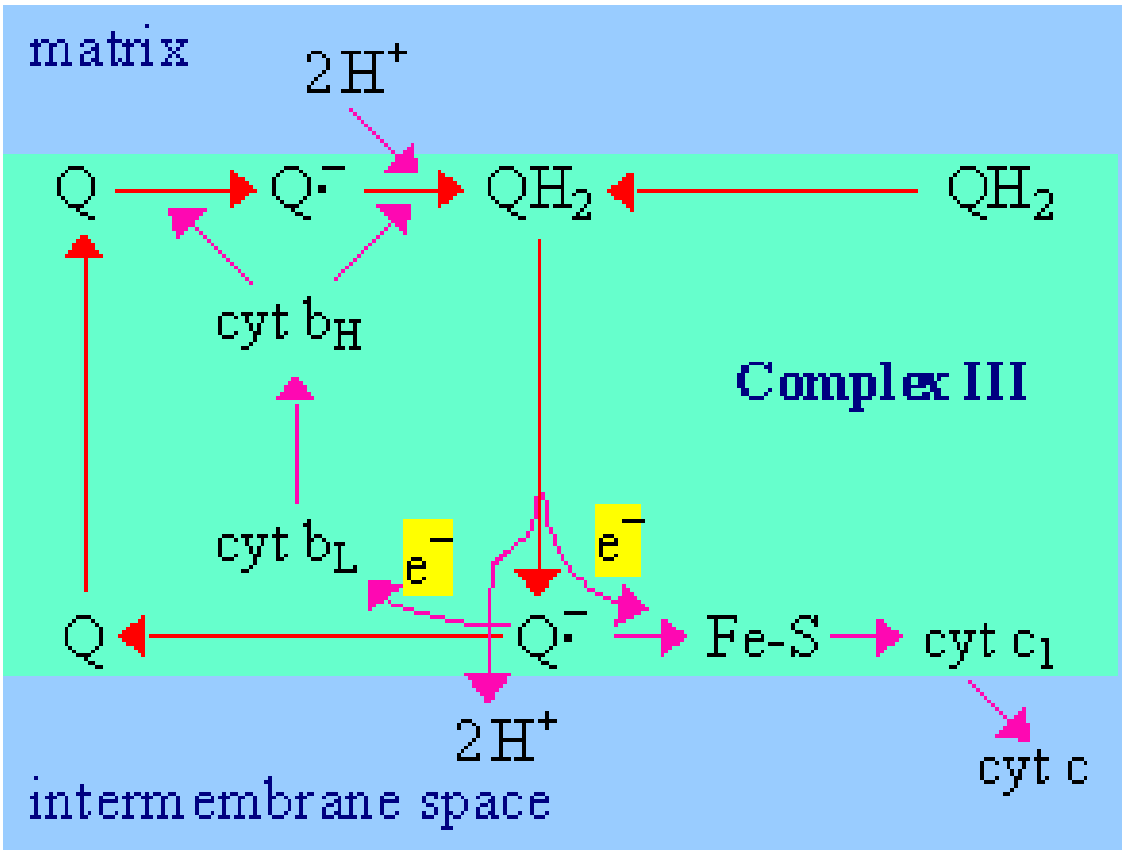

Fig 1: Oxidative Phosphorylation: Chemiosmostic Coupling by Peter Mitchell

1.3 Laser Flash Photolysis Experiment

The laser flash photolysis experiment is based on the idea that a laser induced photochemical event can be used to produce a reactant on the time scale of a laser pulse. Laser pulses as short as picoseconds have been used. The choice of pulse length is generally dictated by the characteristics of the reaction under investigation. A simplified view of the essential equipment is shown in Figure 2.

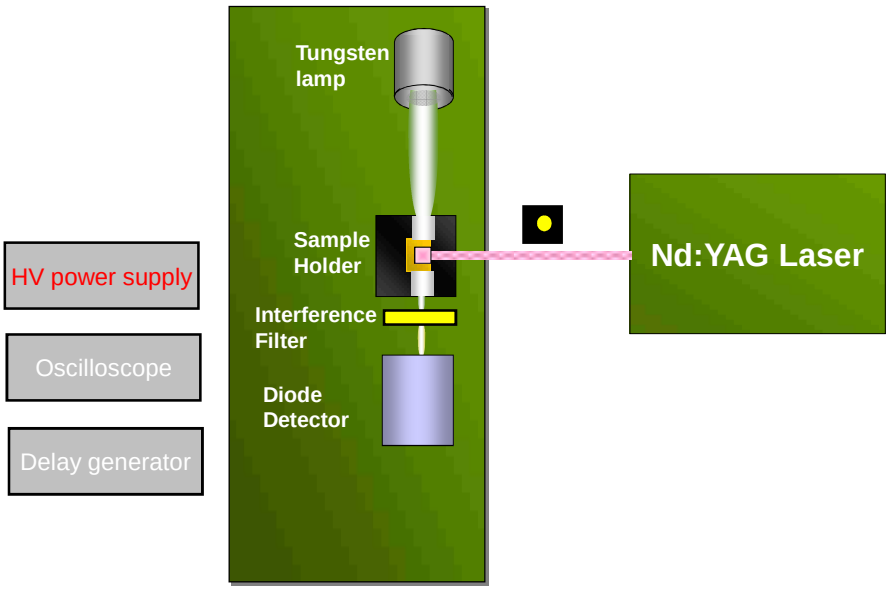

Figure 2. Simplified drawing of the laser flash photolysis apparatus.

The equipment consists of a probe beam which in the current study is a tungsten lamp. The beam is directed through the sample into some type of wavelength selecting component or device. In this example, a simple interference filter with a band pass of 10 nm is shown. A monochromator can also be used.

The light intensity is monitored by a photodiode or a photomultiplier and the time course of the intensity following the laser pulse is monitored with a high speed digitizer. The digitized data is then converted to absorbance with a computer interfaced to the digitizer. Although not shown a shutter is often placed in front of the sample to avoid photolysis from the probe beam. In the example shown, the laser is a Nd: YAG laser which has a pulse width of about 10 nanoseconds. Longer pulses can be provided by flash pumped dye lasers or simply a flash lamp.

1.4 Reactions between Ruthenium (II) Complexes and Proteins

In the early 90's, several reaction schemes were been devised to use the photochemical and redox properties of ruthenium complexes to study electron transfer reactions in biological systems. In one of these experiments, cytochrome *c* was covalently linked to a derivative of $[Ru(bpy)_3]^{2+}$ [12]. Excitation of the ruthenium label with a very short laser pulse results to a very rapid reduction of Fe(III) of cytochrome c to Fe(II). Under appropriate conditions, cytochrome c is electrostatically bound to cytochrome c oxidase which in turn is reduced by cytochrome c). (Scheme 1).

A number of ways to covalently linked ruthenium complexes to cytochrome c have been developed. One of these methods relies on the use of genetically engineered cytochrome c in which a specific amino acid on the surface is replaced by cysteine which then reacts with a derivative of the ruthenium complex that contains α-bromomethylmethylbipyridine.[11, 13-15]. The reagent reacts specifically with the cysteine under appropriate conditions to form a thio ether bond and HBr.

The photoinitation process is illustrated in Scheme 1 in which Ru(II)-Fe(III) represents ruthenium and the heme iron states in a ruthenium cytochrome c derivative. Irradiation of the

complex with a short laser pulse results in the formation of Ru(II)* metal-to-ligand charge excited state. The excited state can undergo electron transfer reaction (k_1) to yield Ru(III)-Fe(II). The intermediate Ru(III) can reoxidized the Fe(II) and return the system to the starting point with no net reaction. This unproductive back reaction is prevented by a donor (e.g. aniline) which reacts irreversibly to reduce Ru(III) and yield Ru(II)-Fe(II). At this point, the photoinitiator is restored to the original oxidation state and is ready for the next laser pulse. Decay of the excited state back to the ground state by processes that do not involve electron transfer is represented by k_d. When the ruthenium cytochrome c (Ru-Cc) derivative is added to solutions of cytochrome c oxidase (CcO), then photoinitiation of the ruthenium complex results in rapid reduction of heme c, followed by electron transfer to Cua, heme a and finally the heme a_3, Cu_b binuclear center in CcO.[11].

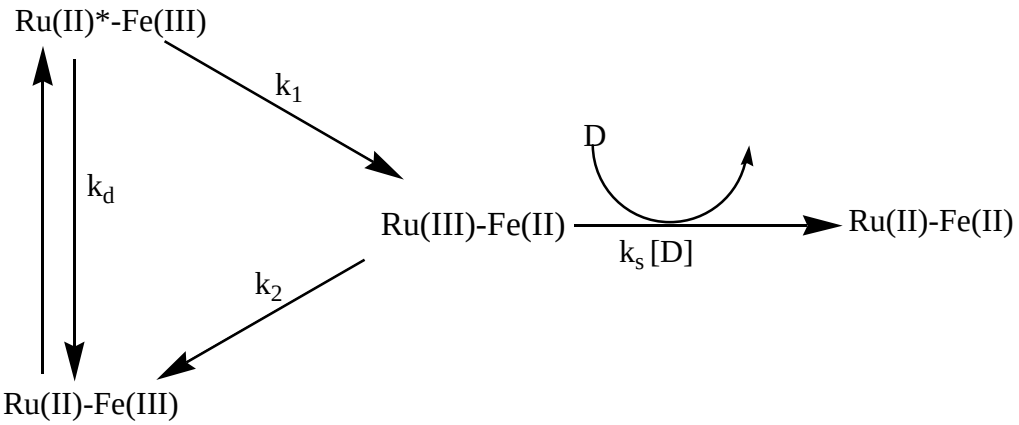

Scheme 1

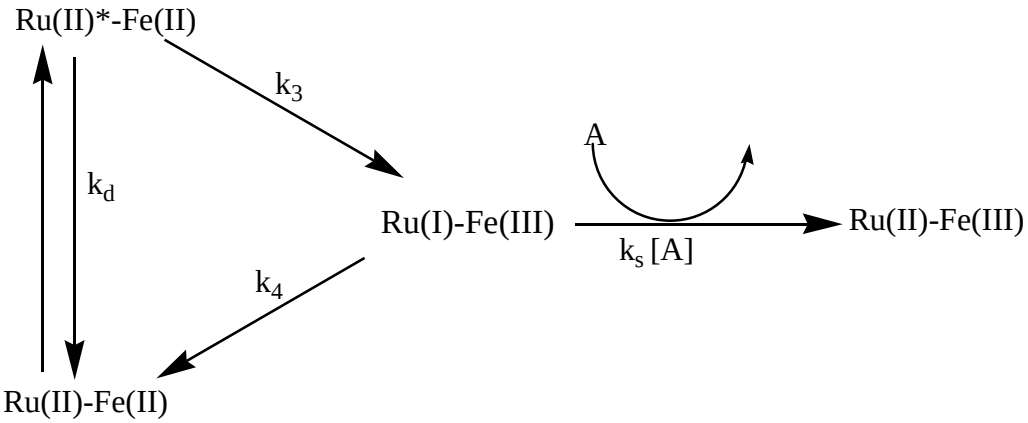

Scheme 2

In scheme 2, the reduced form of the protein system Ru(II)-Fe(II) is excited by a laser to form Ru(II)*-Fe(II). There is an electron transfer reaction between the Ru(II) center and the iron center in which case the Ru(II) is reduced to Ru(I) and the Fe(II) is oxidized to Fe(III). Just like in scheme 1, two pathways are possible at this stage. In one pathway, there is an electron transfer from the iron center to the ruthenium center bringing the system back to its initial resting stage (Ru(II)-Fe(II)). In the second pathway, a sacrificial acceptor accepts an electron from Ru(I) thereby oxidizing the ruthenium center to a Ru(II) while the iron center remains unchanged as an Fe(III). This scheme results in the rapid production of a protein with an iron center containing Fe(III).

Scheme 3 shows yet another reactions pathway that can be utilized. This scheme shows a series of reactions in which the ruthenium (II) complex reacts with a quencher Q producing $[Ru(bpy)_3]^{+}$. The Ru (I) complex subsequently reacts with an iron center of a protein and reduces the Fe(III) to an Fe(II). The net result is the same as that provided by Scheme 1. The sacrificial donor and quencher involved in both schemes respectively share similar properties and one molecule may perform both functions. The end product of both schemes is a Ru (II)-Fe (II)

complex. It is worth noting that, ideally, the quencher is a small molecule that reacts irreversibly and does not interact with the protein reaction of interest.

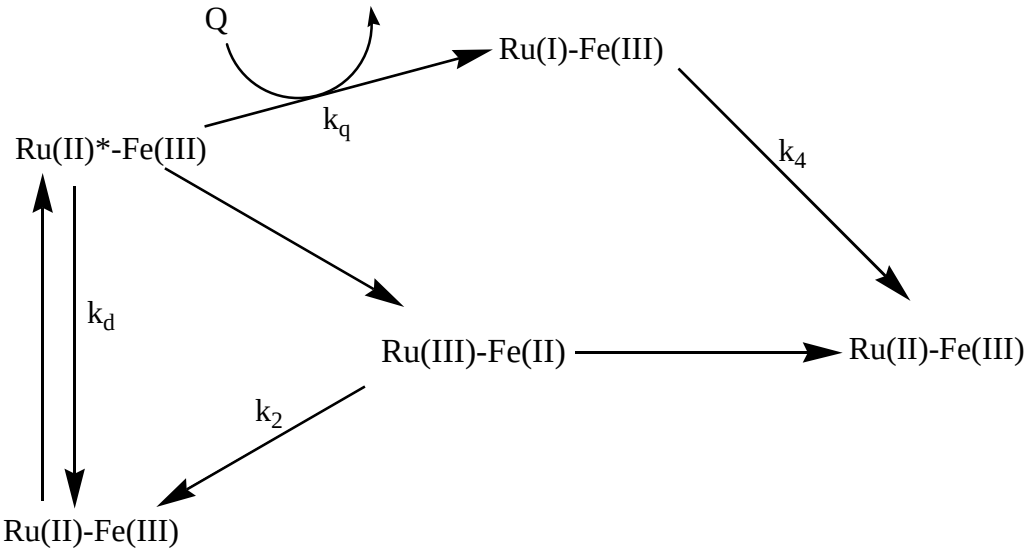

Scheme 3

Pioneer work by the Nilsson group [16] showed that $[Ru(bpy)_3]^{2+}$ electrostatically associates with cytochrome c oxidase with sufficient stereospecificity to allow the excited state of the ruthenium complex to donate an electron to the metal center of a protein. The binding efficiency was found to be strongly correlated to the charge on the complex which led to the synthesis of several dimeric complexes with +4 overall charge. The dimeric complexes have been used to investigate the electron transfer processes inside cytochrome c oxidase which contains four metal centers but only one is involved in the electron transfer from another protein. The emphasis in this case was on the reactions after the electron was injected into the protein. The dimers have also proven to be invaluable in the investigations of the reactions of the bc1 complex.

A constant theme in the above mentioned process is the creation of systems that provide a very high yield of photochemical products. High yields imply large amounts of proteins are reduced

or oxidized and the signal to noise ratio of subsequent measurements is high. Some parameters are extremely important in increasing the overall efficiency of the photochemical initiation reaction and these include:

- The excited state lifetime of the complex.
- The charge on the complex.
- The redox potential of the complex.

By increasing the excited state lifetime, one increase the chances of an electron transfer reaction taking place and therefore complexes with excited state lifetime greater than one micro second are desirable. The overall charge on the complex is only important when the complex is electrostatically bonded to a protein. Based on past and current research, the binding efficiency is optimum when the charge on the complex is +4. The redox potential of a complex can either increase or decrease the overall photochemical yield of the product. According to Marcus theory for simple electron transfer, the rate of reaction increases and then decreases with increasingly strong oxidizing complexes and the effect has been demonstrated with the reactions shown in Scheme 1. Scheme 3 offers some additional flexibility in the choice of reactants and previous choices have resulted in a general trend of high yields with strongly oxidizing complexes.

1.5 Photochemistry and photophysics of $[Ru(bpy)_3]^{2+}$

The long-lived excited state of $[Ru(bpy)_3]^{2+}$ was a key factor that led to great interest in the study of ruthenium (II) polypyridine complexes. Ruthenium (II) complex is a d^6 complex with the t_{2g} orbitals being completely filled and the $e_{.g.}$ orbital unfilled. Excitation of an electron from the t_{2g} orbital to the π^* orbital gives rise to an intense metal to ligand charge transition

(MLCT) at 452 nm [17]. Weak bands in the UV region of the spectrum are a result of π-π^* transitions.

Over the last 4 decades many investigators have focused their attention on the nature of the excited state of $[Ru(bpy)_3]^{2+}$ and related compounds. The current state of the investigations is summarized by Figure 3 which shows the excited state energy diagram.

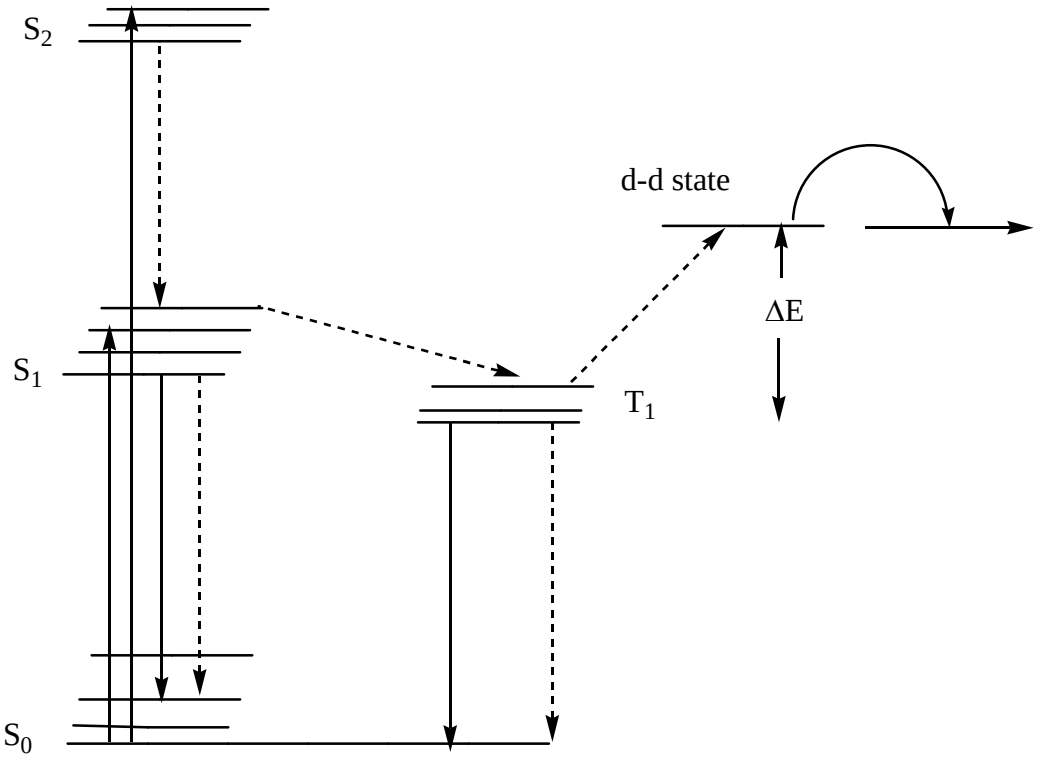

Figure 3: Excited State Diagram of $[Ru(bpy)_3]^{2+}$

The ground state of $Ru(bpy)_3^{2+}$ is a singlet ground state designated S_0. Absorption of light leads to population of the S_1, S_2 and other spin allowed transitions. Following the initial absorption event the triplet state, designated T_1, is populated with 100 % efficiency [17, 18] The triplet state is the long-lived excited state responsible for the photoredox events and it has been characterized by Raman and UV-Vis spectroscopy and other techniques [19-22].R.J Watts et al showed that the temperature dependence of the lifetime is correlated with a lower set of emission levels which undergo weakly coupled non radiative deactivation and a higher set of emission levels which undergo strongly coupled non radiative deactivation [23].

The excited state decays by a combination of processes. It decays by emission of light centered at about 600 nm and by a nonradiative process which simply degrades the excited state energy

into heat. Near room temperature a third process occurs which the principle route for decay. The process involves thermal population of a higher excited state, labeled d-d state. The d-d state decays rapidly to the ground state by a nonradiative process. The small but measurable photochemical loss of bipyridine from the complex has been postulated to be a consequence of population of this state. The temperature dependence of the excited state lifetime is the primary source of information leading to Figure 4 and is mathematically described by equation (1).

$$1/t = knr + kr + kexp\ (\Delta E/RT) \qquad (1)$$

Where knr is the rate constant for non-radiative decay, kr is the rate constant for radiative decay (emission), k is the rate constant for decay of the excited state and ΔE is the energy gap between the triplet state and the d-d state. Watts et al reported values of 3600 cm^{-1} for the upper set of levels which give rise to ligand substitution photochemistry. The upper set of levels is assigned to the d-d state.[23] Other investigators have suggested additional states but the three state model is generally accepted as a minimum.

Low temperature emission study (77 K) done by Crosby et al [24-27] showed that the excited state consist of three close lying emitting states. Van Houten and Watts [28] showed that the emission of $[Ru(bpy)_3]^{2+}$ displayed a blue shift in ethylene glycol upon cooling. In an alcoholic medium at 77 K, the emission lifetime of $[Ru(bpy)_3]^{2+}$ is approximately 5 µs. This order of magnitude of emission lifetime is common in metal complexes which have MLCT excited states. Those with ligand centered excited states have emission lifetimes in the millisecond range.[27-29,30-34].R.J Watts et al studied the luminescent behavior of $[Ru(bpy)_3]^{2+}$ at -196°C and 100° C respectively. They observed that the spectrum broadens and red shift as the temperature was raised.

The rate of radiative transition such as fluorescence and phosphorescence were found to be determined by the spin and symmetry of the complex where as the rate of the non-radiative transitions were found to increase with decreasing excited state energy [35, 36]. The emission lifetime was found to decrease as temperature increases. The relationship between the emission lifetime and temperature is given by the equation below [37]:

$$1/\tau = \kappa_0 + \sum_i \kappa_i^{nr}(\mathrm{T}) \qquad 2$$

τ = Life time of the excited state

k_0 = rate constant of the ground state

k_i = rate constant of the excited state

k^{nr} = non radiative transition

T = temperature

The temperature dependence on the non radiative emission lifetime was found to be dependent on:

I. The crossing of an activated surface to another excited state which is described by the Arrhenius equation.
II. Vibrational modes that favor non radiative decay which are absent at low temperature due to a frozen molecular environment.

At high temperatures, the luminescence lifetime is also related to an activated surface crossing from a ^{3}MLCT to a ^{3}MC energy level which is described by an Arrhenius equation

The excited state of *$[Ru\ (LL)_3]^{2+}$ is described as either localized ($[Ru^{3+}\ (LL)_2(LL^{-})]^{2+}$) or delocalized ($[Ru^{3+}(LL^{-1/3})_3]^{2+}$) model respectively . The localized excited state theory postulates that the promoted electron resides in a single ligand in a hypothetical Ru-LL unit and assumes a C_{2v} symmetry.[38, 39]. This model has been used to explain charge transfer absorption of complexes containing nonequivalent ligands. Experimental evidence to support the localized model is strong in a fluid solution but is less convincing in the solid state or in low temperature glasses. Molecular orbital calculations of the C2v point group symmetry corresponds to that of low temperature spectrum of $[Ru(bpy)_3]^{2+}$.[40]. This model also matches with the electrochemical experiments of $[Ru(bpy)_3]^{2+}$. Electrochemical studies show that the singly reduced species $[Ru(bpy)_3]^{+}$ is formed with the added electrons delocalized on one bpy ring rather than being delocalized on all three.[41].

The delocalized model on the other hand describes a situation in which the electron is either shared by the three ligands or it undergoes hopping from ligand to ligand. In this model, it is assumed the promoted electron resides in an orbital with a D_3 symmetry. The lowest energy configurations d $\rightarrow\pi^*$ is described as a set of three levels, [42]. In this model, the splitting of the energy level is as a result of the interaction between the excited electron and the electron remaining in the d^5 orbital whereas ligand – ligand interaction is neglected. The delocalized or electron ion coupling model has been used to describe the excited state of complexes such as $[Ru(bpy)_n(phen)_{3-n}]^{2+}$[35] , $[Ru(bpy)_3]^{2+}$

1.6 Electrochemistry of $[Ru(bpy)_3]^{2+}$

Ruthenium (II) polypyridine complexes undergo a reversible one electron oxidation and reduction whose redox potential is solvent independent.[43]. Oxidation of ruthenium (II)

polypyridine involves the loss of electron from a metal t_{2g} orbital resulting to the formation of a low spin $4d^5$ ruthenium (III) complex which is inert to ligand substitution [44].

$$[Ru^{II}(LL)_3]^{2+} \leftrightarrow [Ru^{III}(LL)_3]^{3+} + e \quad . \qquad 3$$

The redox potential of Ru (II) / (III) polypyridine complexes is 1.25 V with respect to normal hydrogen electrode (NHE).

Reduction of ruthenium (II) polypyridine complexes may involve either a metal centered or a ligand centered orbital [43]. When the ligand field is strong or the ligand can easily be reduced, reduction occurs through a ligand centered orbital π^*_L. During this process, the reduced form has a low spin $4d^6$ configuration which is inert and the reduction process is reversible.[37, 45, 46]. On the other hand, when the ligand field is weak or the ligand cannot be easily reduced, reduction occurs in the metal centered orbital. If this were the case, an unstable low spin d^7 complex would be formed giving rise to ligand dissociation and the process will be irreversible.

$$[Ru^{II}(LL)_3]^{2+} + e \rightarrow [Ru^{II}(LL)_2(LL^-)]^+ \qquad 4$$

$$[Ru^{II}(LL)_3]^{2+} + e \rightarrow [Ru^{+}(LL)_3]^+ \rightarrow [Ru^{+}(LL)_2]^+ \; LL \qquad 5$$

This scenario has never been observed for ruthenium (II) polypyridine complexes.

1.7 Mixed Valence Complexes

The Creutz-Taube ion $[(NH_3)_5Ru\text{-}(\mu\text{-pyrazine})\text{-}Ru(NH_3)_5]^{4+}$ first synthesized in 1969 was the first mixed valence complex to be studied [4748]. A key feauture in the Creutz – Taube ion is the presence of a large separation in the oxidation potential between the first and second metal (0.4 V and 0.76 V) respectively. For the mixed valence complex Ru(II)-Ru(III) there is a band at about 565 nm and an intervalence band at 1570 nm is also observed. The mechanism for the

interaction of the metal centers in a pyrazine bridged complex is thought to occur through a bridged mediated super exchange process rather than by the overlap of metal orbitals [49-51]. Since the first report on the Creutz-Taube mixed valence complex, was done, pyrazine bridged metal complexes have attracted a lot of attention [52-54]. Most of the research in this field have been predominantly on the electrochemical and spectrochemical properties of these complexes as well as the measurements on the degree of delocalization in the mixed valence complex Ru (II)-Ru(III)[55, 56]. By substituting one ammonia by a water molecule (in the Creutz-Taube ion) resulted to a slight shift of the intervalence band from 1570 nm to 1530 nm. On the other hand, when the ammonia molecule was substituted with a chloride or a pyrazine ion, there was a blue shift in the λmax of the intervalence band to 1450 nm and 1160 nm respectively [48]. The changes in the energy of the intervalence band have been described in terms of the effect of substitution on the barrier of electron transfer. By substituting ammonia with a strong field ligand such as chloride ion, the metal center becomes more difficult to oxidize. Increasing the asymmetry of the complex by replacing one $Ru(NH_3)_5$ moiety by $RuCl(bpy)_2$, $Ru(NO_2)(bpy)_2$ or $Ru(CH_3CN)(bpy)_2$ results in a blue shift of the intervalence transfer band [48,57, 58]. Studies on 4,4'-bipyridine bridged analogue of the Creutz-Taube ion also showed a much reduced level of interaction for symmetric systems with increasing oxidation potential of the ruthenium centers[59]. Meyer et al have studied the intervalence properties of the Creutz-Taube ion analogue $[(bpy)_2Cl$ M-(μ-pyrazine)-MCl(bpy)2$]^{2+}$ (where M = Ru or Os)and have shown that the extent of delocalization in this mixed valence complex is small[60-63]. The difference in the oxidation potential of the metals in the ruthenium dimer is 120 mV and the intervalence transfer band occurs at 1300 nm. For the $[(bpy)_2Cl$ Ru-(μ-pyrimidine)-$RuCl(bpy)_2]^{2+}$ mixed valence complex, the interaction between the two metal centers is equal to that of the pyrazine mixed valence complex but the intervalence

transfer band occurs at 1360 nm.[48]. Calculations on the delocalization of the pyrimidine based mixed dimer is lower than that of pyrazine [60]. Meyers and Powers have done molecular orbital calculations on the free ligands (pyrazine and pyrimidine) and shown that the disparity in the strength of interaction of these ligands is due to the lower π^* level of the pyrazine ligand compared to pyrimidine.

Dinuclear nuclear ruthenium complexes form the largest group of mixed valence system because they are cheap and form stable ruthenium (II) and ruthenium (III) coordination compounds.[64]. The study of mixed valence complexes gained a lot of attention in 1967 with the publication of two review articles in 1967 by Allen and Hush [65] and Robin and Day [66]. Robin and Day classified mixed valence complexes into three main categories:

- Class I complex
- Class II complex
- Class III complex

In a class I complex, there is no electronic coupling between the two metal centers involved. A class II complex has the metal centers weakly coupled together. A class III complex has a strong coupling between the two metal centers. The nature of the bridging ligand is extremely important in determining what type of mixed dimer we have.

Electron transfer processes from a ground state to an excited state molecule can be rationalized based on the Marcus theory.[67]. According to this theory, the rate constant for an electron transfer process can be expressed as:

$$\kappa_{el} = \upsilon_{\mathrm{N}} \kappa el\ exp(-\Delta G^{\ddagger}/RT) \qquad 6$$

Where υ_{N} is the average nuclear factor

κ_{el} is the electronic transmission coefficient and

$\Delta G^{\ddagger}$ is the free energy of activation.

The asymmetric mixed dimers we studied were oxidizing dimers with a charge of +4. Upon irradiation with a laser, the dimers got oxidized resulting to a new complex with a +5 charge. We were interested in mixed dimers because we wanted to enhance the possibility of quenching the excited state. Also by studying the mixed dimer, we can gain insight into the parameters that determine the excited state by carrying out electrochemical studies to see how the two metal centers interact with each other.

Dinuclear complexes of ruthenium had been previously studied by the Durham's group and found to be the best photoinitiators to initiate photoredox reactions. They were found to have a long lived excited state lifetime compared to their monomeric counterpart. Symmetric dimers such as $[Ru(bpy)_2diphen(bpy)_2](PF_6)_4$, $[Ru(TAP)_2diphen(TAP)_2](PF_6)_4$ and the asymmetric dimer $[Ru(bpy)_2diphen(dmbpy)_2](PF_6)_4$ were studied because they were easy to synthesize and were compatible with biological systems.

Fig 4: **Structure of Ruthenium dimer complexes**

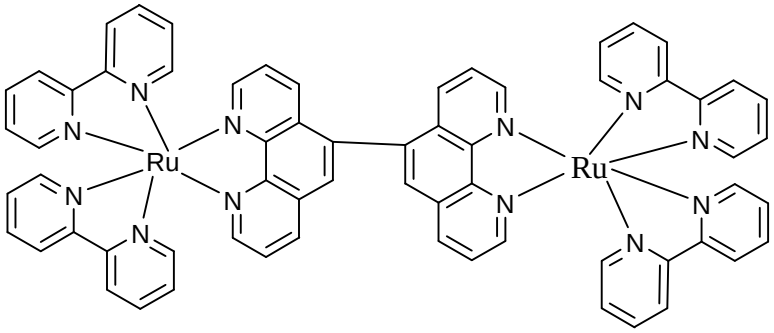

$[Ru(bpy)_2diphen(bpy)_2Ru]^{4+}$

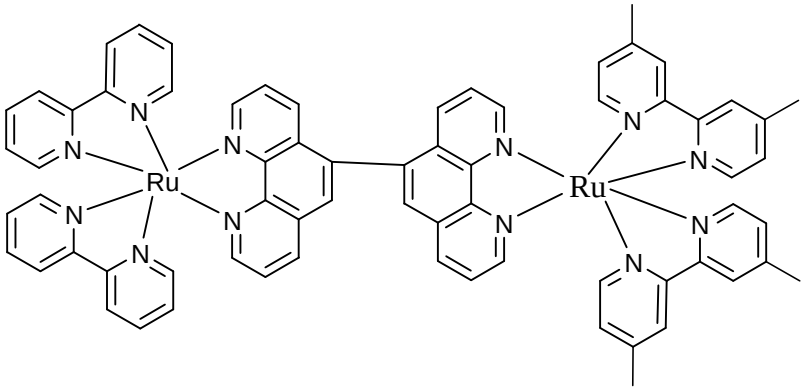

$[Ru(bpy)_2diphen(dmbpy)_2Ru]^{4+}$

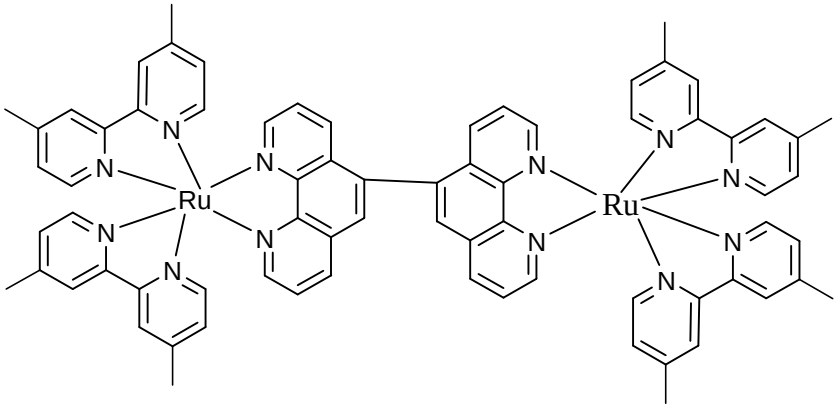

$[Ru(dmbpy)_2diphen(dmbpy)_2Ru]^{4+}$

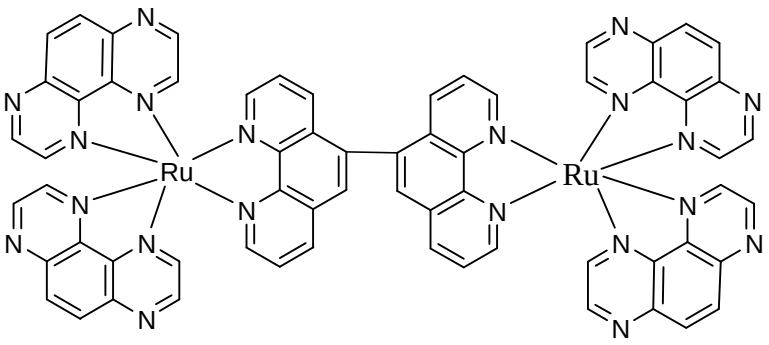

$[Ru(TAP)_2diphen(TAP)_2Ru]^{4+}$

CHAPTER 2: EXPERIMENTAL

2.1 Materials

Aluminum oxide, (basic, grade 1, 58 Å), lithium chloride anhydrous, 2, 2'-bipyridyl (99% assays) and 4-nitro-o-phenylene diamine, triphenyl phosphine flake (99%), glyoxal (40% w/w aqueous solution), potassium hydroxide pellets (85 %) and hydroxylamine hydrochloride (96+ %) were purchased from Alfa Aesar. Silica gel 60Å, (high purity 60 – 200 µm) and chloroform were purchased from BDH. Palladium, 10 weight % on activated carbon , 4,4'dimethyl 2, 2'-bipyridine, Sp Sephadex C-25, (strong acidic cation exchanger bead size 40 - 120µm), tetrabutylammonium hexafluorophosphate (98%) were purchased from Sigma Aldrich. Ruthenium (III) chloride trihydrate which contained 35 – 40 % Ru was manufactured by Acros Organics. Tetraethylammonium iodide purchased from Fluka. Zinc dust was purchased from Fischer Scientific. 1, 10-phenanthroline monohydrate was purchased from GFS Chemicals. Sodium chloride crystals and sand (washed and dried) were purchased from Mallinckrodt chemicals. Ammonium hexafluorophosphate was purchased from Oakwood product Inc. Pyrazine carboxylic acid and triethylamine N-oxide anhydrous were purchased from TCI. N, N - dimethylformamide (99.8 % extra dry over molecular sieves) was purchased from Acros Organics. 2-Methoxyethanol was purchased from Alfa Aesar. Methyl alcohol anhydrous (99%) was purchased from Acros Organic. Acetonitrile, dichloromethane, ethyl ether anhydrous, methanol and toluene were purchased from EMD. Dimethylformamide, ammonium hydroxide (28 – 30 %) was purchased from J.T. Baker. Ethanol (200 proof) was purchased from Koptec. Acetonitrile d_3 (99.8 %) was purchased from Cambridge Isotope, chloroform d (99.8 + atom % D) and methyl sulfoxide d_6 (99.8 atom % D) were purchased from Acros Organics. Acetone-d_6 was purchased from Aldrich Chemical.

2.2 Instrumentation

CHI Instruments model 600 C Series Electrochemical Analyzer/Work station was used for cyclic voltammetry

The counter and reference electrodes were made of platinum wire, whereas the working electrode was a platinum disc. The platinum disc had diameter of 1.6 mm and an area of 2.0 mm^2. In order to avoid artifacts from leakage of a KCl based reference electrode a platinum wire quasi-reference electrode was used in many experiments and was calibrated against ferrocene. A saturated Ag/AgCl solution in saturated KCl was used in all other experiments.

For ESI-MS and MALDI-TOF characterization, an ESI-Quadruple Ion Trap Mass Spectrometer (ESQUIRE-LC, Bruker Daltonics) and MALDI-TOF Mass Spectrometer (Reflex III, Bruker Daltonics) were used respectively. The HPLC was equipped with an auto sampler, a quaternary pump and a variable wavelength detector. The sample was pumped to the mass spectrometer at a flow rate of 0.05 mL/min. Nitrogen was used both as a nebulizing gas and a drying gas with a flow rate of 12 L / min. The mass spectrometer was fitted with an atmospheric pressure electrospray ionization source. The flow rate of the mass spectrometer was set at 0.05 mL/min. A 300 MHz Avance I and 400 MHz Avance III Bruker Spectrometer with z gradient and broad band probe was used for ^{1}H-NMR and ^{13}C NMR spectroscopy.

UV-Vis spectra were obtained with a Hewlett Packard 8452 A Diode Array Spectrophotometer. The data were plotted using Microsoft Excel.

Fluorescence spectra were obtained with a Jobin Yvon Horiba Fluorolog 3 Fluorimeter. The excitation wavelength was set at 450 nm whereas the emission wavelength was set at 480-890 nm. Spectra recorded at 77 K were held in a specially designed dewar with a extended

bottom which was no silvered. The dewar was held in the spectrometer with a ring stand and clamps in the sample location as the normal sample holder which had been removed. The spectra were recorded as soon as the liquid nitrogen in the dewar stopped bubbling. The samples were held in pyrex NMR tubes and air saturated. A 4:1 (v:v) ethanol/methanol mixture was used as the glass-forming solvent.

Excited state measurements were obtained by excitation of the samples with the third harmonic (355 nm) of a Quanta-Ray DCR-1 Nd:YAG laser. Tow series of experiments were performed. In one the samples were held in fluorescence cuvettes with no attempt to remove oxygen from the solvent. The samples were prepared to have concentrations very close to 14 µM. The emitted light was directed to monochromator through a focusing lens. A photomultiplier tube (R-765) was used to monitor the emitted light intensity at 620 nm. The signal from the photomultiplier was connected to a unity gain amplifier by way of a 10" coaxial cable. The output from the amplifier was recorded with a Lecroy 7200 precision Digital Oscilloscope. Approximately 100 shots were averaged before the data was recorded on a PC interfaced to the oscilloscope.

The emission decay rate constants were obtained by fitting the time dependence of the emission intensity following laser excitation to a simple first-order rate equation. In general the signal to noise ratio was very large with almost no visible noise in the averaged signals. A fitting procedure described previously by Matheson was used to obtain the rate constants.

2.3 Syntheses

$[Ru(bpy)_2(Cl\text{-}phen)](PF_6)_2$ [68]

$Ru(bpy)_2Cl_2.2H_2O$ (0.5356 g, 1.03 mmol) and Cl-phen (0.2188 g, 1.02 mmol) were combined in a 100 mL RBF containing 25 mL of a 3:1 (v/v) EtOH / H_2O. The solution was refluxed for 24 hr. under nitrogen. The solution was cooled to room temperature and filtered. To the filtrate was added 10mL of saturated solution of NH_4PF_6 to precipitate the product. An orange precipitate was recovered by vacuum filtration and the product was dried in a desiccator. Yield 0.8842 g, (94 %). The product was characterized by CV, ESI-MS: ($[M]^{2+}$, m/z = 313.9) and UV-Vis: (CH_3CN, λ_{max} = 452nm).

$[Ru(bpy)_2(Cl\text{-}phen)]Cl_2$ [69]

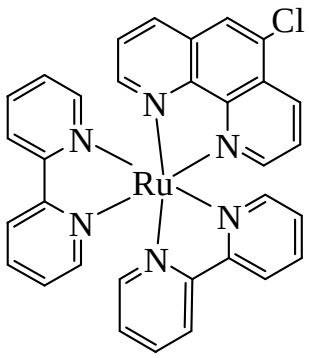

$Ru(CO)_2Cl_2$Cl-phen (0.583 g, 1.32 mmol), bpy (0.467 g, 2.99 mmol) and Me_3NO (0.521 g, 6.95 mmol) were combined and transferred to a three neck RBF. To this was added 70 mL of dry 2-methoxyethanol which was nitrogen purged. The solution was refluxed for 2 hr., cooled to room temperature and then filtered. The filtrate was concentrated by evaporating the solvent on a rotavap and the concentrated solution was added dropwise to anhydrous ethyl ether. The orange solution was kept overnight in a freezer to precipitate the product which was recovered by vacuum filtration and dried in a desiccator. Yield 0.6304 g, (68 %). The product was characterized by CV and ESI-MS: ($[M]^{2+}$, m/z = 313.9).

5, 5'-Bi-1, 10-phenanthroline (diphen) [70]

A 100 mL 3-neck RBF was oven dried and purged with Ar. Through the central neck of the flask was added $NiCl_2$.

$6H_2O$ (0.538 g, 2.26 mmol) and PPh_3 (2.202 g, 8.40 mmol). Then 20 mL of dry DMF was added through a syringe and the resulting blue solution was stirred and purged with argon for 30 min. Zn dust (0.164g, 2.5 mmol) was then added and the mixture stirred for 3 hr resulting in an orange solution. Tetraethyl ammonium iodide (Et_4NI) (0.45 g, 1.75 mmol) and Cl-phen (0.5 g, 1.91 mmol) were then added to the RBF and the solution stirred for 14 hr.at 55 °C under Ar. The resulting reddish solution was transferred to a beaker with a solution of 2.16 g of KCN in 70 mL of 10 % aq. NH_3 solution. A grayish green precipitate which resulted was stirred for 30 min and then filtered. The precipitate was then washed with hexane (2 X 100 mL) and then recrystallized in methanol. Recrystallization was done by dissolving the crude product in a small amount of methanol and warming the solution. At this point a small amount of toluene was added and the solution was further heated gently until clear. The solution was then allowed to slowly cool to room temperature in a flask wrapped with a paper towel. Yield 0.272 g, (74%). The product was characterized by ^{1}H-NMR (300 MHz, $CDCl_3$) δ (ppm): 7.49 (2H, dd), 7.75 (2H, dd), 7.78 (2H, dd), 7.96 (2H, s), 8.33 (2H, dd), 9.24 (2H, dd), 9.31 (2H, dd).and ESI-MS. ($[M\ H]^+$, m/z = 359.1)

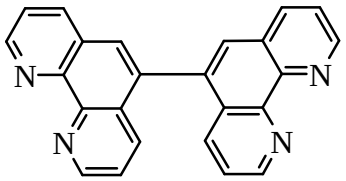

[Ru(bpy)$_2$diphenRu(bpy)$_2$] (PF_6)$_4$ [70]

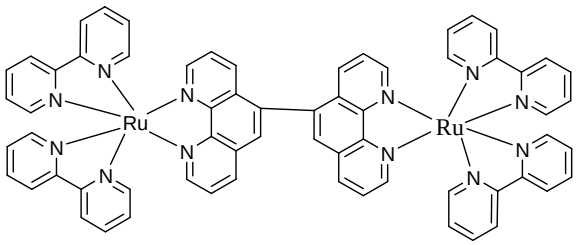

A 100 mL 3-neck RBF was oven dried and purged w/Ar. Through the central neck of the flask was added $NiCl_2.6H_2O$ (0.1524 g, 0.641 mmol) and PPh_3 (0.5587 g, 2.13 mmol). Then 20 mL of dry DMF was added through a syringe and the resulting blue solution was stirred and purged w/ argon for 30 min. Zn dust (0.0405g, 0.619 mmol) was then added and stirred for 3 hr resulting in an orange solution. Tetraethyl ammonium iodide (Et_4NI) (0.137 g, 0.534 mmol) and [Ru (bpy)$_2$(Cl-phen)] (PF_6)$_2$ (0.490 g, 0.534 mmol) were then added to the RBF and the solution stirred for 14 hr. at 55 °C under Ar. The solution was allowed to cool to room temperature and filtered. To the filtrate was added 10 mL of saturated NH_4PF_6 to precipitate the product. Further dilution was carried out with DDI water to obtain maximum precipitate of product. The orange product was recovered by vacuum filtration and was dried in a desiccator. Yield 0.787 g, (84 %). The product was characterized by ESI-MS ($[M]^{4+}$, m/z = 296.5), CV and UV-VIS (CH_3CN, λ_{max} = 452nm).

[Ru(CO)$_2$Cl$_2$]$_n$ [71]

$RuCl_3.3H_2O$ (1.01 g, 3.87 mmol) was transferred to a 100 mL RBF. To this was added 50 mL of a 1:1 (v/v) concentrated HCl/HCOOH solution. The solution was refluxed for 24 hr. under nitrogen atmosphere. The resulting yellow solution was vacuum filtered and the filtrate was heated on a hot plate to evaporate solvent. The resulting yellow product was collected and allowed to cool to room temperature. Yield 0.874 g, (79 %).

[Ru(CO)$_2$Cl$_2$(Cl-phen)] [69]

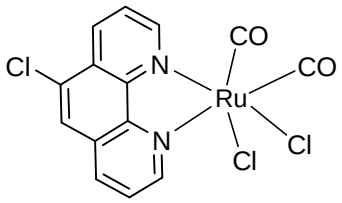

[Ru(CO)$_2$Cl$_2$]$_n$ (0.464 g, 2.03 mmol) was dissolved in 60 mL of hot 2-methoxyethanol and filtered to remove impurities. Cl-phen (0.553 g, 2.58 mmol) was also dissolved in 20 mL of 2-methoxyethanol at room temperature while stirring. The Cl-phen solution was combined with the [Ru(CO)$_2$Cl$_2$]$_n$ solution and boiled on a hot plate to concentrate the solution. The concentrated solution was then kept in a freezer at -18^{o}C to precipitate the product. The reddish brown precipitate was recovered by vacuum filtration and dried in a desiccator. Yield 0.700 g, (78%).

6-Nitroquinoxaline [72]

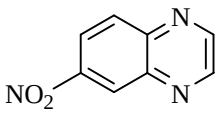

1,2-diamino-4-nitroquinoxaline (1g, 6.529 mmol) and 40 % glyoxal (2.273 g, 39.1 mmol) were combined and transferred to a RBF. To this flask was added 25 mL of ethanol. The solution was heated to 75^{o}C for 1 hr. and then stirred overnight. An orange precipitate was recovered by vacuum filtration, washed with ethanol and dried in a desiccator. Yield 0.857 g, (75%). The product was characterized by ^{1}H-NMR (300 MHz, d_6-DMSO) δ (ppm): 8.35 (s, 1H), 8.1 (d, 1H), 7.78 (d, 1H), 7.55 (dd, 1H), 7.51 (d, 1H) and GC/MS = 175.

5-Amino-6-Nitroquinoxaline [72]

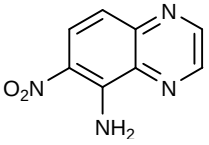

6-Nitroquinoxaline (3.5 g, 20 mmol), hydroxyl amine hydrochloride (8.2 g, 120 mmol) was dissolved in 200 mL of ethanol in a 500 mL RBF. Potassium hydroxide (16.4 g, 300 mL) was placed in a 150 mL beaker and dissolved in 80 mL of ethanol and added dropwise to the RBF for 4 hr.while stirring. The resulting brown solution was then stirred at room temperature for 90 min and poured into a beaker containing 500

g of ice. The solution was refrigerated overnight and filtered to give a yellow brown precipitate. This was then loaded on a short alumina column and eluted with methylene chloride. The product was recovered by rotary evaporation to give a yellow solid. Yield 1.190 g, (31.3%). The product was characterized by ^{1}H-NMR (300 MHz, d_6-DMSO) δ (ppm): 9.1 (d, 1H), 8.9 (d, 1H), 8.9 (d, 1H), 8.5 (br s, 2H), 8.3 (d, 1H), 7.15 (d, 1H), 7.15 (d, 1H). ESI-MS ($[M H]^+$, m/z = 191).

5,6-Diaminoquinoxaline [72]

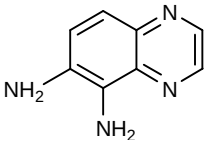

5-amino-6-nitroquinoxaline (0.76 g, 4 mmol) was added to a 100 mL 2-neck RBF under nitrogen. Pd / C 10 % (0.24 g) was also added followed by the addition of 60 mL of ethanol dropwise. 2 mL of hydrazine monohydrate was finally added and the solution was heated to 60 °C for 2 hr. The resulting red solution was then filtered and needle like product was obtained by evaporating the filtrate under vacuum Yield 0.567 g, (88.7 %) The product was characterized by.^{1}H-NMR (300 MHz, d_6-DMSO) δ (ppm): 8.5 (d, 1H), 7.25 (dd, 2H), 5.25 (d, 1H), 3.5 (br s, 4H).ESI-MS: ($[M H]^+$, m/z = 161).

TAP (1,4,5,8-tetraazaphenanthrene) [72]

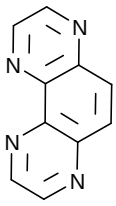

5, 6-diaminoquinoxaline (0.1 g, 0.625 mmol) and 40 % glyoxal (0.288 g, 4.968 mmol) were transferred to a 25 mL RBF and 5 mL of EtOH was added. The RBF was refluxed for 1 hr. at 60°C and then cooled to room temperature. The crude product was purified on an alumina column using chloroform as the eluent. The brownish yellow product was obtained by evaporating the yellow fraction Yield 0.105 g, (92%). The product was characterized by ^{1}H-NMR (300 MHz, d_6-DMSO) δ (ppm): 9.19 (d, 2H), 9.1 (d, 2H), 8.35 (s, 2H). ^{13}C-NMR (300 MHz, d_6-DMSO) δ (ppm): 146.5, 145, 144.4, 141 and 131.9. ESI-MS: ($[M H]^+$, m/z = 183).

$Ru(TAP)_2(Cl\text{-}phen)](PF_6)_2$[69]

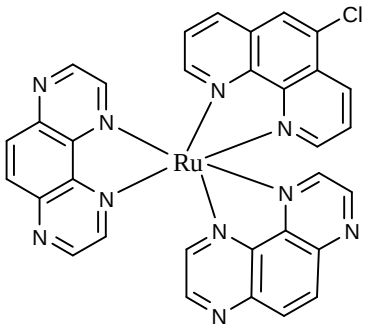

$[Ru(CO)_2Cl_2(Cl\text{-}phen)]$ (0.2915 g, 0.6586 mmol), TAP (0.272 g, 1.495 mmol) and Me_3NO (0.2605 g, 3.473 mmol) were combined and transferred to a three neck RBF. To this was added 35 mL of dry 2-methoxyethanol and the solution was purged with nitrogen for 10 min. The solution was refluxed for 2 hr. under nitrogen atmosphere. Aqueous NH_4PF_6 solution was added to the hot solution and allowed to cool down to room temperature. The solution was filtered and the filtrate was evaporated under reduced pressure. The solution was added dropwise to ca 500 mL of anhydrous ethyl ether to precipitate the product. The product was recovered by vacuum filtration and dried in a dessicator. Yield 0.5390 g, (84.4 %). The product was characterized by ESI-MS: ($[M]^{2+}$, m/z = 339.9)

$[Ru(TAP)_2diphenRu(TAP)_2](PF_6)_4$ [70]

A 100 mL 3-neck RBF was oven dried and purged w/ Ar. Through the central neck of the flask was added $NiCl_2.6H_2O$ (0.1452 g, 0.611 mmol) and PPh_3 (0.535 g, 2.04 mmol). Then 20 mL of dry DMF was added through a syringe and the resulting blue solution was stirred and purged w/ argon for 30 min. Zn dust (0.038g, 0.581 mmol) was then added and stirred for 3 hr resulting in an orange solution. Tetraethylammonium iodide (Et_4NI) (0.1308g, 0.508 mmol) and $Ru(TAP)_2(Cl\text{-}phen)](PF_6)_2$ (0.200 g, 0.206 mmol) were then added to the RBF and the solution stirred for 14 hr. at 55 °C under Ar. The solution was allowed to cool to room temperature, filtered and to the filtrate was added saturated NH_4PF_6 solution to precipitate the product. The orange brown product was recovered by vacuum filtration and dried in a desiccator. Yield 0.1888g (52%). The product was characterized by CV and ESI-MS: ($[M]^{4+}$, m/z = 322.5).

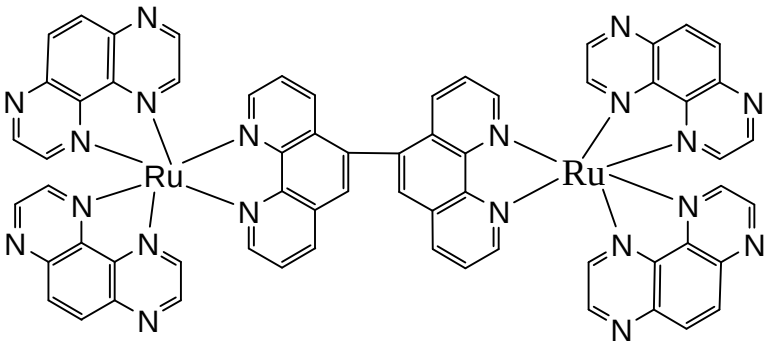

$[Ru(dmbpy)_2Cl\text{-}phen](PF_6)_2$[69]

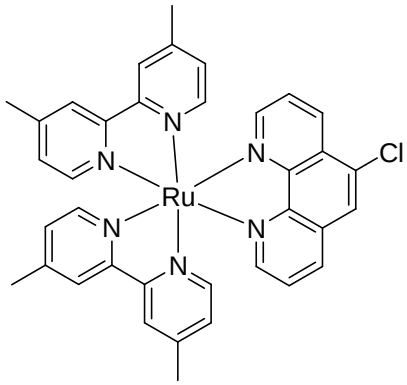

$[Ru(CO)_2Cl_2]_n$ (0.507 g, 2.223 mmol) was dissolved in 50 mL of hot 2-methoxyethanol. Cl-phen (0.534 g, 2.488 mmol) was also dissolved in 5mL of 2-methoxyethanol at room temperature and the two solutions were combined and heated for a short while. To the boiled solution was added 30 mL of 2-methoxyethanol. The solution was nitrogen purged for 35 min. Finally, dmbpy (0.856 g, 4.646 mmol) and Me_3NO (0.846 g, 11.26 mmol) were added and the solution was refluxed for 2 hr. under nitrogen atmosphere. The resulting dark red solution was filtered and to the filtrate was added aq. NH_4PF_6. The solution was then concentrated by evaporating the solvent under vacuum and was added to 300 mL of ethyl ether anhydrous to precipitate the product. The orange product was collected on a filter paper via vacuum filtration and dried in a desiccator. Yield 3.3515 g, (77.4%). The product was characterized by CV and ESI-MS: ($[M]^{2+}$, m/z = 342).

$[Ru(dmbpy)_2diphenRu(dmbpy)_2(PF_6)_4$[69]

$[Ru\ (CO)_2Cl_2]_n$ (0.042 g, 0.184 mmol) was dissolved in 15 mL of hot 2-methoxyethanol. Diphen (0.058 g, 0.162 mmol) was also dissolved in 2-methoxyethanol at room temperature and combined with the previous solution. The combined solution was then heated on a hot plate to concentrate the solution and was added to a 3 neck RBF containing 30 mL of 2-methoxyethanol which was argon purged for 30 min. Finally, dmbpy (0.065 g, 0.352 mmol) and Me_3NO (0.076 g, 1.012 mmol) were added and the solution was refluxed for 2 hr. under nitrogen atmosphere. The resulting dark red solution was filtered and to the filtrate was added aq. NH_4PF_6. The solution was then concentrated by evaporating the solvent under vacuum and was added to 300 mL of anhydrous ethyl ether to precipitate the product. The orange product was recovered by

vacuum filtration and dried in a desiccator. Yield 0.133 g, (38.5%). The product was characterized by CV and ESI-MS: ($[M]^{4+}$, m/z = 324.4)

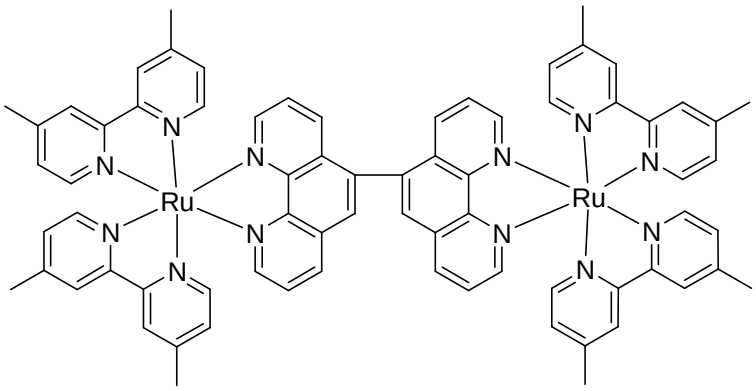

$[Ru(CO)_2Cl_2$ dmbpy] [69]

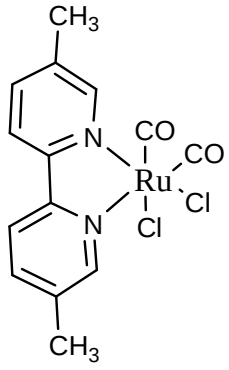

$[Ru(CO)_2Cl_2]_n$ (0.464 g, 2.03 mmol) was dissolved in 60 mL of hot 2-methoxyethanol. Dmbpy (4,4'-dimethyl, 2,2'-bipyridine) (0.475 g, 2.58 mmol) was also dissolved in 20 mL of 2-methoxyethanol at room temperature while stirring. The two solutions were combined and heated on a hot plate to ca 5mL. The concentrated solution was stored overnight in a refrigerator at -18°C to precipitate product. The product was recovered by vacuum filtration and dried in a desiccator. Yield 0.700g, (84%). The product was characterized by ^{1}H-NMR (300 MHz, d_6-$(CD_3)_2CO$) δ (ppm): 2.64 (6H, s, CH_3), 7.66 (2H, d, $H^{5,5'}$), 8.54 (2H, s, $H^{3,3'}$) and 9.06 ppm (2H, d, $H^{6,6'}$).

$[Ru(dmbpy)_2(CO)_2](PF_6)_2 . H_2O$ [73]

$[Ru(dmbpy(CO)_2Cl_2]$ (0.151 g, 0.37 mmol) and dmbpy (0.081 g, 0.44 mmol) were weighed and transferred to a 250 mL RBF. To this flask was added 150 mL of a 3:1 (v/v) MeOH / H_2O and the solution was refluxed for 24 hr. The solution was then allowed to cool to room temperature and filtered. To the filtrate was added 10 mL of saturated NH_4PF_6 to precipitate the product. The orange product was recovered by vacuum filtration and was dried in a desiccator. Yield 0.2715 g,

(88%). The product was characterized by ^{1}H-NMR (300 MHz, d_6-$(CD_3)_2CO$) δ (ppm): 2.56 (6H, s, CH_3), 2.76 (6H, s, CH_3'), 7.49 (2H, d, H^5), 7.65 (2H, d, H^6), 7.94 (2H, d, $H^{5'}$), 8.70 (2H, s, H^3), 8.76 (2H, s, $H^{3'}$) and 9.28 (2H, d, $H^{6'}$).

$Ru(dmbpy)_2diphenRu(bpy)_2(PF_6)_4$[74]

$[Ru(dmbpy)_2(CO)_2](PF_6)_2.H_2O$ (0.8652g, 1.0 mmol), $[Ru(bpy)_2diphen](PF_6)_2$ (1.2738 g, 1.2 mmol) and Me_3NO (0.2253 g, 3.0 mmol) were weighed and transferred into a 150 mL RBF. To this was added 70 mL of 2-methoxyethanol. The solution was refluxed for 2 hr. under nitrogen atmosphere. Saturated NH_4PF_6 was added unto the hot solution and allowed to cool down. Red orange solution was concentrated and added drop wise to approx. 300 mL of anhydrous diethyl ether to precipitate product. Red orange product was recovered by vacuum filtration and dried in a desiccator. Yield 1.6188 g, (89 %). The product was characterized by CV and ESI-MS: ($[M]^{4+}$, m/z = 310.5).

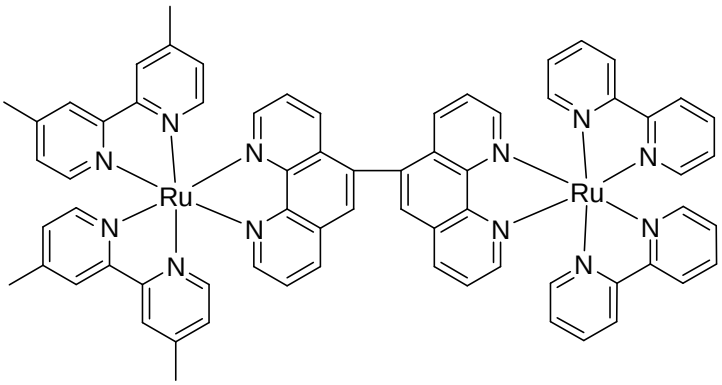

[Ru (bpy)$_2$diphen](PF$_6$)$_2$[68]

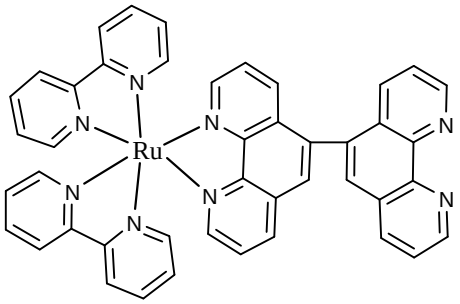

$Ru(bpy)_2Cl_2.2H_2O$ (0.2603 g, 0.50 mmol) and diphen (0.2150 g, 0.60 mmol) were weighed and transferred into a 50 mL RBF. To this was added 12.5 mL of a 3: 1 (v/v) EtOH / H_2O. The solution was refluxed for 24 hr. The solution was filtered and to the filtrate was added aq NH_4PF_6 to precipitate product. The orange product was obtained via vacuum filtration and dried in a desiccator. Yield 0.4778 g, (90%). The product was characterized by CV and ESI-MS: ($[M]^{2+}$, m/z = 385.9)

[Ru(bpy)$_2$CO$_3$[75]

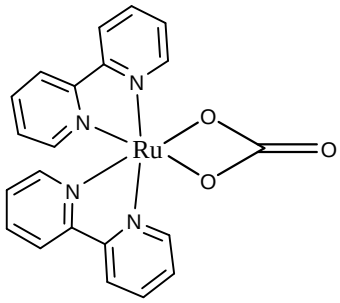

$Ru(bpy)_2Cl_2.2H_2O$ (2.0 g, 3.85 mmol) was added to a 250 mL RBF and dissolved in 150 mL of DDI water while stirring. Sodium carbonate (6.6 g, 62.3 mmol) was added and the solution was refluxed for 2 hr. The heat was turned off and the solution was allowed to cool slowly overnight.The dark red solution was vacuum filtered and black needle like solid was collected. It was washed several times with water, isopropanol and anhydrous ethyl ether and dried in a desiccator. Yield 0.9870 g, (54%).

[Ru(bpy)$_2$Cl$_2$.2H$_2$O][76]

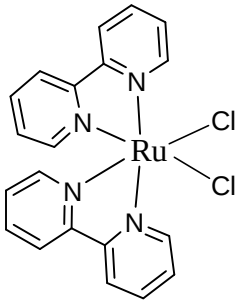

$RuCl_3.3H_2O$ (7.80 g, 29.8 mmol), bpy (9.36 g 60 mmol) and LiCl (8.4 g, 197.6 mmol) was weighed and transferred to a 100 mL RBF. To this was added 50 mL of DMF and the solution was refluxed for 18 hr. The solution was then allowed to cool down to room temperature and filtered. The black product was recovered

by vacuum filtration, washed with ethyl ether and DDI water and dried in a desiccator. Yield 13.0 g, (84%). The product was characterized by CV.and UV-VIS (CH_3CN, λ_{max} = 540 nm)

$[Ru(dmbpy)_2CO_3]$[75]

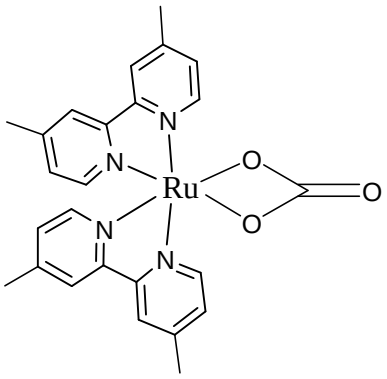

$[Ru(dmbpy)_2Cl_2$ (1.717 g, 3.18 mmol) was placed in a 150 mL RBF and dissolved in 80 mL of DDI water while stirring. Sodium carbonate (6.00 g, 56.68 mmol) was also added and the solution was refluxed for 2h. The heat was turned off and the solution was allowed to cool slowly overnight.The dark red solution was vacuum filtered and black solid was collected. It was washed several times with water, isopropanol and anhydrous ethyl ether and dried in a desiccator. Yield 1.6084 g, (96%).

$[Ru(dmbpy)_2Cl_2.2H_2O]$[77]

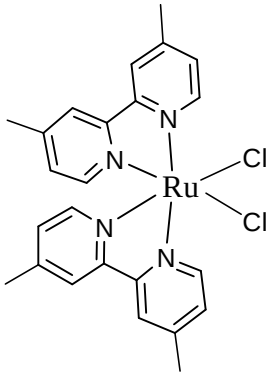

$RuCl_3.3H_2O$ (4.30 g, 16.5 mmol), dmbpy (7.08 g, 38.5 mmol) and LiCl (5.5 g, 42.5 mmol) was weighed and transferred to a 100 mL RBF. To this was added 30 mL of DMF and the solution was refluxed for 8 hr. After cooling, the dark solution was added to 300 mL of rapidly stirring acetone in a 500 mL Erlenmeyer flask. The solution was kept overnight in the refrigerator. The dark brown solid was collected by vacuum filtration, washed with anhydrous ethyl ether and dried in a desiccator. In order to remove the last traces of DMF, the solid was suspended in 100 mL of ethyl ether anhydrous and then recovered by vacuum filtration. This procedure was repeated until a pure product was obtained. Yield 9.054 g, (95%).

4,4'-dicarboxy-2,2'-bipyridine[78]

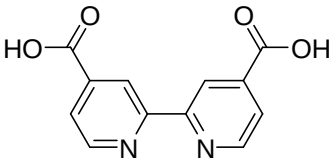

4,4'-dimethyl-2, 2-bipyridine (4.926 g, 26.7 mmol) was weighed and transferred to a 100 mL RBF. To this was added 37 mL of concentrated sulfuric acid. Chromium oxide (8.047 g, 80.5 mmol) was added in 0.2 g portion to keep the temperature less than 70 °C. The solution was allowed to stir until it had cooled to 30 °C. The solution was poured over 500 g of crushed ice. The product was recovered by vacuum filtration and allowed to dry in a desiccator. Yield 4.5604 g, (70%).

4,4'-diethoxycarbonyl-2,2'-bipyridine[79]

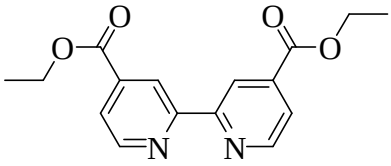

4,4'-dicarboxy-2,2'-bipyridine (2.964g,12.15mmol) was weighed and transferred to a 1L RBF. To this were added 400 mL of 200 proof pure ethanol and 5 mL of concentrated sulfuric acid. The solution was refluxed for 80 hr. under nitrogen atmosphere. The precipitate was obtained by the addition of 400 mL of DDI water. The product was recovered by vacuum filtration and dried in a desiccator. Yield 2.85 g, (78%). The product was characterized by ^{1}H-NMR (300 MHz, $CDCl_3$) δ (ppm): 8.77 (s, 1H), 8.69 (d, 1H), 7.73 (d, 1H), 4.28 (q, 2H), 1.26 (t, 3H).

2, 2'-bipyrazine [80]

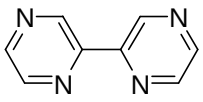

2-pyrazine carboxylic acid (12.5 g, 101 mmol) was dissolved in a beaker containing 100 mL of 15 M ammonia while stirring. The solution was heated to dryness under vacuum in a rotatory evaporator. The resulting white solid was added to 500 mL of aqueous copper (II) acetate solution and stirred for 1 hr. The resulting blue solution was filtered giving a blue precipitate which was dried in an oven. The blue solid was pyrolysed at 253°C in a sublimator. The ligand was collected from the inner tube of the sublimator and was washed with anhydrous ethyl ether and dried in a desiccator. The crude product was purified by

column chromatography using silica gel 60 as the absorbent and DCM / THF (v/v: 20:1) as the eluents. Yield 1.005 g, (6.3%). The product was characterized by ^{1}H-NMR (300 MHz, $CDCl_3$) δ (ppm): 9.59 (1H, s), 8.64 (1H, s).

$[Ru(bpz)_3](PF_6)_2$ [80]

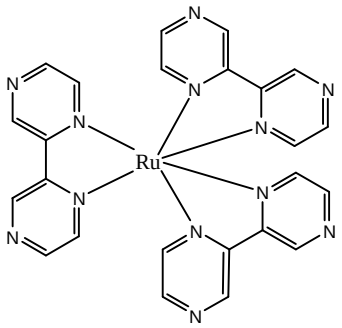

$RuCl_3.3H_2O$ (0.0108 g, 0.0413 mmol), bpz (0.0282 g, 0.178 mmol) were weighed and transferred to a 10 mL microwave vessel containing 7.5 mL of ethylene glycol. The suspension was microwaved at 200 ^{0}C for 30 min. The suspension was then allowed to cool down to room temperature and filtered to remove unreacted $RuCl_3.3H_2O$. To the filtrate was added 5 mL of saturated NH_4PF_6 to precipitate the product. The orange product was recovered by vacuum filtration and dried in a desiccator. The crude product was purified by column chromatography using alumina as the absorbent and acetonitrile as the eluent. Yield 0.0322 g, (90%). The product was characterized by ^{1}H-NMR (300 MHz, $CDCl_3$) δ (ppm): 9.59 (1H, s), 8.64 (1H, s) and UV-VIS (CH_3CN, λ_{max} = 450 nm)

$[Ru(bpy)_3](PF_6)_2$ [80]

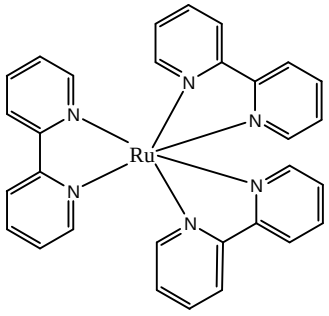

$Ru(bpy)_2Cl_2$ (0.013 g, 0.02 mmol) was dissolved in a 250 mL RBF containing 150 mL EtOH / H_2O (v/v : 1: 1). The solution was heated for 30 min under nitrogen atmosphere. Bpy (0.09 g, 0.576 mmol) was then added and the solution was refluxed overnight. The solution was then allowed to cool to room temperature and filtered. To the filtrate was added 5 mL of saturated NH_4PF_6 to precipitate the product. The orange product was obtained via vacuum filtration, washed with 10 mL of H_2O, 2 x 10 mL of 2-propanol and 2 x 25 mL of ethyl ether anhydrous. The sample was dried in a desiccator and

purified by column chromatography using alumina as the adsorbent and CH_3CN / CH_2Cl_2 (V/V: 1: 10) as eluents. The product was characterized by ^{1}H-NMR (300 MHz, CD_3CN) δ. (ppm): 8.49 (d, 6H), 8.05 (t, 6H), 7.72 (d, 6H), 7.39 (t, 6H) and CV.

[Ru(Cl-phen)]Cl_4 [81]

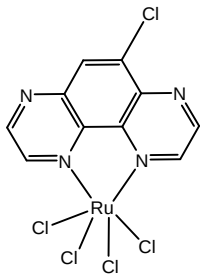

$RuCl_3.3H_2O$ (1.00 g, 3.82 mmol) and Cl-phen (0.838 g, 3.91 mmol) were weighed and transferred to a 50 mL RBF. To this was added 5 mL of 1M HCl drop wise while stirring. The mixture was further stirred to ensure that all unreacted solid had dissolved. The RBF was then sealed and allowed to stand for 7 days in the dark. The suspension was filtered and black product was collected and washed with anhydrous ethyl ether and dried in a desiccator. Yield 1.5732 g, (90%).

CHAPTER 3: RESULTS

3.1 Synthesis and Basic Characterization

Investigation of the electronic coupling was pursued through the synthesis and extensive characterization of three dinuclear ruthenium complexes. The dinuclear complex $(bpy)_2Ru$ diphen $Ru(bpy)_2^{4+}$ was the initial focus of the investigation. The complexes $(dmbpy)_2Ru$ diphen $Ru(dmbpy)_2^{4+}$ and $(bpy)_2Rudiphen(dmbpy)_2^{4+}$ were synthesized as a control and as a comparison to a complex containing two distinctly different redox centers, respectively.

3.2 Synthesis and Characterization of $[(bpy)_2RudiphenRu(bpy)_2](PF_6)_4$

This dimer was synthesized by modifying the protocol of Toyota et al [70]. The complex cis-$Ru(bpy)_2Cl_2$ was prepared as previously [77]described. This complex was reacted with 7-chlorophenanthroline by simple reflux in ethanol/water to produce $[(bpy)_2Ru(7\text{-chlorophenanthroline})](PF_6)_2$. Two mononuclear complexes were combined by a nickel coupling reaction in moderate yield.

The scheme for this synthesis is illustrated below.

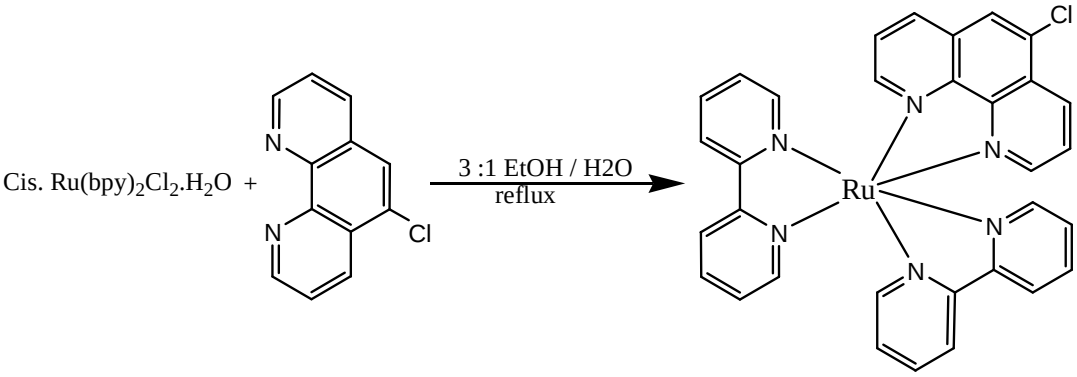

Scheme 3.2.1. Synthesis of $[Ru(bpy)_2(7\text{-chlorophenanthroline})](PF_6)_2]$

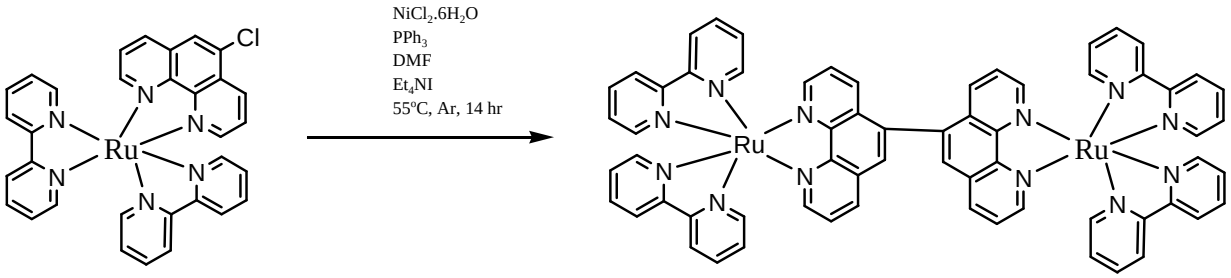

Scheme 3.2.2. Synthesis of $[(bpy)_2RudiphenRu(bpy)_2](PF_6)_4$

The product was purified by column chromatography with CH_3CN / MeOH as the eluent and alumina as the adsorbent. Identity of the intermediates and the final product was confirmed by NMR, mass and UV/Vis spectroscopy.

Of the three dimers described in this dissertation, $[(bpy)_2RudiphenRu(bpy)_2](PF_6)_4$ is the most thoroughly characterized. Several of the intermediates are common to the other two dimeric complexes. $[Ru(bpy)_2(Cl\text{-}phen)](PF_6)_2$ was a key intermediate in several of the pathways. The mass spectrometry results are perhaps the most informative. Figures 3.2.1 and 3.2.2 show mass spectrometry obtained using a MALDI TOF instrument and an electrospray-based instrument. The two different ionization methods yield different results and is consistent with previous reports. Specifically MALDI-TOF generally produces singly charge ions with complexes such as the one sunder investigation. In the present case the MALDI-TOF spectrum shows a very clean major ion at M/Z = 629.97 with an isotopic distribution consistent with a charge of one (peaks separated by 1) in the presence of one ruthenium (7 naturally occurring isotopes) and one chloride (2 naturally occurring isotopes). The electrospray-based spectrum is consistent with a charge of two (peaks separated by 0.5) with the appropriate isotopic splitting. The masses in both cases agree with the monoisotopic mass of expected structure for the +1 and +2 ions, M/Z =

628.07 and 314.03, respectively. In both cases simulated spectra match the actual spectral within experimental expectations.

The NMR spectrum shown in Figure 3.2.3 is very complex and substantially more difficult to interpret. However, the singlet at 8.32 ppm is distinctive for the proton at carbon 5 of Cl-phen and overall integration agrees with the presence of one Cl-phen. Figure 3.2.4 shows the UV/Vis absorption spectrum of the complex in acetonitrile. The major peak at 450 nm with a should at higher energy is typical of ruthenium(II) complexes containing three polypyridine ligands. The peak has been assigned to a MLCT transition.

The intermediate complex $[Ru(bpy)_2diphen](PF_6)_2$ was also characterized by electrospray mass spectroscopy which is shown in Figure 3.2.5. The parent ion with M/Z = 385.9 agrees with the expected monoisotopic M/Z = 285.05. The isotopic distribution of a complex containing one ruthenium atom is clearly evident. In this some additional peaks were also present in the spectrum. The peak at M/Z = 296 is due to a small amount of the dimer $[(bpy)_2RudiphenRu(bpy)_2]^{4+}$. The peak at M/Z = 359 lacks the ruthenium isotopic distribution and therefore does not contain ruthenium.

The ^{1}H-NMR and the ^{13}C-NMR are shown in Figures 3.2.6 and 3.2.7, respectively and are consistent with the assigned structure.

The electrospray mass spectrum of the final product, $[(bpy)_2RudiphenRu(bpy)_2]^{4+}$ is shown in Figure 3.2.8. The spectrum shows a clean major peak centered at 296.3 which is consistent with an ion with Z = 4. The isotopic distribution is also consistent with the +4 charge and the presence of two ruthenium atoms. The ^{1}H-NMR, illustrated in Figure 3.2.9 is very complex and is provided only for comparison to other samples and future reference. The UV/Vis absorption

spectrum is shown in Figure 3.2.10 and is essentially identical to the spectrum of the monomeric intermediates as expected.

Figure 3.2.1. Maldi TOF Spectra of $[Ru(bpy)_2Cl\text{-}phen](PF_6)_2$

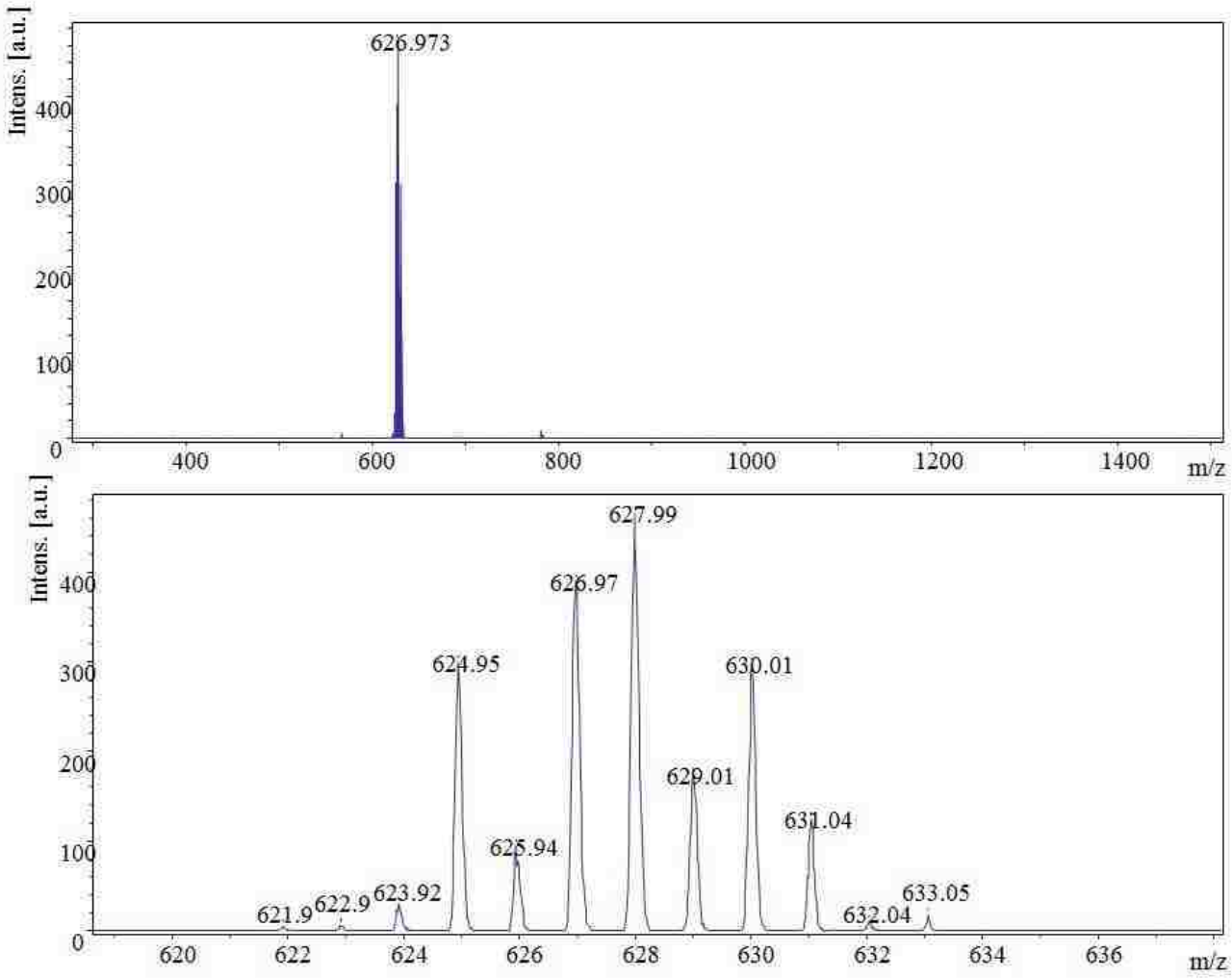
Intens. [a.u.]
626.973
m/z
Intens. [a.u.]
627.99
626.97
624.95
630.01
629.01
631.04
625.94
621.9
622.9
623.92
632.04
633.05
m/z

Figure 3.2.2. ESI-MS spectra of $[Ru(bpy)_2Cl\text{-}phen](PF_6)_2$

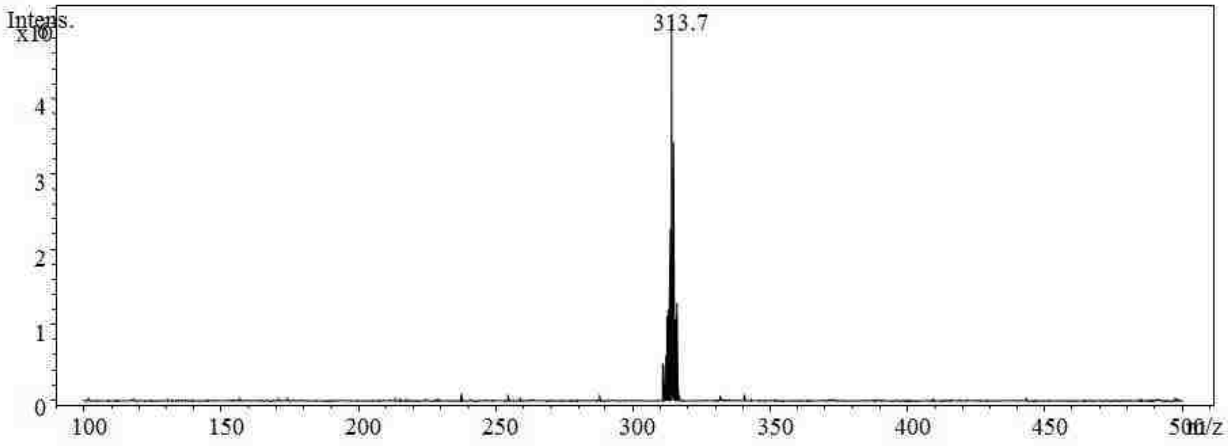
Intens.
313.7
100
150
200
250
300
350
400
450
m/z

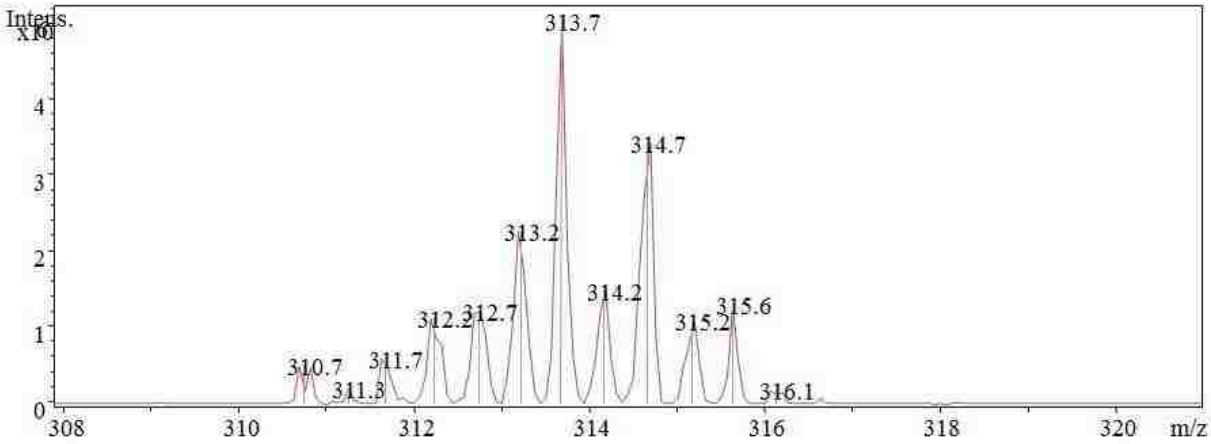
Intens.
313.7
314.7
313.2
314.2
312.2
312.7
315.6
315.2
310.7
311.7
311.3
316.1
308
310
312
314
316
318
320
m/z

Figure 3.2.3. ^{1}H-NMR of $[Ru(bpy)_2Cl\text{-}phen]^{2+}$ in d_3-acetonitrile.

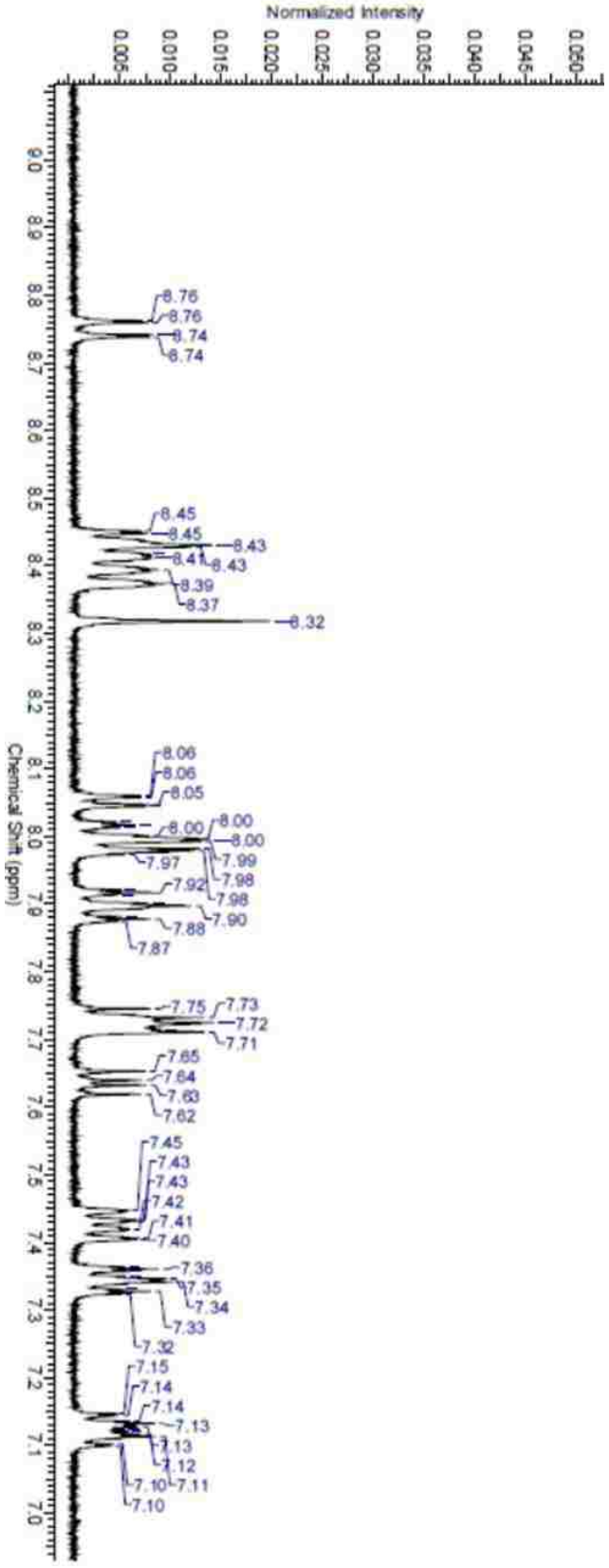
Normalized Intensity
0.005
0.010
0.015
0.020
0.025
0.030
0.035
0.040
0.045
0.050
Chemical Shift (ppm)
9.0
8.9
8.8
8.7
8.6
8.5
8.4
8.3
8.2
8.1
8.0
7.9
7.8
7.7
7.6
7.5
7.4
7.3
7.2
7.1
7.0
8.76
8.76
8.74
8.74
8.45
8.45
8.43
8.41
8.43
8.39
8.37
8.32
8.06
8.06
8.05
8.00
8.00
8.00
7.99
7.98
7.98
7.97
7.92
7.90
7.88
7.87
7.75
7.73
7.72
7.71
7.65
7.64
7.63
7.62
7.45
7.43
7.43
7.42
7.41
7.40
7.36
7.35
7.34
7.33
7.32
7.15
7.14
7.14
7.13
7.13
7.12
7.11
7.10
7.10

Figure 3.2.4. UV-Vis Absorption of $[Ru(bpy)_2Cl\text{-}phen](PF_6)_2$ in acetonitrile.

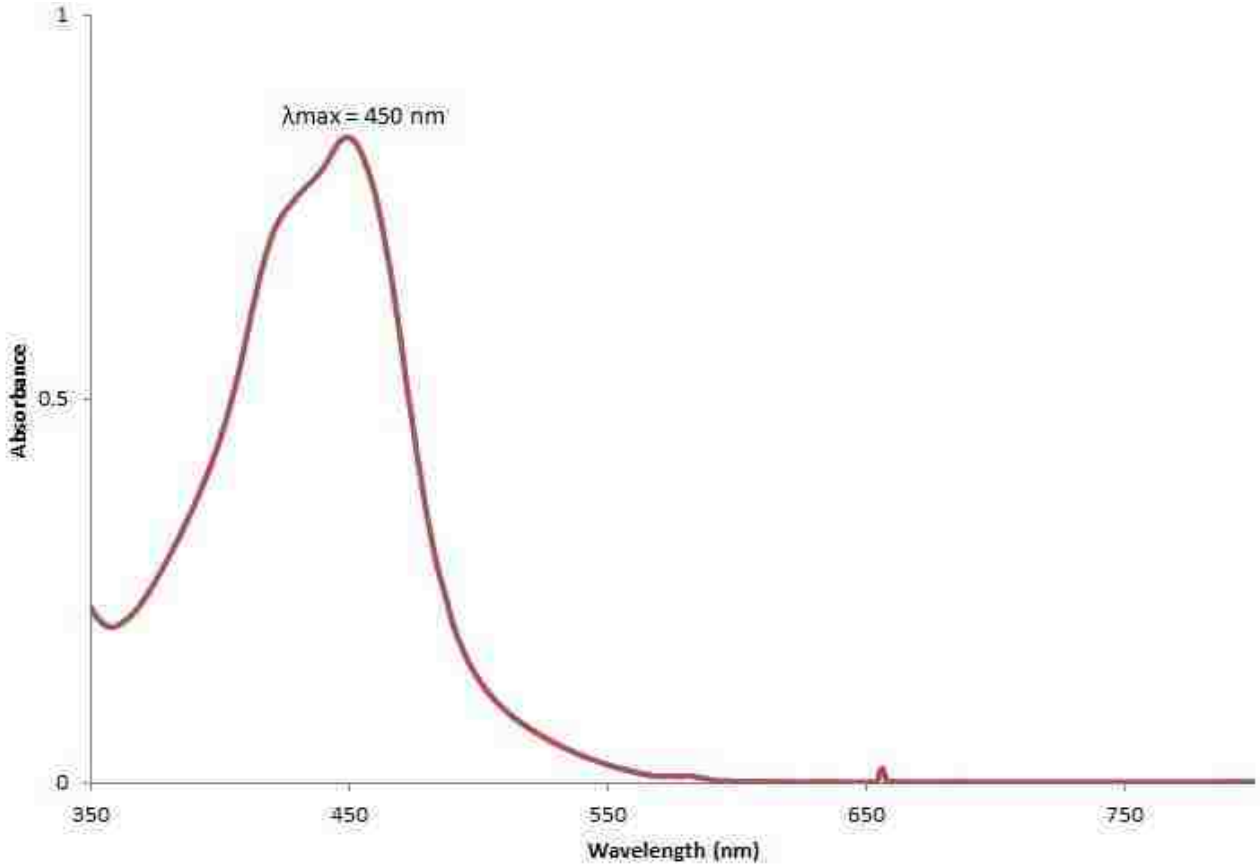
λmax = 450 nm
Absorbance
1
0.5
0
350
450
550
650
750
Wavelength (nm)

Figure 3.2.5. ESI-MS spectra of $[Ru(bpy)_2diphen]^{2+}$

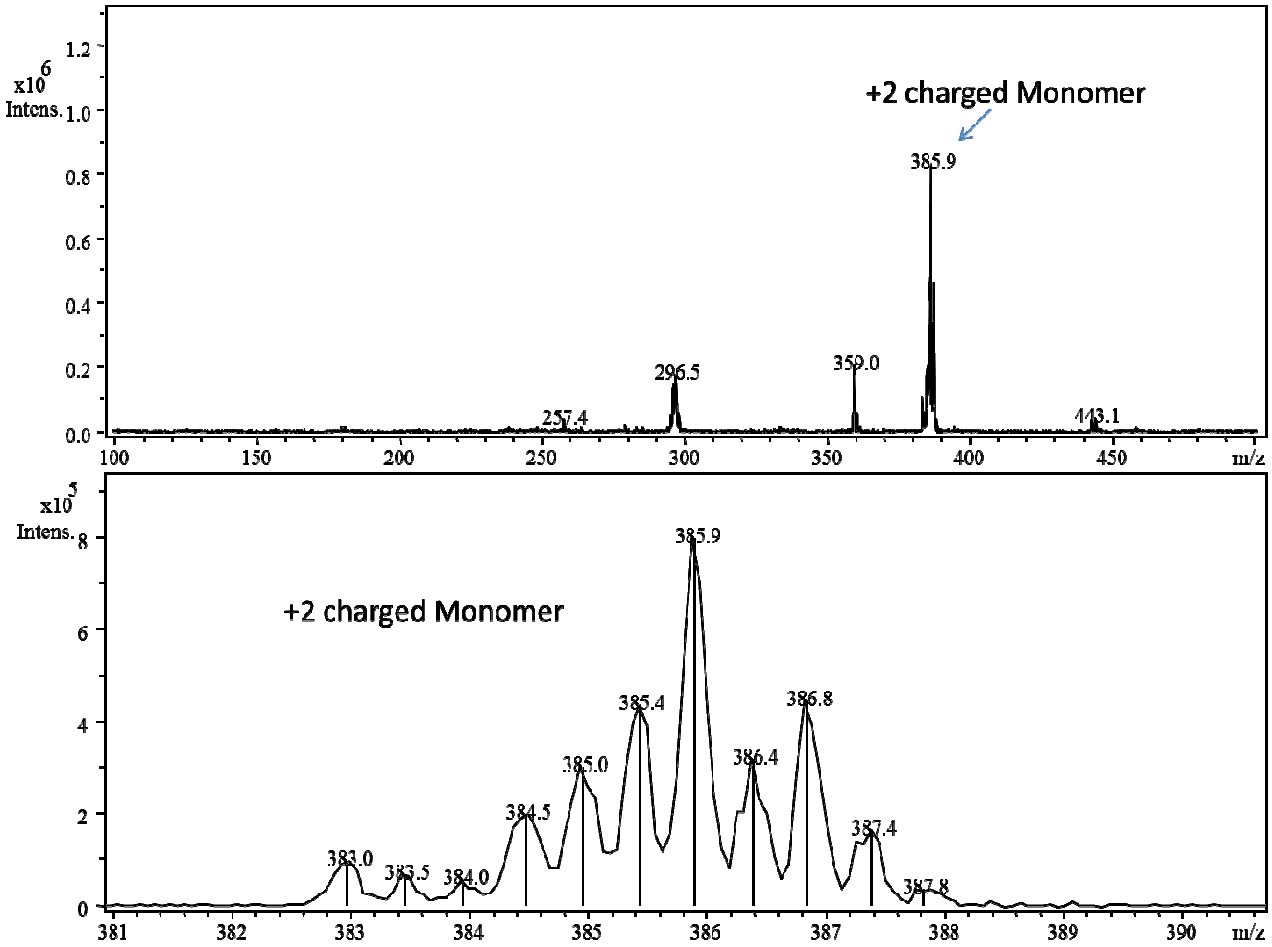
x10 6
Intens.
1.2
1.0
0.8
0.6
0.4
0.2
0.0
+2 charged Monomer
385.9
359.0
296.5
257.4
443.1
100
150
200
250
300
350
400
450
m/z
x10 5
Intens.
8
6
4
2
0
+2 charged Monomer
385.9
385.4
386.8
385.0
386.4
384.5
387.4
383.0
383.5
384.0
387.8
381
382
383
384
385
386
387
388
389
390
m/z

Figure 3.2.6. ^{1}H-NMR of $[Ru(bpy)_2diphen]^{2+}$in d_3-CD_3CN .

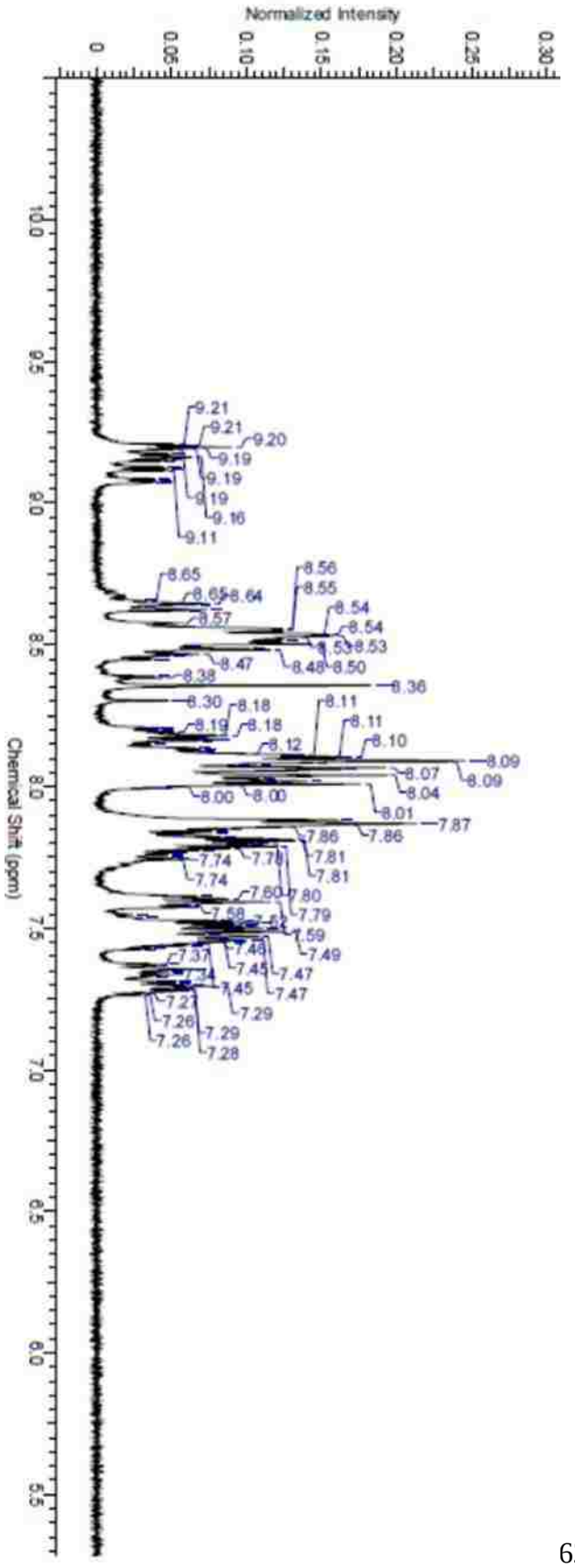
Normalized Intensity
0
0.05
0.10
0.15
0.20
0.25
0.30
Chemical Shift (ppm)
10.0
9.5
9.0
8.5
8.0
7.5
7.0
6.5
6.0
5.5
9.21
9.21
9.20
9.19
9.19
9.19
9.16
9.11
8.65
8.65
8.64
8.57
8.56
8.55
8.54
8.54
8.53
8.53
8.47
8.48
8.50
8.38
8.36
8.30
8.18
8.19
8.18
8.12
8.11
8.11
8.10
8.09
8.07
8.09
8.04
8.00
8.00
8.01
7.87
7.86
7.86
7.74
7.78
7.81
7.81
7.74
7.60
7.80
7.79
7.58
7.59
7.49
7.37
7.46
7.45
7.47
7.45
7.47
7.27
7.29
7.26
7.29
7.26
7.28

Figure 3.2.7. ^{13}C-NMR of $[Ru(bpy)_2diphen]^{2+}$ in d_3-CD_3CN.

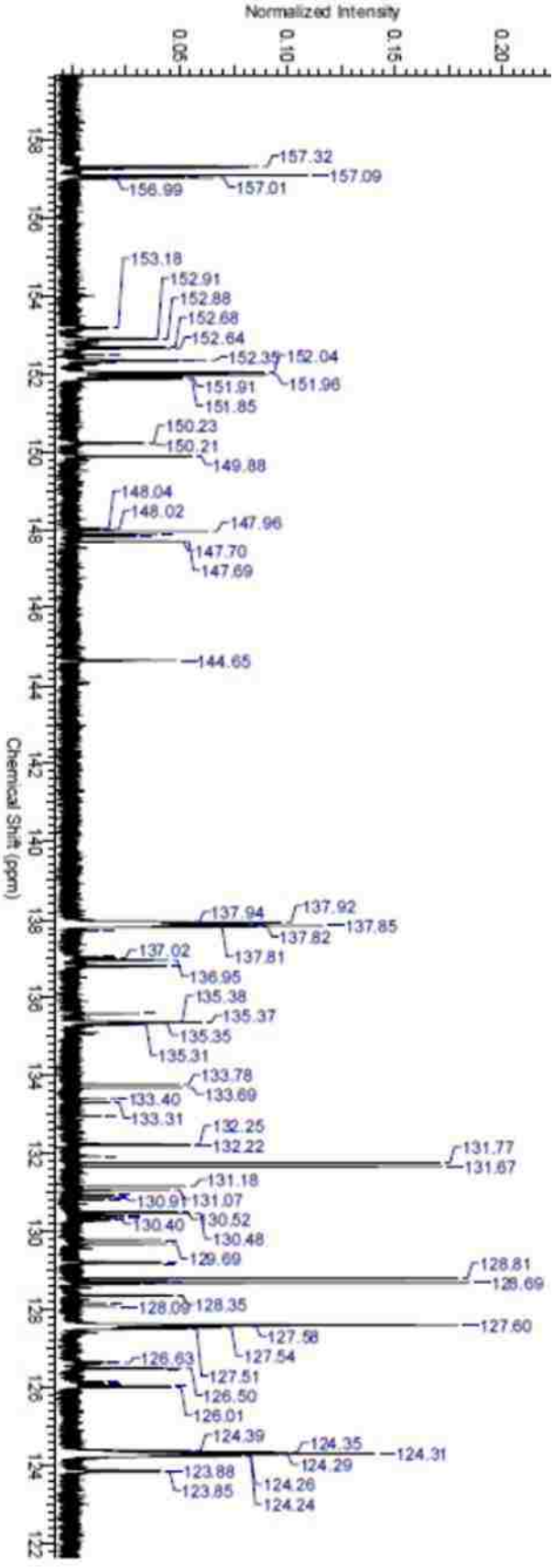
Normalized Intensity
0.05
0.10
0.15
0.20
Chemical Shift (ppm)
158
156
154
152
150
148
146
144
142
140
138
136
134
132
130
128
126
124
122
157.32
157.09
156.99
157.01
153.18
152.91
152.88
152.68
152.64
152.35
152.04
151.96
151.91
151.85
150.23
150.21
149.88
148.04
148.02
147.96
147.70
147.69
144.65
137.94
137.92
137.85
137.82
137.81
137.02
136.95
135.38
135.37
135.35
135.31
133.78
133.69
133.40
133.31
132.25
132.22
131.77
131.67
131.18
130.91
131.07
130.40
130.52
130.48
129.69
128.81
128.69
128.09
128.35
127.60
127.58
127.54
126.63
127.51
126.50
126.01
124.39
124.35
124.31
124.29
123.88
123.85
124.26
124.24

Figure 3.2.8. ESI-MS spectra of $[Ru(bpy)_2diphen(bpy)_2Ru]^{4+}$

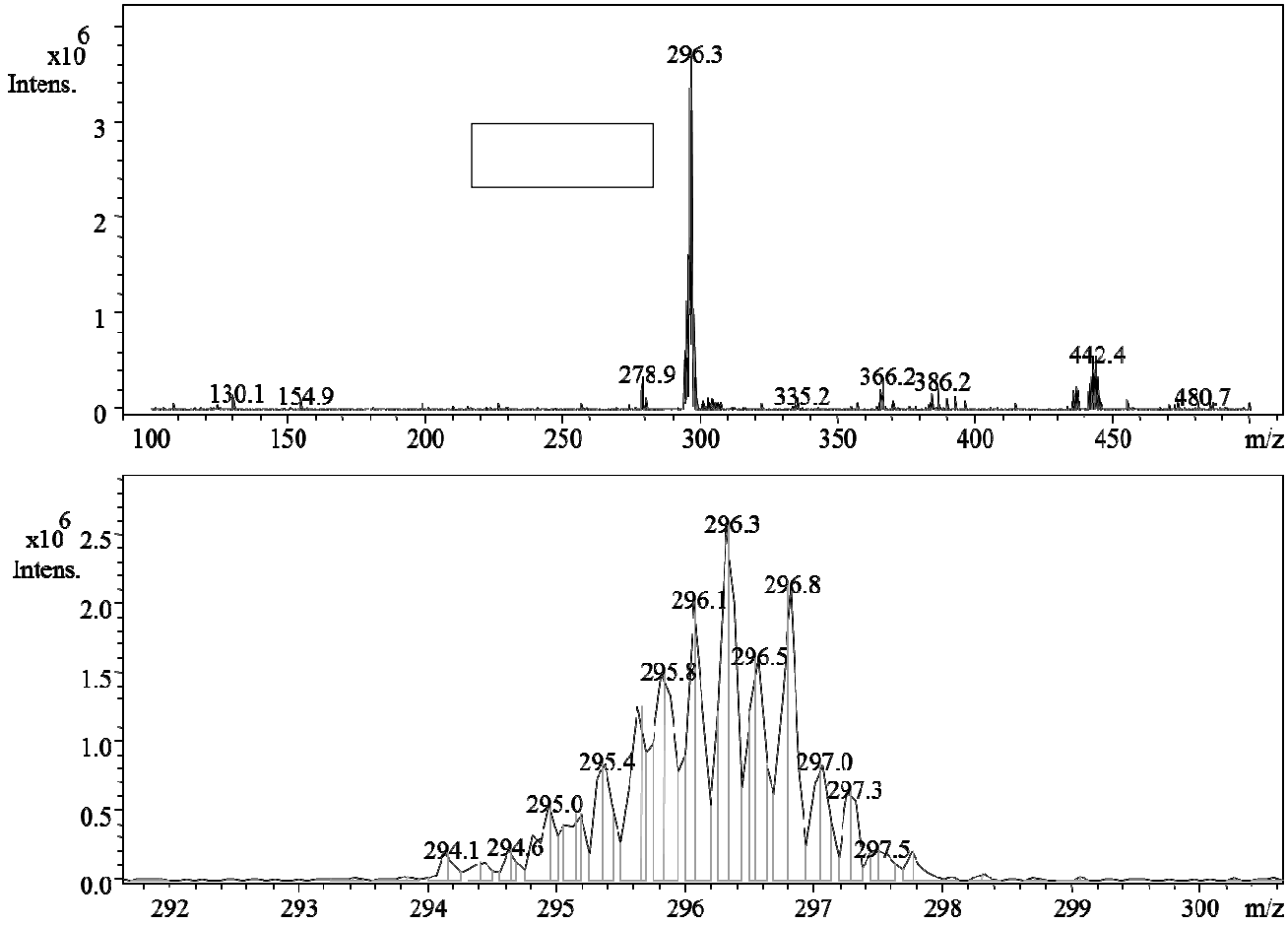
x10 6
Intens.
296.3
278.9
130.1
154.9
335.2
366.2
386.2
442.4
480.7
m/z
x10 6
Intens.
296.3
296.1
296.8
296.5
295.8
295.4
295.0
297.0
297.3
294.1
294.6
297.5
m/z

Figure 3.2.9. ^{1}H-NMR of $[Ru(bpy)_2diphen(bpy)_2Ru]^{4+}$ in acetonitrile.

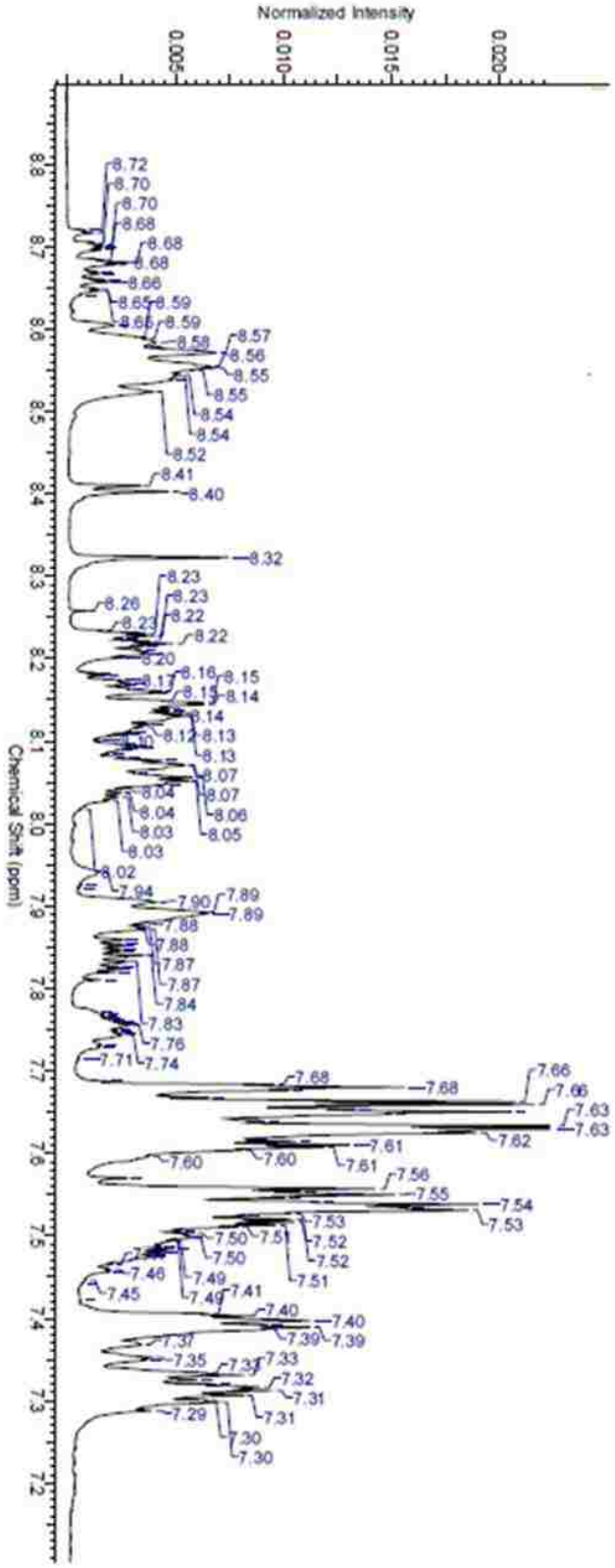
Normalized Intensity
0.005
0.010
0.015
0.020
Chemical Shift (ppm)
8.8
8.7
8.6
8.5
8.4
8.3
8.2
8.1
8.0
7.9
7.8
7.7
7.6
7.5
7.4
7.3
7.2
8.72
8.70
8.70
8.68
8.68
8.68
8.66
8.65
8.59
8.65
8.59
8.58
8.57
8.56
8.55
8.55
8.54
8.54
8.52
8.41
8.40
8.32
8.23
8.26
8.23
8.23
8.22
8.22
8.20
8.16
8.15
8.15
8.14
8.14
8.12
8.13
8.13
8.07
8.04
8.07
8.04
8.06
8.03
8.05
8.03
8.02
7.94
7.90
7.89
7.89
7.88
7.88
7.87
7.87
7.84
7.83
7.76
7.71
7.74
7.68
7.68
7.66
7.66
7.63
7.63
7.62
7.61
7.60
7.60
7.61
7.56
7.55
7.54
7.53
7.53
7.50
7.51
7.52
7.50
7.52
7.46
7.49
7.51
7.45
7.49
7.41
7.40
7.40
7.39
7.39
7.37
7.35
7.33
7.32
7.31
7.29
7.31
7.30
7.30

Figure 3.2.10. UV-Vis absorption of $[Ru(bpy)_2diphen(bpy)_2Ru]^{4+}$ in acetonitrile.

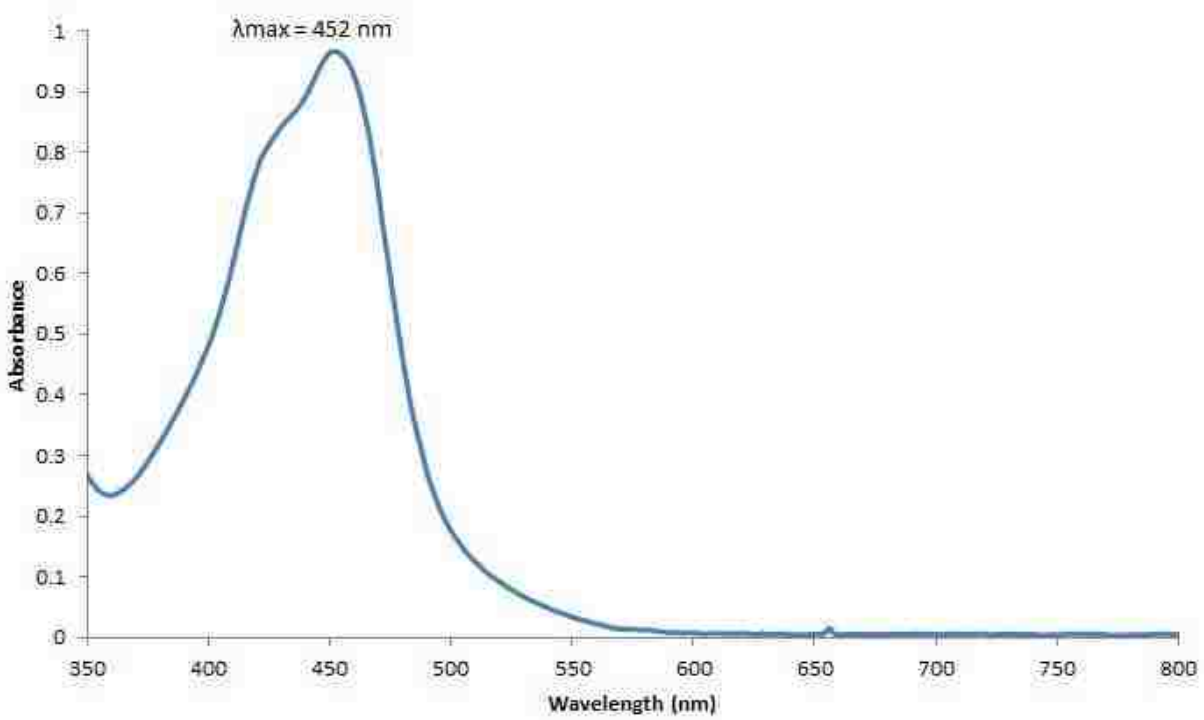
λmax = 452 nm
Absorbance
Wavelength (nm)
1
0.9
0.8
0.7
0.6
0.5
0.4
0.3
0.2
0.1
0
350
400
450
500
550
600
650
700
750
800

3.3 Synthesis and Characterization of $(dmbpy)_2RudiphenRu(dmbpy)_2](PF_6)_4$

The procedure described above for the synthesis of $[(bpy)_2Ru\ diphen\ (bpy)_2]^{4+}$ was unsuccessful. To overcome this difficulty, a different scheme was used based on a well-documented decarbonylation reaction described by Thomas et al [69].

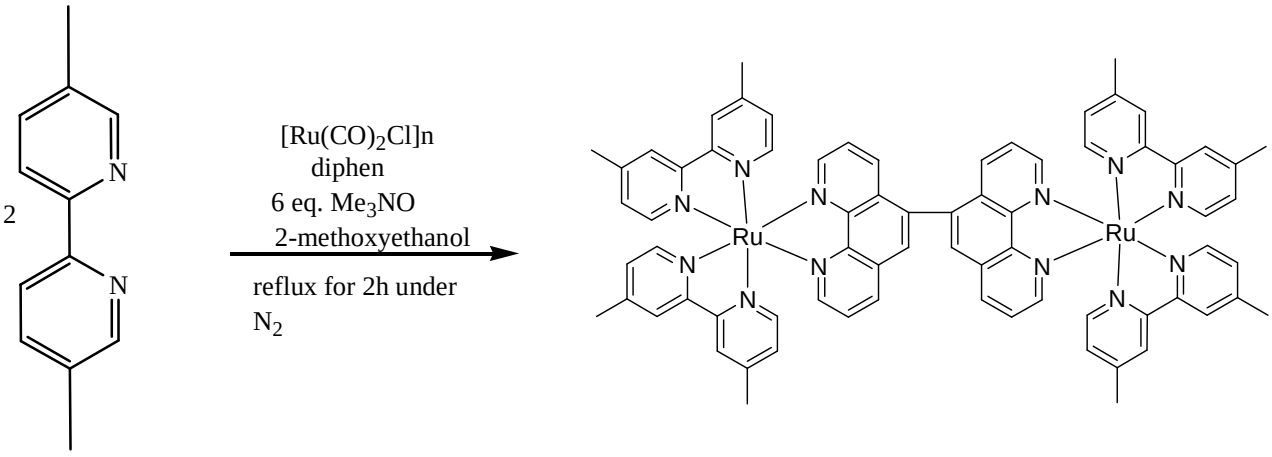

Scheme 3.3.1. Synthesis of $[(dmbpy)_2RudiphenRu(dmbpy)_2](PF_6)$

The product was characterized by electrospray mass spectroscopy and the spectrum is shown in Figure 3.3.1. Unfortunately, the spectrum is dominated by a parent peak at M/Z = 185. The peak, however, is not associated with the characteristic isotopic distribution of ruthenium and, therefore, is not significant in the investigations described in this dissertation. The expected peak for the dimeric product is evident at M/Z = 324.5. The calculated monoisotopic M/Z = 324.2. Mass spectrum also reveals an impurity containing ruthenium with a similar M/Z. In this case the impurity has been identified as a monomeric ruthenium complex with as yet to be determined structure.

Figure 3.3.1.ESI-MS spectra of $[Ru(dmbpy)_2diphen(dmbpy)_2Ru]^{4+}$

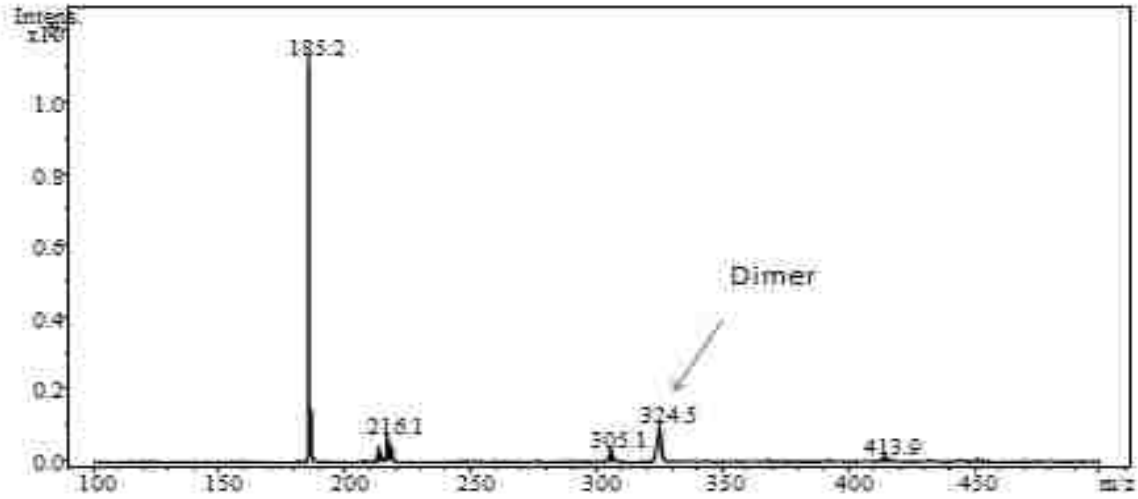
185.2
Dimer
216.1
305.1
324.5
413.9
m/z

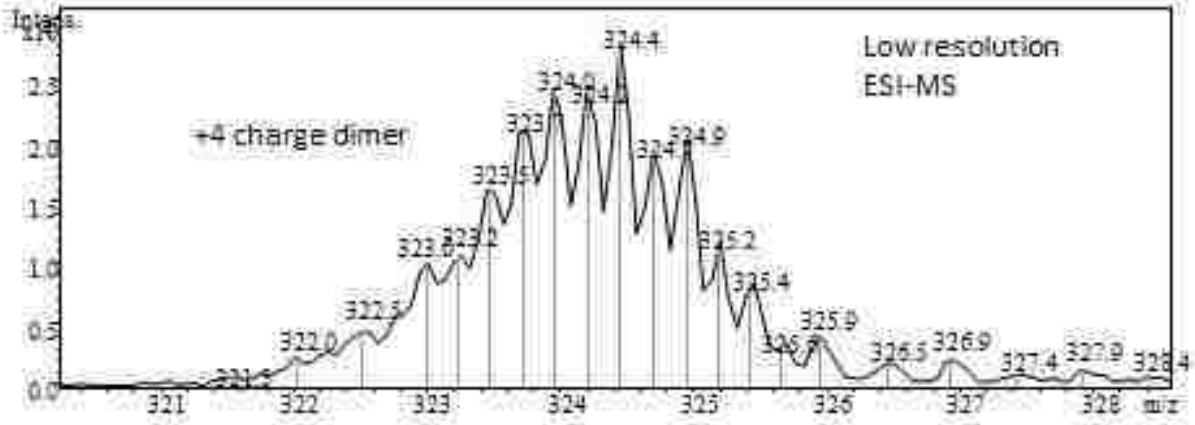
Low resolution
ESI-MS
+4 charge dimer
324.4
324.9
325.2
325.4
325.9
326.5
326.9
327.4
m/z

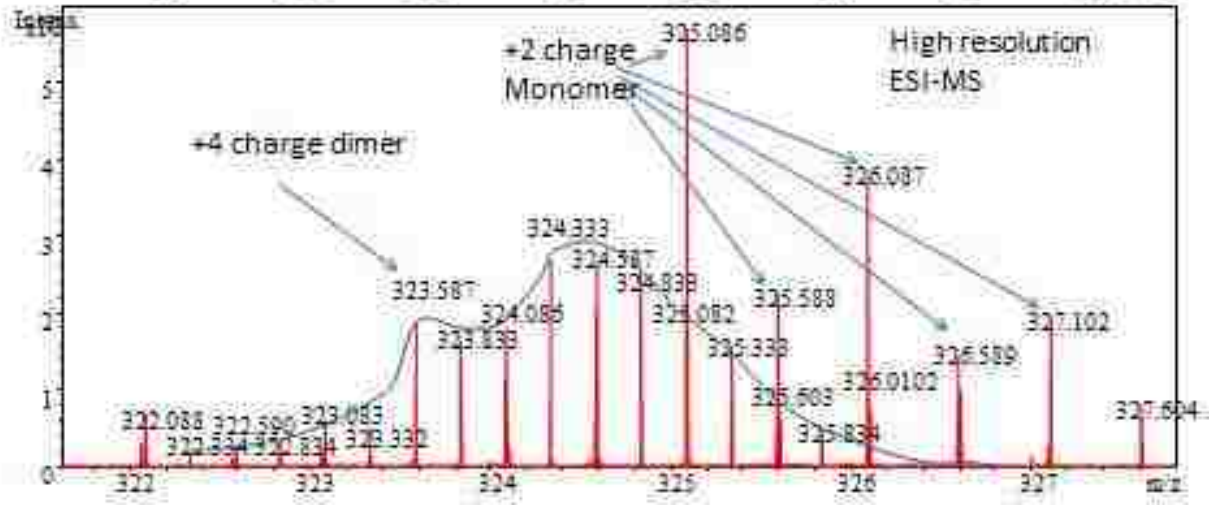
High resolution
ESI-MS
+2 charge
Monomer
+4 charge dimer
325.086
326.087
324.333
323.587
325.588
327.102
326.589
326.0102
327.604
m/z

3.4 Synthesis and Characterization of $[(bpy)_2\ RudiphenRu(dmbpy)_2](PF_6)_4$

The dinuclear ruthenium (II) complex, $[Ru(dmbpy)_2diphen(bpy)_2]^{4+}$ was synthesized a by combining the two monomeric complexes, $Ru(dmbpy)_2(CO)_2]^{2+}$ and $[Ru(bpy)_2diphen]^{2+}$, in a decarbonylation reaction.

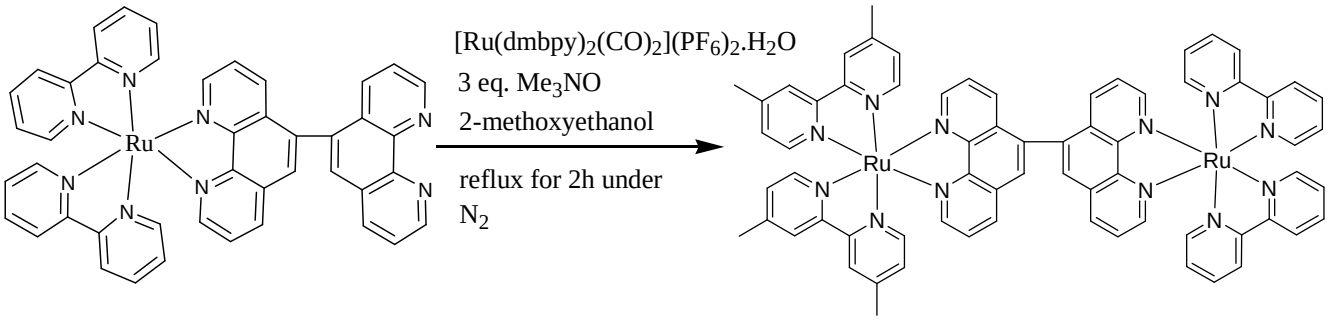

Scheme 3.4.1. Synthesis of $[(bpy)_2RudiphenRu(dmbpy)_2](PF_6)_4$

The final product of the synthesis was characterized by electrospray mass spectrometry. The spectrum is shown in Figure 3.4.1. The spectrum indicates the complex is contaminated with both symmetric dimers but does contain the desired product. This was a consistent result independent of the method of preparation. At the present time there is a question about the validity of the mass spectrometry in this application. Based on the fact that identical results were obtained with a variety of samples it is possible that scrambling of ligands is occurring in the mass spectrometer. Further research will be required to determine whether or not this is the case.

Figure 3.4.1. ESI-MS spectra of $[Ru(bpy)_2diphen(dmbpy)_2Ru]^{4+}$ in acetonitrile

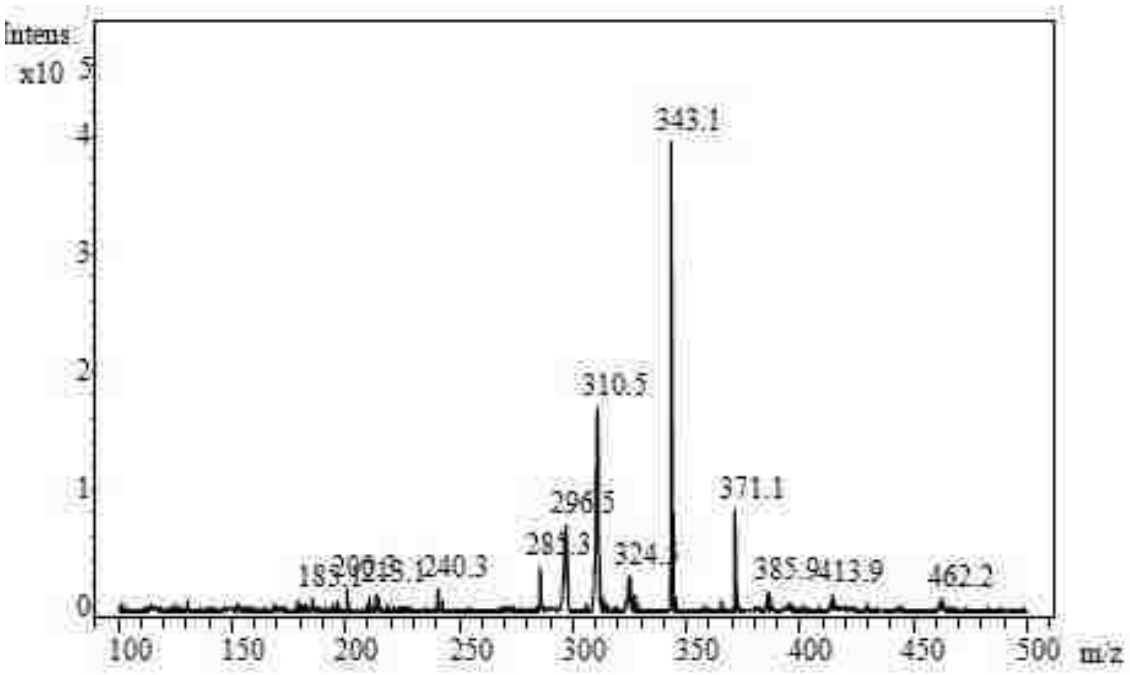
Intens.
x10 5
4
3
2
1
0
343.1
310.5
296.5
371.1
283.3
324.2
240.3
385.9
413.9
462.2
100
150
200
250
300
350
400
450
500
m/z

.

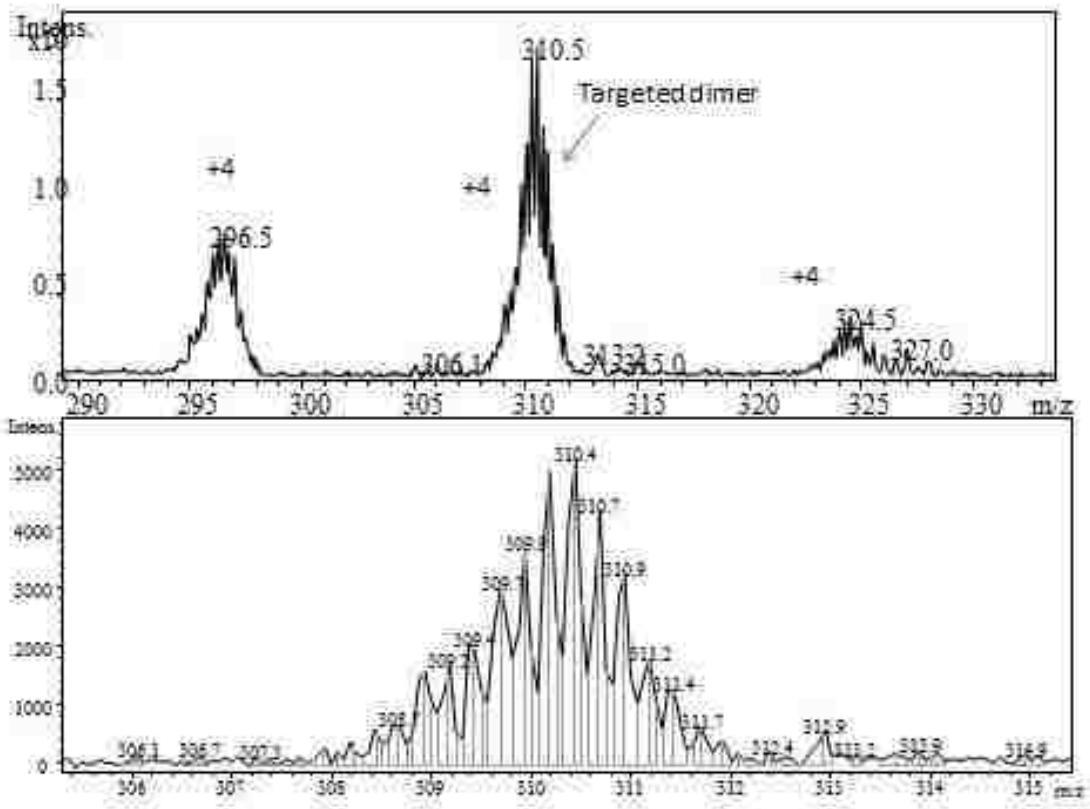
Intens.
1.5
1.0
0.5
0.0
310.5
Targeted dimer
+4
+4
+4
296.5
306.1
314.5
327.0
290
295
300
305
310
315
320
325
330
m/z
Intens.
5000
4000
3000
2000
1000
0
310.4
310.7
309.9
310.9
309.1
309.4
309.7
311.2
311.4
308.7
311.7
312.9
306.1
306.7
307.3
316.9
306
307
308
309
310
311
312
313
314
315
m/z

3.5. Intervalence Charge Transfer Studies of $[Ru(bpy)_2diphen(bpy)_2Ru]^{4+}$

Although difficult to observe, intervalence transfer bands are central to the theoretical treatments of electron transfer in covalently linked complexes. With this in mind, visible absorption spectra of $[Ru(bpy)_2diphen(bpy)_2Ru]^{4+}$ under the condition expected to produce an intervalence transfer band were recorded over the limits of the available instrumentation. In these experiments a strong oxidizing agent ceric ammonium nitrate ($(NH_4Ce(NO_3)_6$) was used to partially oxidize the dimer to the mixed valence state, i.e. Ru(II)-Ru(III). No new bands were observed as indicated by the spectra shown in Figure 3.5.1.

Figure 3.5.1. Titration of $[Ru(bpy)_2diphen(bpy)_2Ru]^{4+}$ with Ce(IV) ions in 0.5 M TFA acetonitrile solution.

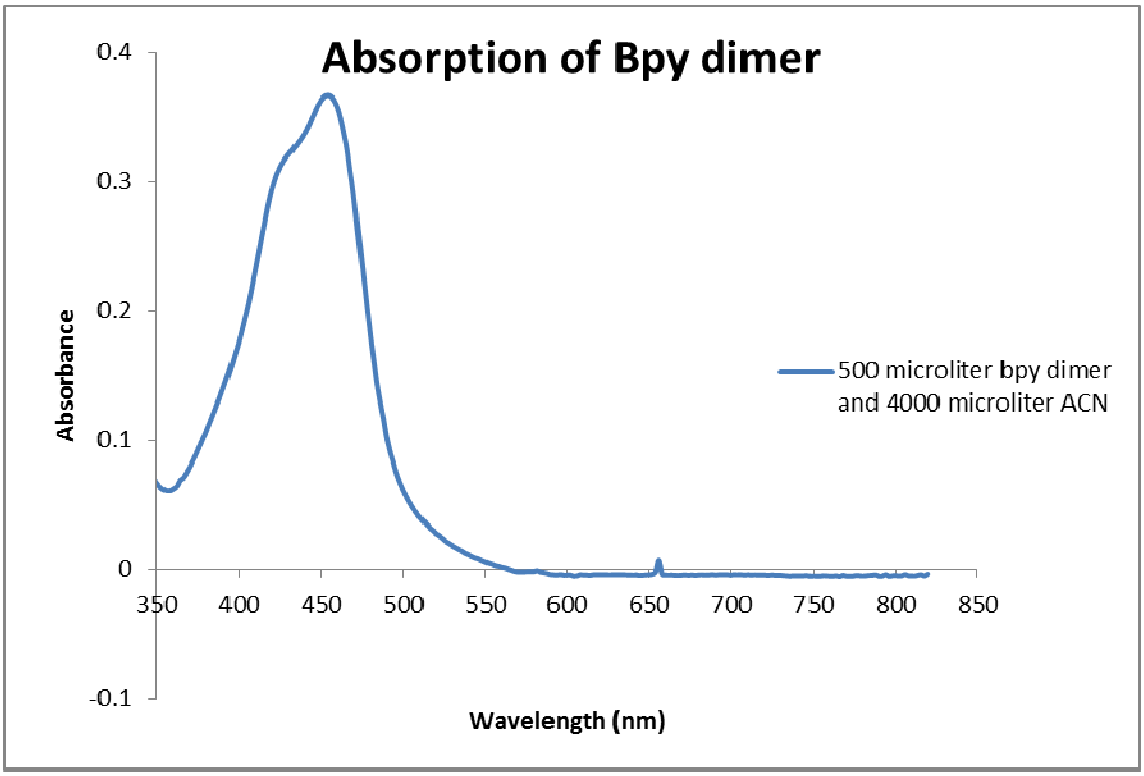
Absorption of Bpy dimer
Absorbance
Wavelength (nm)
0.4
0.3
0.2
0.1
0
-0.1
350
400
450
500
550
600
650
700
750
800
850
500 microliter bpy dimer and 4000 microliter ACN

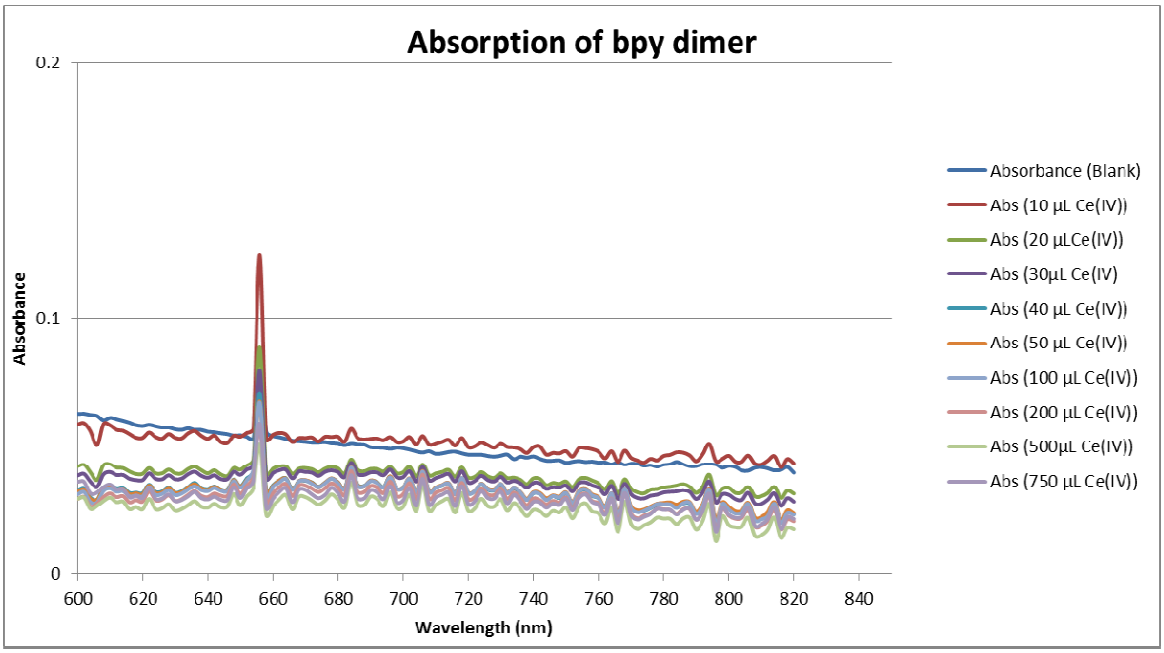
Absorption of bpy dimer
Absorbance
Wavelength (nm)
0.2
0.1
0
600
620
640
660
680
700
720
740
760
780
800
820
840
Absorbance (Blank)
Abs (10 µL Ce(IV))
Abs (20 µLCe(IV))
Abs (30µL Ce(IV)
Abs (40 µL Ce(IV))
Abs (50 µL Ce(IV))
Abs (100 µL Ce(IV))
Abs (200 µL Ce(IV))
Abs (500µL Ce(IV))
Abs (750 µL Ce(IV))

3.6 Fluorescence emission studies of Ru (II) Dimers and Monomers

Emission spectra of dinuclear and mononuclear complexes were recorded at 77 K in a frozen glass consisting of (v/v) (4:1) ratio of EtOH /MeOH. No attempt was made to exclude air. This experiment was done at low temperature in order to obtain sharper emission peaks with measurable differences in the maximum for the various complexes.

Table 3.6.1: Summary of the emission spectra maxima obtained with the indicated Ru(II) complexes at 77 K in ethanol/methanol glass excited at 450 nm.

Ru(II) complexes	Absorbance	λ_{max} emission (nm)
$[(bpy)_2RudiphenRu(bpy)_2]^{4+}$	0.20685	606
$[(dmbpy)_2RudiphenRu(dmbpy)_2]^{4+}$	0.20187	625
$[(bpy)_2RudiphenRu(dmbpy)_2]^{4+}$	0.20074	618
$[Ru(bpy)_2(Cl\text{-}phen)]^{2+}$	0.20576	612
$[Ru(dmbpy)_3]^{2+}$	0.20267	629
$[Ru(bpy)_3]^{2+}$	0.20432	609

Figure 3.6.1. Emission spectra of $[(bpy)_2RudiphenRu(bpy)_2]^{4+}$, $[(dmbpy)_2RudiphenRu(dmbpy)_2]^{4+}$ and $[(bpy)_2RudiphenRu(dmbpy)_2]^{4+}$ recorded at 77 K in ethanol/methanol frozen glass. The upper panel shows the three spectra. The lower panel shows a comparison of the spectrum of $[(bpy)_2RudiphenRu(dmbpy)_2]^{4+}$ with the sum of the spectra of $[(bpy)_2RudiphenRu(bpy)_2]^{4+}$, $[(dmbpy)_2RudiphenRu(dmbpy)_2]^{4+}$.

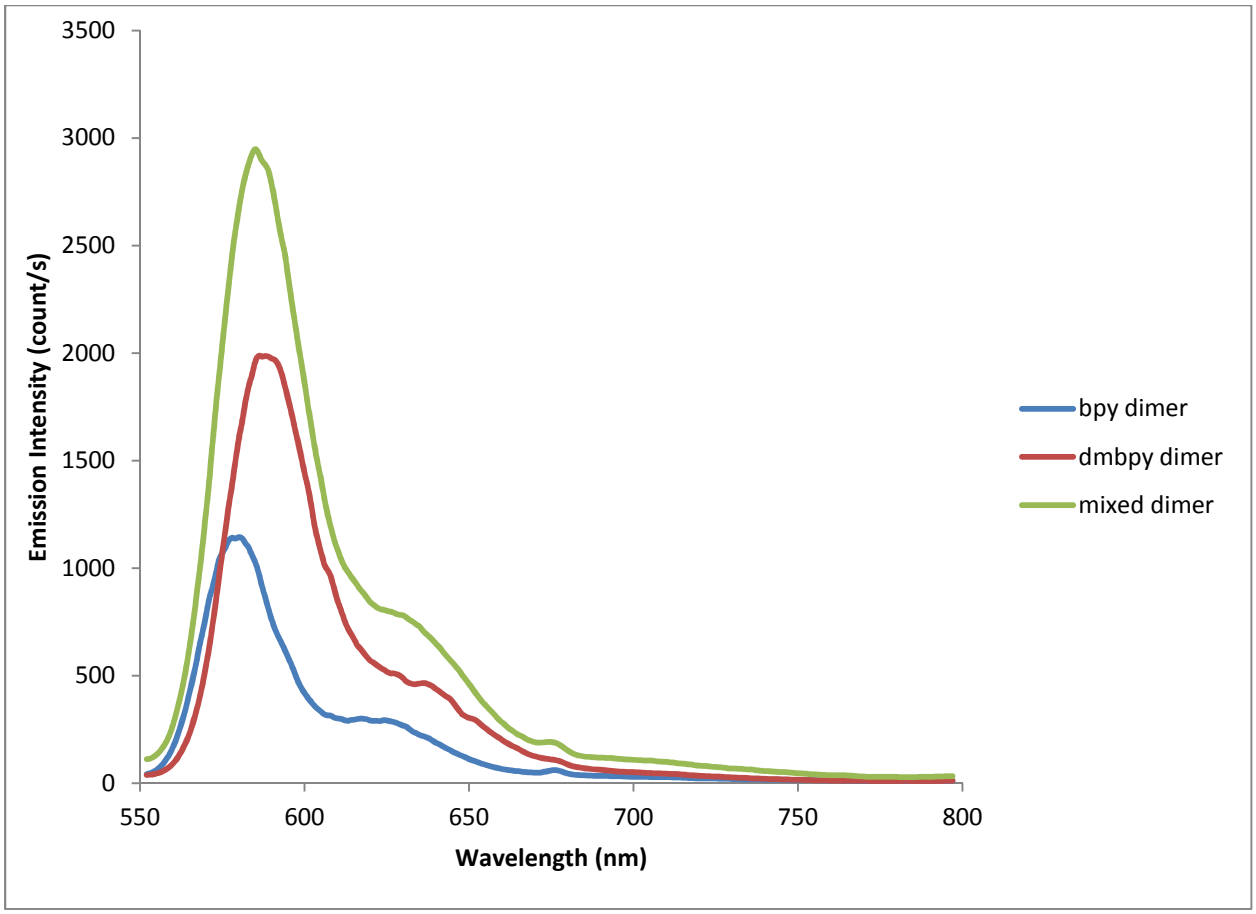
3500
3000
2500
2000
1500
1000
500
0
Emission Intensity (count/s)
550
600
650
700
750
800
Wavelength (nm)
bpy dimer
dmbpy dimer
mixed dimer

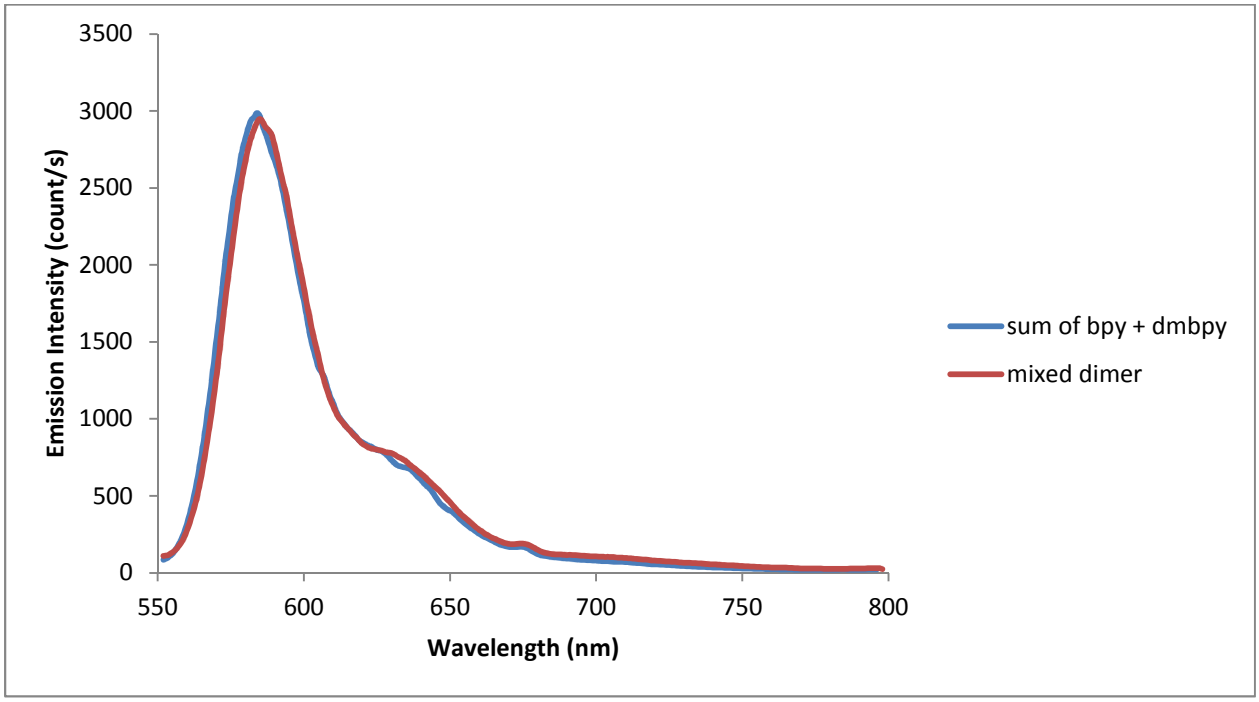
3500
3000
2500
2000
1500
1000
500
0
Emission Intensity (count/s)
550
600
650
700
750
800
Wavelength (nm)
sum of bpy + dmbpy
mixed dimer

The emission spectra recorded at 77 K all show the expected major peak and low energy shoulder normally associated with $Ru(bpy)_3^{2+}$. In these cases the emitting state is the long-lived triplet state and the shoulder has been assigned as vibrational component of that state. It is important to note that the dimeric complexes have emission spectra which are very similar to the monomeric complexes. The only difference are maxima.

The lower panel of Figure 3.5.2 shows a comparison of the spectrum of $[(bpy)_2RudiphenRu(dmbpy)_2]^{4+}$ with the sum of the spectra $[(bpy)_2RudiphenRu(bpy)_2]^{4+}$ and $[(dmbpy)_2RudiphenRu(dmbpy)_2]^{4+}$. The summation spectra were created using Excel and a 1:1 ratio of the two emission spectra. The results of the summation are nearly superimposable with the spectrum of the mixed dimer suggesting that the individual ruthenium centers emit independently at 77 K.

Figure 3.6.2 Emission spectra of $[(bpy)_2RudiphenRu(bpy)_2]^{4+}$,

$[(dmbpy)_2RudiphenRu(dmbpy)_2]^{4+}$,$[(bpy)_2RudiphenRu(dmbpy)_2]^{4+}$,$[Ru(bpy)_3]^{2+}$and

$[Ru(dmbpy)_3]^{2+}$ in air saturated acetonitrile at 22 ^{o}C.

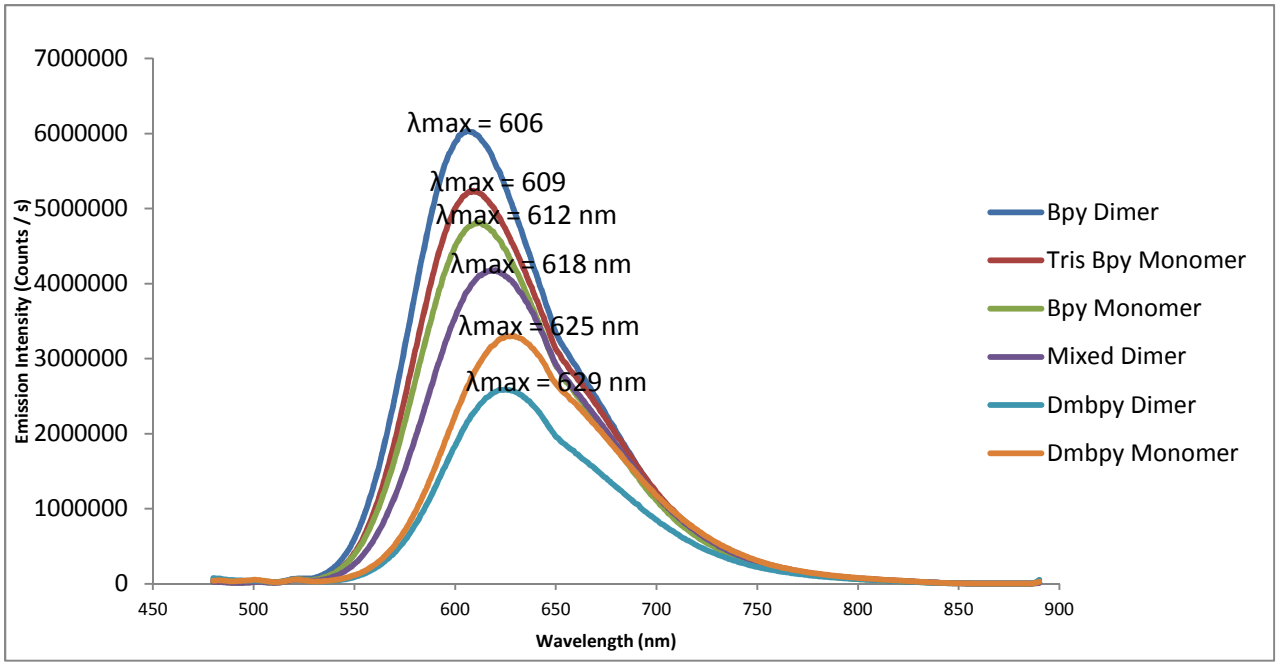
7000000
6000000
5000000
4000000
3000000
2000000
1000000
0
Emission Intensity (Counts / s)
450
500
550
600
650
700
750
800
850
900
Wavelength (nm)
λmax = 606
λmax = 609
λmax = 612 nm
λmax = 618 nm
λmax = 625 nm
λmax = 629 nm
Bpy Dimer
Tris Bpy Monomer
Bpy Monomer
Mixed Dimer
Dmbpy Dimer
Dmbpy Monomer

As expected the room temperature spectra of the various ruthenium(II) complexes are significantly broader at higher temperatures and the vibration-related shoulder is just barely visible. The maxima are clearly defined and show that the mixed dimer emits at a wavelength midway between the two symmetric dimers in keeping with the low temperature observations. The emission spectra are consistent with the excited state picture currently accepted for $Ru(bpy)_3^{2+}$ and show no indication of a deviation from the behavior of the monomeric complexes, i.e., the ruthenium centers in the dimeric complexes appear to behave as monomeric units.

3.7 Excited-State Lifetime Measurements

The excited-state lifetimes of the following ruthenium (II) complexes $Ru(bpy)_2diphen(bpy)_2Ru]^{4+}$,$[Ru(bpy)_2diphen(dmbpy)_2Ru]^{4+}$,$[Ru(bpy)_2diphen(dmbpy)_2Ru]^{4+}$, $[Ru(bpy)_2(Cl\text{-}phen)]^{2+}$ and $[Ru(dmbpy)_2(Cl\text{-}phen)]^{2+}$ were determined in air saturated acetonitrile solutions. The results show a striking similarity in the excited state lifetimes and provide no indication of additional decay pathways for the triplet excited state of the individual ruthenium centers.

A more detailed temperature dependence of the $[(bpy)_2RudiphenRu(bpy)_2]^{4+}$ was also performed. In this case the samples were dissolved in acetonitrile, freeze-thaw-pump degassed and sealed in glass tubes. The observed rate constants were plotted as a function of temperature in an Arhenius plot and fitted to the equation discussed in chapter 1.

$$k_{obs} = k_{nr} + k_r + A\exp(\Delta E/RT)$$

This equation was previously reported by Allsopp et al and used to describe the temperature dependence of the excited state lifetime of $[Ru(bpy)_3]^{2+}$ in acetonitrile. The manual fitting procedure provided the value of three parameters, $k_{nr} + k_r = 6.0 \times 10^5$, $A = 4.0 \times 10^{14}$ and ΔE = 50100 kJ/mol with $[(bpy)_2RudiphenRu(bpy)_2]^{4+}$. Allsopp et al reported 6.3×10^5, 3.9×10^{14} and 50300 kJ/mol, respectively for $[Ru(bpy)_3]^{2+}$.

Table 3.7.1: Excited State Lifetimes for the indicated Ru(II) complexes in air saturated acetonitrile solutions at 22 ^oC.

Ru(II) complexes	First-Order Rate Constant	Lifetime (1/k), nsec
$[(bpy)_2RudiphenRu(bpy)_2]^{4+}$	7.45×10^6	134
$[(dmbpy)_2RudiphenRu(dmbpy)_2]^{4+}$	8.43×10^6	118
$[(bpy)_2RudiphenRu(dmbpy)_2]^{4+}$	7.95×10^6	125
$[Ru(bpy)_2(Cl\text{-}phen)]^{2+}$	7.16×10^6	139
$[Ru(dmbpy)_2(Cl\text{-}phen)]^{2+}$	7.75×10^6	129

Figure 3.7.1. Transient Emission decay plots obtained with $Ru(bpy)_2diphen(bpy)_2Ru]^{4+}$, $[Ru(bpy)_2diphen(dmbpy)_2Ru]^{4+}$,$[Ru(bpy)_2diphen(dmbpy)_2Ru]^{4+}$,$[Ru(bpy)_2(Cl\text{-}phen)]^{2+}$, $[Ru(dmbpy)_2(Cl\text{-}phen)]^{2+}$ and $[Ru(bpy)_3]^{2+}$ in air saturated acetonitrile solutions.

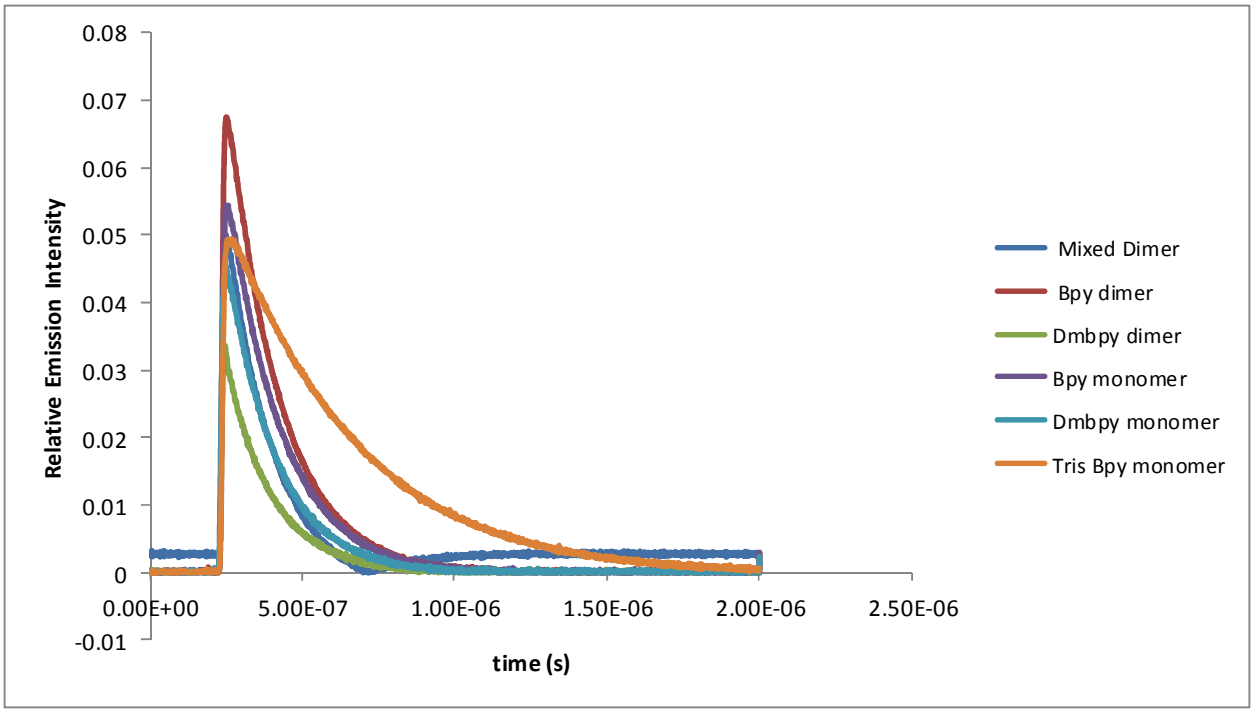
0.08
0.07
0.06
0.05
0.04
0.03
0.02
0.01
0
-0.01
Relative Emission Intensity
0.00E+00
5.00E-07
1.00E-06
1.50E-06
2.00E-06
2.50E-06
time (s)
Mixed Dimer
Bpy dimer
Dmbpy dimer
Bpy monomer
Dmbpy monomer
Tris Bpy monomer

Figure 3.7.2. The temperature dependence of the emission decay rate constants of $Ru(bpy)_2diphen(bpy)_2Ru]^{4+}$ in acetonitrile (♦). Solid line is the theoretical fit based on the equation $k_{obs} = k_{nr} + k_r + Aexp(\Delta E/RT)$ where $k_{nr} + k_r = 6.0 \times 10^5\ sec^{-1}$, $A = 4.0 \times 10^{14}\ sec^{-1}$ and $\Delta E = 50100$ kJ/mol.

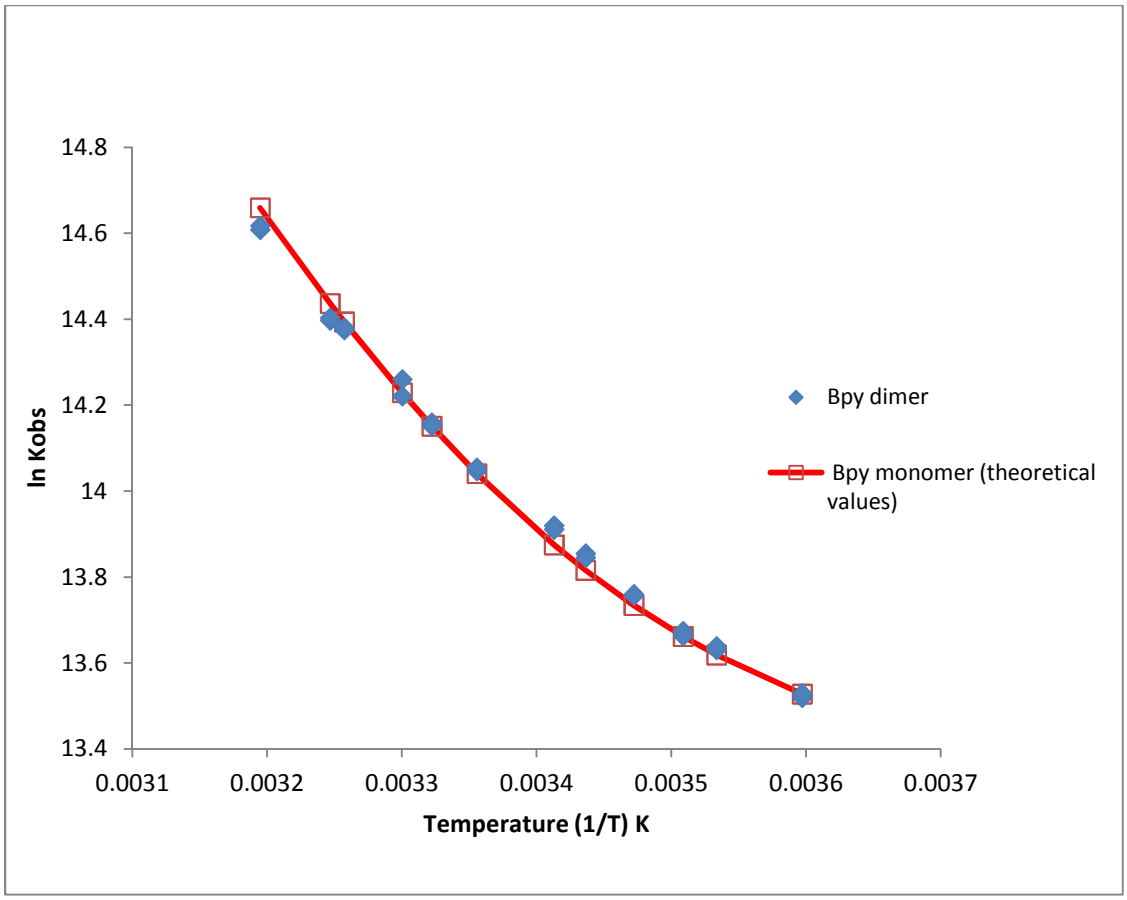
14.8
14.6
14.4
14.2
14
13.8
13.6
13.4
ln Kobs
0.0031
0.0032
0.0033
0.0034
0.0035
0.0036
0.0037
Temperature (1/T) K
Bpy dimer
Bpy monomer (theoretical values)

3.8 Electrochemical Studies

The electrochemistry of ruthenium(II) polypyridine systems have been studied extensively and have been shown to be very well behaved. For example, one electron oxidations of most complexes generally show reversible cyclic voltammetry at a platinum disk electrode. Electrochemical investigation of the dimeric complexes was expected to reveal evidence of interaction between the metal centers if such interaction was sufficiently strong. The theoretical behavior of multicomponent systems has been addressed previous and is well developed. Bard and Faulkner for example describe the expectations for various levels of interaction.

Application of the theory requires high quality electrochemical data with care taken to develop well defined controls. One particular problem frequently encounter is leakage of chloride ion into the electrochemical cell from reference electrode. This produces an artifact at approximately 1.1 volts and interfers significantly with the interpretation of the data since the ruthenium complexes are oxidized at a similar potential. In order to avoid this complication a Pt wire pseudo reference calibrated against ferrocene was employed as needed. Figure 3.8.1 shows the cyclic voltammogram of ferrocene with a Pt wire as the reference. The pseudoreference is more than adequate for investigations of the scan rate dependence and to a lesser extent the concentration dependence because the absolute potential is not critical to the analysis. If an accurate measure of the potential was required ferrocene was added to the solution as shown in for example figure 3.8.3.

Cyclic voltammetry of $[Ru(bpy)_2(Cl\text{-}phen)]^{2+}$ shows a single reversible wave with $E^{0'}$ = 0.83 V vs ferrocene or 0.128 V vs NHE and is illustrated in figure 3.8.4. The potential is independent of

scan rate and concentration as indicated in figures 3.8.5 and 3.8.6. The peak current is expected to depend on the concentration and scan rate as indicated by the Randles –Sevcik equation:

$$I_p = \left(2.69 \times 10^5\right) n^{3/2} A D^{1/2} C v^{1/2}$$

where I_p = peak current, n = number of electrons transferred in the redox event , A = electrode area in cm^2, D =diffusion coefficient in cm^2/s, C = Concentration in mol / cm^3 and v = scan rate V/s.

A plot of peak current I_p versus the square root of the scan rate shows a linear dependence with $R^2 = 0.997$ and a slope of 1.02×10^{-5}. In this experiment the electrode area was 0.02 cm^2, $n = 1$ and $C = 2.4 \times 10^{-6}$ mol/cm^3. The calculated diffusion coefficient was 6×10^{-7} cm^2/sec. Analogous measurements, not shown, with [Ru(bpy)3]2+ revealed a comparable value for the diffusion coefficient of 7.8×10^{-7} cm^2/sec.

Figure 3.8.4 shows the effect of concentration on the peak potentials of $[Ru(bpy)_2Cl\text{-}phen]^{2+}$. There appears to be a small dependence on concentration but this may be an artifact of using the pseudo reference electrode. Figure 3.8.5 shows the cyclic voltammogram of $[Ru(bpy)_2Cl\text{-}phen]^{2+}$ at potentials that expected to show reductions of ths ligands. The voltammogram reveals four electrochemical events at -1.2932 V, -1.668 V, -1.929 V and -2.23 V. The first three probably correspond to the success one electron reductions of the ligands. The last is most likely an artifact associate with an impurity in the supporting solvent. The observation of the reductions at these potentials is consistent with previously published results obtained with other polypyridine complexes.

Figure 3.8.6 shows the scan rate dependence of $[Ru(dmbpy)_2Clphen]^{2+}$. A plot of peal current versus the square root of the scan rate revealed a linear dependence as expected with a slot comparable to that obtained with $[Ru(bpy)_2Cl\text{-}phen]^{2+}$. Figure 3.8.7 shows the concentration dependence which reveals considerable scatter in the peak potentials with no obvious relation between concentration and peak current.

Figure 3.8.8 shows the cyclic voltammogram of $[Ru(bpy)_2diphen(bpy)_2Ru]^{4+}$ with ferrocene added as an internal standard. The peak potential for the oxidation/reduction of the dimer is 1.30 versus SCE under the conditions of the experiment. The scan rate dependence is illustrated in Figure 3.8.9. The slope of the plot of peak current versus the square root of the scan rate is 1×10^{-5} and the calculated diffusion constant is approximately 2×10^{-7} cm^2/sec. Figure 3.8.10 shows the concentration dependence of the peak potential and peak current. The data is similar to that shown in Figure 3.8.7 and may reflect difficulties with the use of a Pt wire reference electrode is this type of investigation. Unfortunately the data does not show trend and further investigation will be required.

Figure 3.8.11 shows the cyclic voltammogram of $[Ru(dmbpy)_2diphen(dmbpy)_2Ru]^{4+}$. The peak potentialfor the oxidation/reduction of the dimer is 1.190 versus SCE. The reduction in the peak potential is consistent with the presence of the methyl substitutients and has been previous reported.

Figure 3.8.13 shows the cyclic voltammogram of $[Ru(bpy)_2diphen(dmbpy)_2Ru]^{4+}$. The voltammogram clearly shows evidence of two electrochemical process. The peak potentials are substantially less oxidizing than expected for the mixed dimer composed. The scan rate

dependence shown in Figure 3.8.14 is similar to that observed with symmetric dimer in Figure 3.8.8. The ligand reductions are also similar to those found in the monomeric complexes.

Figure 3.8.1. Cyclic Voltammogram of Ferrocene vs platinum wire in acetonitrile.

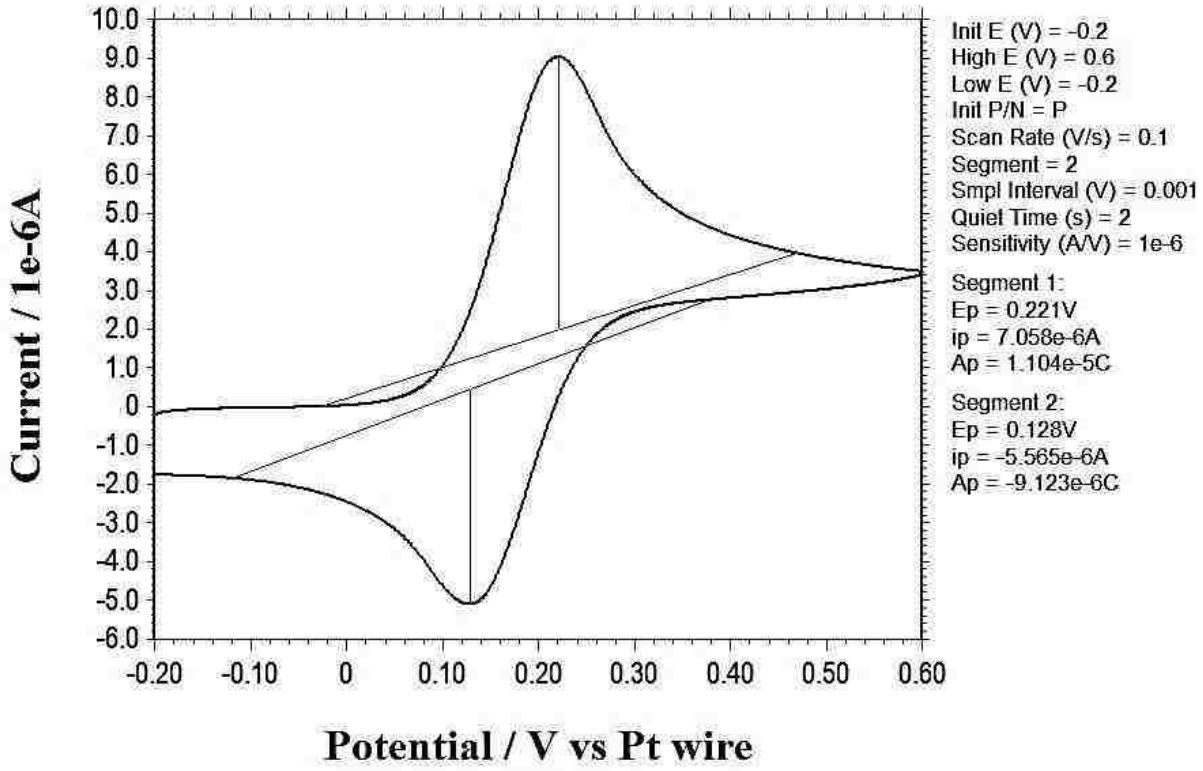
Current / 1e-6A
Potential / V vs Pt wire
Init E (V) = -0.2
High E (V) = 0.6
Low E (V) = -0.2
Init P/N = P
Scan Rate (V/s) = 0.1
Segment = 2
Smpl Interval (V) = 0.001
Quiet Time (s) = 2
Sensitivity (A/V) = 1e-6
Segment 1:
Ep = 0.221V
ip = 7.058e-6A
Ap = 1.104e-5C
Segment 2:
Ep = 0.128V
ip = -5.565e-6A
Ap = -9.123e-6C

V)

Figure 3.8.2. Cyclic Voltammogram of $[Ru(bpy)_2Cl\text{-}phen]^{2+}$ in acetonitrile.

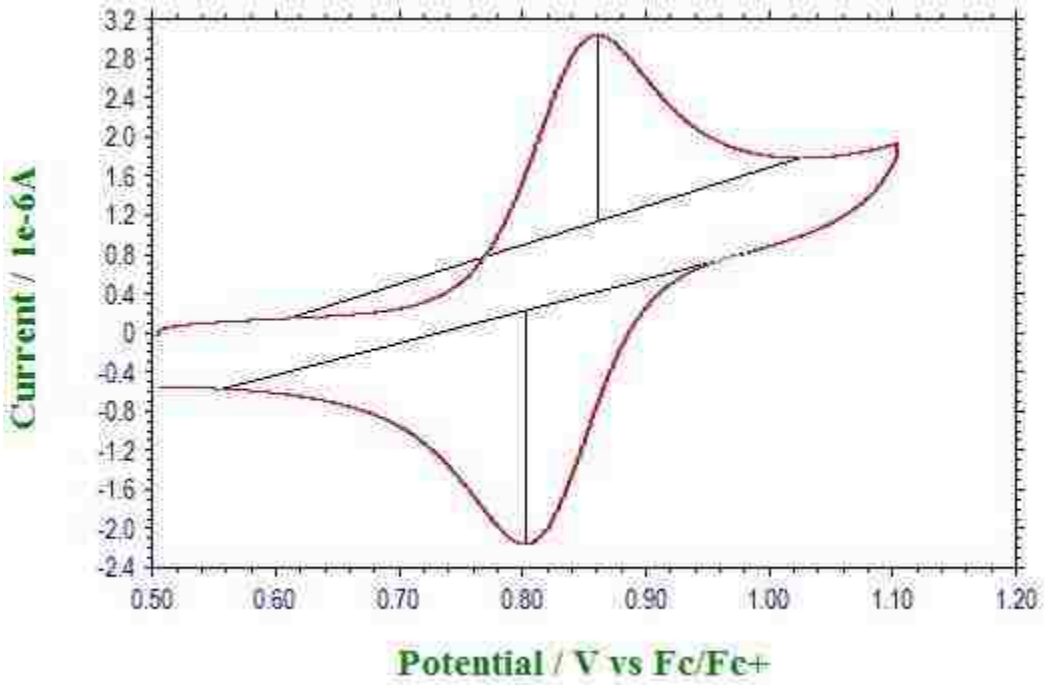
Current / 1e-6A
3.2
2.8
2.4
2.0
1.6
1.2
0.8
0.4
0
-0.4
-0.8
-1.2
-1.6
-2.0
-2.4
0.50
0.60
0.70
0.80
0.90
1.00
1.10
1.20
Potential / V vs Fc/Fc+

Figure 3.8.3. Cyclic voltammetric scan rate dependence of $[Ru(bpy)_2Cl\text{-}phen]^{2+}$ in acetonitrile.

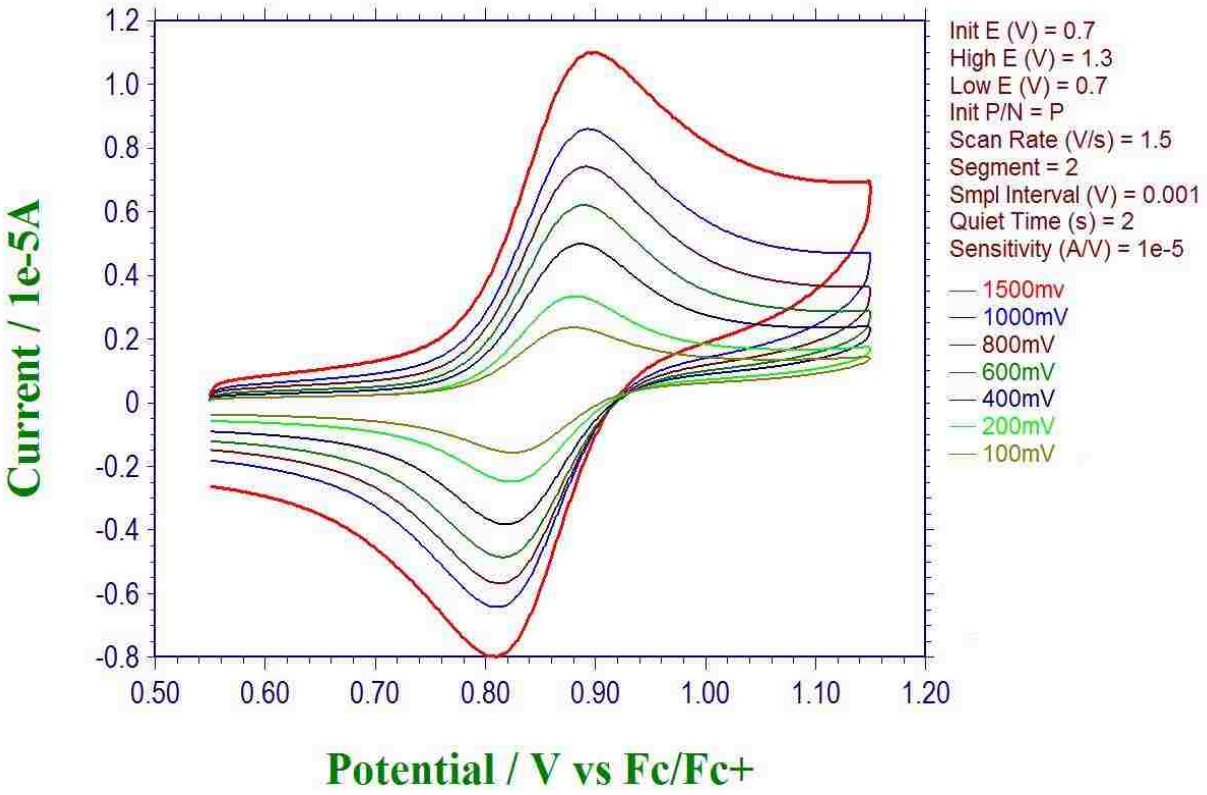
Current / 1e-5A
Potential / V vs Fc/Fc+
Init E (V) = 0.7
High E (V) = 1.3
Low E (V) = 0.7
Init P/N = P
Scan Rate (V/s) = 1.5
Segment = 2
Smpl Interval (V) = 0.001
Quiet Time (s) = 2
Sensitivity (A/V) = 1e-5
1500mv
1000mV
800mV
600mV
400mV
200mV
100mV
1.2
1.0
0.8
0.6
0.4
0.2
0
-0.2
-0.4
-0.6
-0.8
0.50
0.60
0.70
0.80
0.90
1.00
1.10
1.20

Figure 3.8.4. Cyclic voltammetric concentration studies of $[Ru(bpy)_2Cl\text{-}phen]^{2+}$ in acetonitrile.

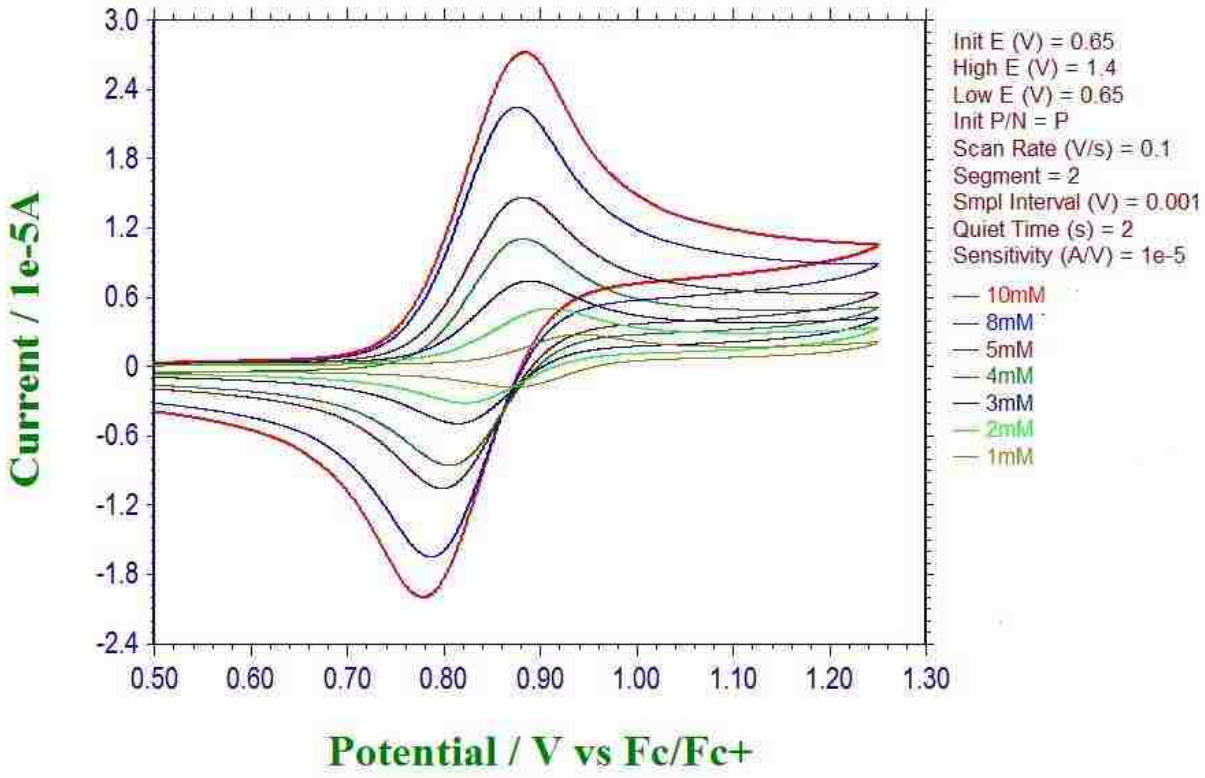
Current / 1e-5A
Potential / V vs Fc/Fc+
3.0
2.4
1.8
1.2
0.6
0
-0.6
-1.2
-1.8
-2.4
0.50
0.60
0.70
0.80
0.90
1.00
1.10
1.20
1.30
Init E (V) = 0.65
High E (V) = 1.4
Low E (V) = 0.65
Init P/N = P
Scan Rate (V/s) = 0.1
Segment = 2
Smpl Interval (V) = 0.001
Quiet Time (s) = 2
Sensitivity (A/V) = 1e-5
10mM
8mM
5mM
4mM
3mM
2mM
1mM

Figure 3.8.5. Cyclic voltammetry of $[Ru(bpy)_2Cl\text{-}phen]^{2+}$ in acetonitrile showing ligand reductions.

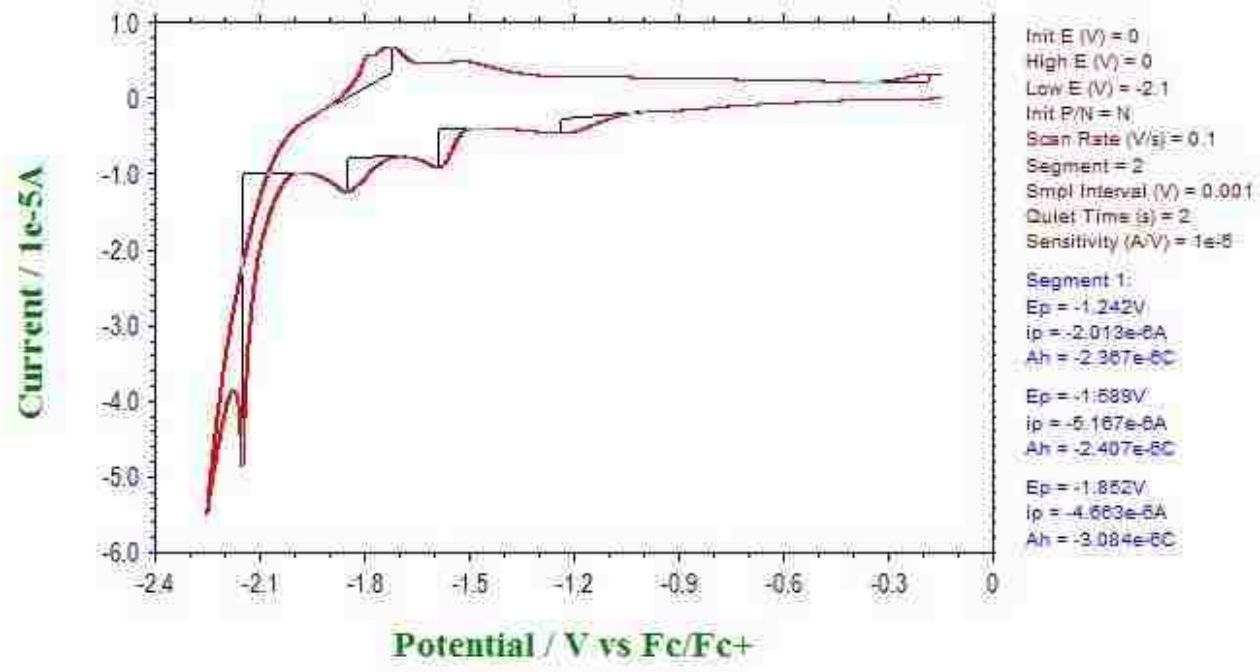
Current / 1e-5A
Potential / V vs Fc/Fc+
1.0
0
-1.0
-2.0
-3.0
-4.0
-5.0
-6.0
-2.4
-2.1
-1.8
-1.5
-1.2
-0.9
-0.6
-0.3
0
Init E (V) = 0
High E (V) = 0
Low E (V) = -2.1
Init P/N = N
Scan Rate (V/s) = 0.1
Segment = 2
Smpl Interval (V) = 0.001
Quiet Time (s) = 2
Sensitivity (A/V) = 1e-5
Segment 1:
Ep = -1.242V
ip = -2.013e-6A
Ah = -2.367e-6C
Ep = -1.589V
ip = -5.167e-6A
Ah = -2.407e-6C
Ep = -1.852V
ip = -4.663e-6A
Ah = -3.084e-6C

Figure 3.8.6. Cyclic voltammetric scan rate dependence of $[Ru(dmbpy)_2Cl\text{-}phen]^{2+}$ in acetonitrile.

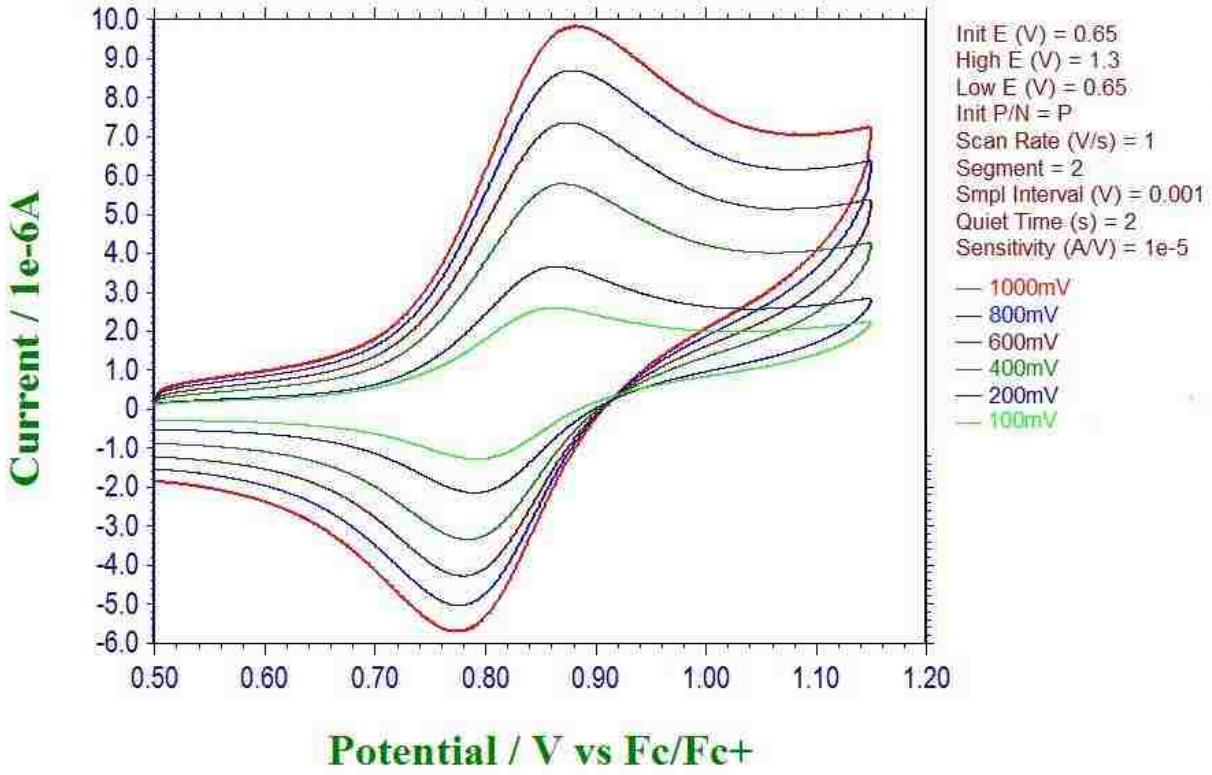
Current / 1e-6A
10.0
9.0
8.0
7.0
6.0
5.0
4.0
3.0
2.0
1.0
0
-1.0
-2.0
-3.0
-4.0
-5.0
-6.0
0.50
0.60
0.70
0.80
0.90
1.00
1.10
1.20
Potential / V vs Fc/Fc+
Init E (V) = 0.65
High E (V) = 1.3
Low E (V) = 0.65
Init P/N = P
Scan Rate (V/s) = 1
Segment = 2
Smpl Interval (V) = 0.001
Quiet Time (s) = 2
Sensitivity (A/V) = 1e-5
1000mV
800mV
600mV
400mV
200mV
100mV

Figure 3.8.7. Cyclic voltammetric concentration studies of $[Ru(dmbpy)_2Cl\text{-}phen]^{2+}$ in acetonitrile.

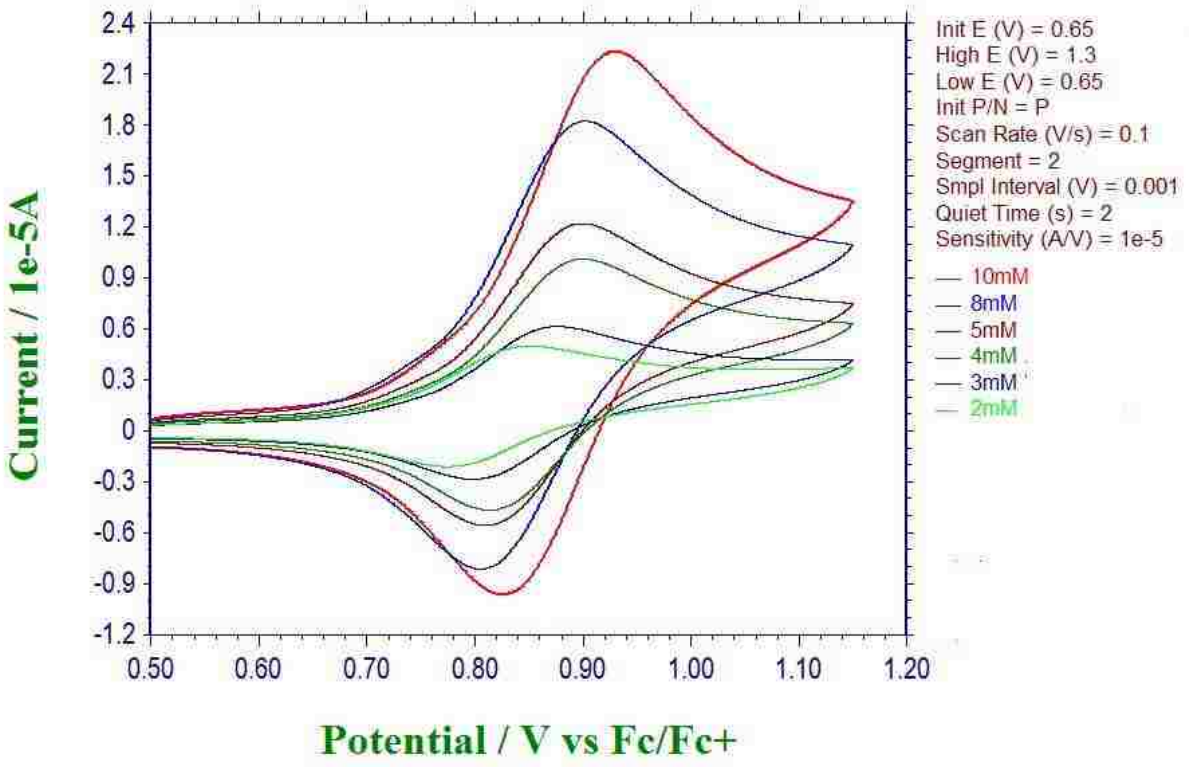
Current / 1e-5A
2.4
2.1
1.8
1.5
1.2
0.9
0.6
0.3
0
-0.3
-0.6
-0.9
-1.2
0.50
0.60
0.70
0.80
0.90
1.00
1.10
1.20
Potential / V vs Fc/Fc+
Init E (V) = 0.65
High E (V) = 1.3
Low E (V) = 0.65
Init P/N = P
Scan Rate (V/s) = 0.1
Segment = 2
Smpl Interval (V) = 0.001
Quiet Time (s) = 2
Sensitivity (A/V) = 1e-5
10mM
8mM
5mM
4mM
3mM
2mM

Figure 3.8.8. Cyclic voltammogram of $[Ru(bpy)_2diphen(bpy)_2Ru]^{4+}$ in acetonitrile.

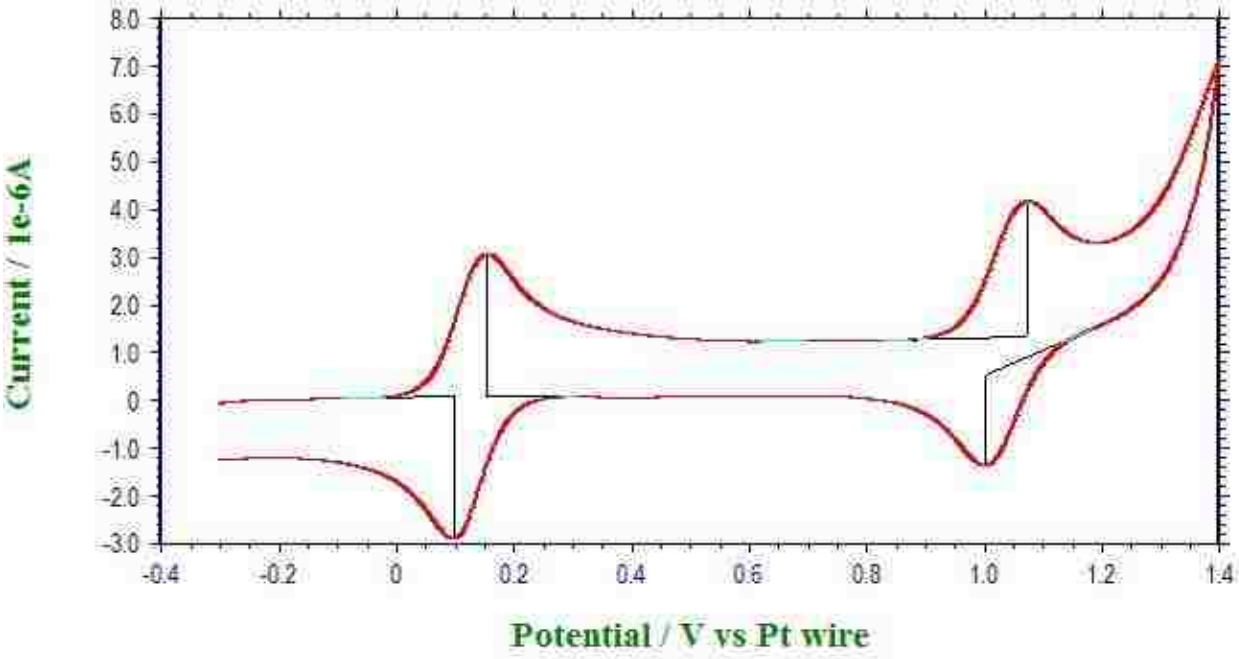
Current / 1e-6A
8.0
7.0
6.0
5.0
4.0
3.0
2.0
1.0
0
-1.0
-2.0
-3.0
-0.4
-0.2
0
0.2
0.4
0.6
0.8
1.0
1.2
1.4
Potential / V vs Pt wire

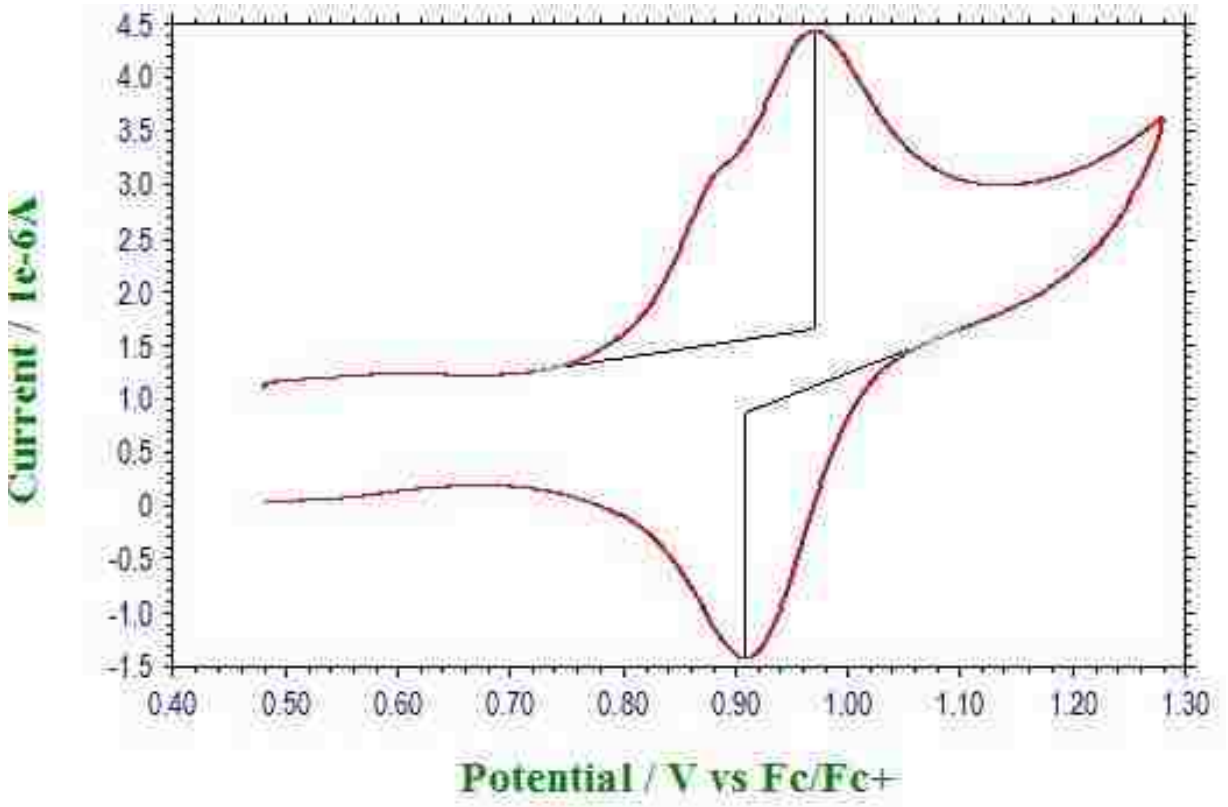
Current / 1e-6A
4.5
4.0
3.5
3.0
2.5
2.0
1.5
1.0
0.5
0
-0.5
-1.0
-1.5
0.40
0.50
0.60
0.70
0.80
0.90
1.00
1.10
1.20
1.30
Potential / V vs Fc/Fc+

Figure 3.8.9. Cyclic voltammetric scan rate studies of $[Ru(bpy)_2diphen(bpy)_2Ru]^{4+}$ in acetonitrile.

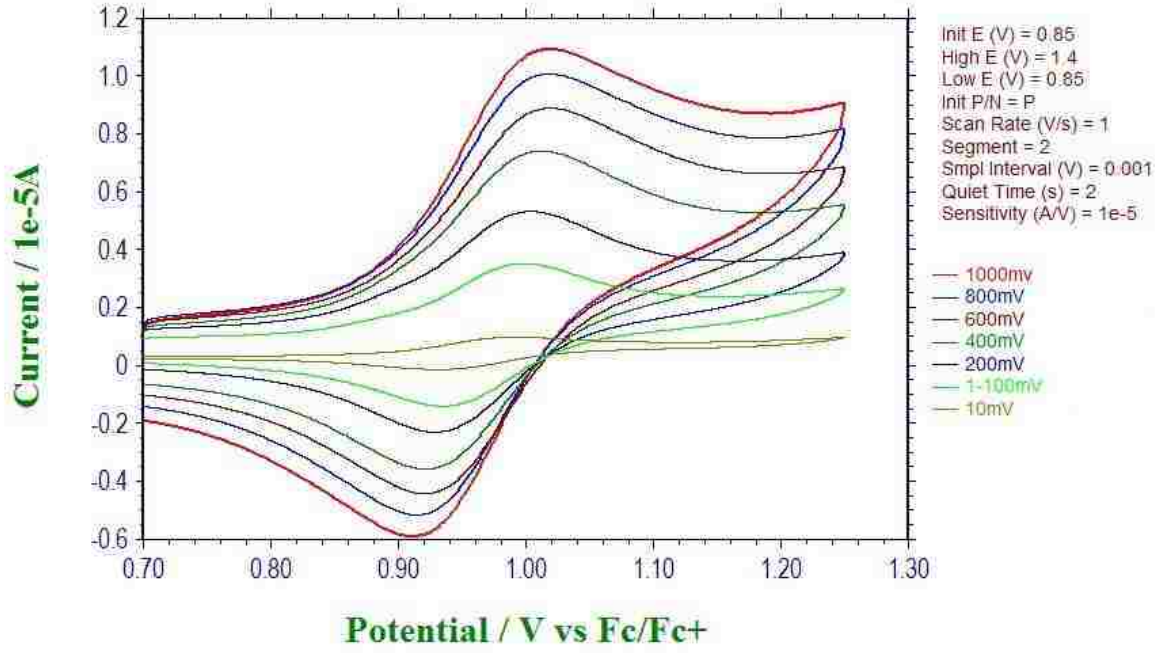
Current / 1e-5A
Potential / V vs Fc/Fc+
Init E (V) = 0.85
High E (V) = 1.4
Low E (V) = 0.85
Init P/N = P
Scan Rate (V/s) = 1
Segment = 2
Smpl Interval (V) = 0.001
Quiet Time (s) = 2
Sensitivity (A/V) = 1e-5
1000mv
800mV
600mV
400mV
200mV
1-100mV
10mV

Figure 3.8.10. Cyclic voltammetric concentration studies of $[Ru(bpy)_2diphen(bpy)_2Ru]^{4+}$ in acetonitrile.

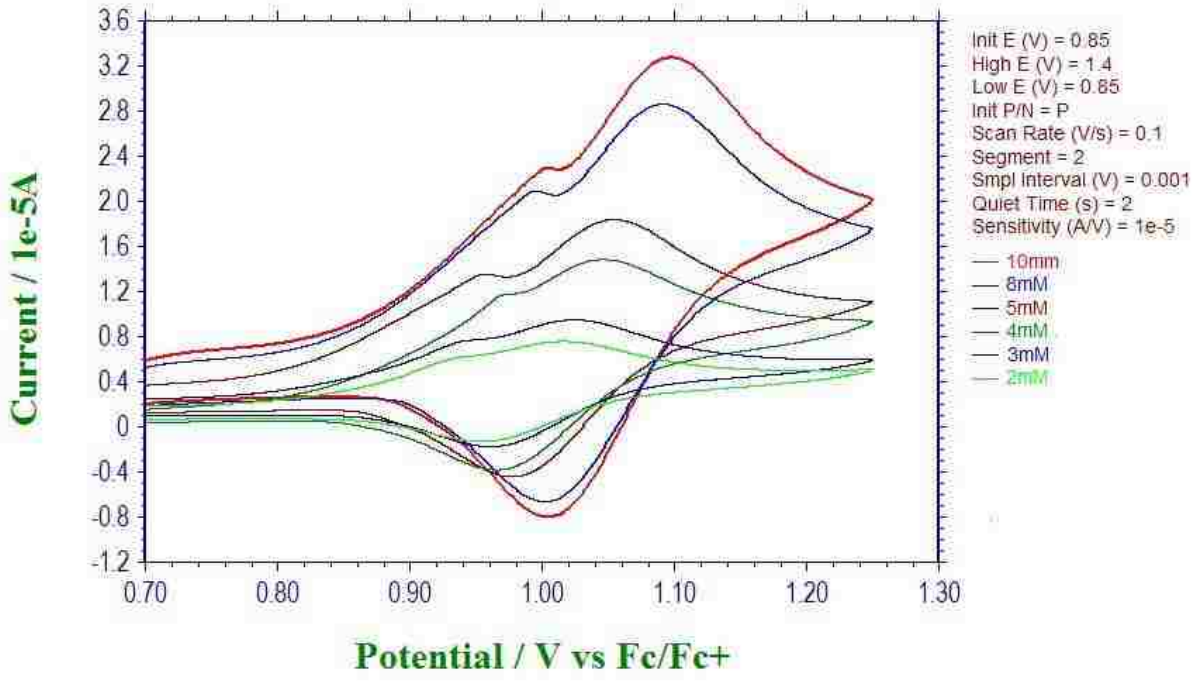
Current / 1e-5A
3.6
3.2
2.8
2.4
2.0
1.6
1.2
0.8
0.4
0
-0.4
-0.8
-1.2
0.70
0.80
0.90
1.00
1.10
1.20
1.30
Potential / V vs Fc/Fc+
Init E (V) = 0.85
High E (V) = 1.4
Low E (V) = 0.85
Init P/N = P
Scan Rate (V/s) = 0.1
Segment = 2
Smpl Interval (V) = 0.001
Quiet Time (s) = 2
Sensitivity (A/V) = 1e-5
10mm
8mM
5mM
4mM
3mM
2mM

Figure 3.8.11. Cyclic voltammogram of $[(bpy)_2RudiphenRu(bpy)_2]^{4+}$ and $[Ru(bpy)_2diphen]^{2+}$ showing ligand reductions

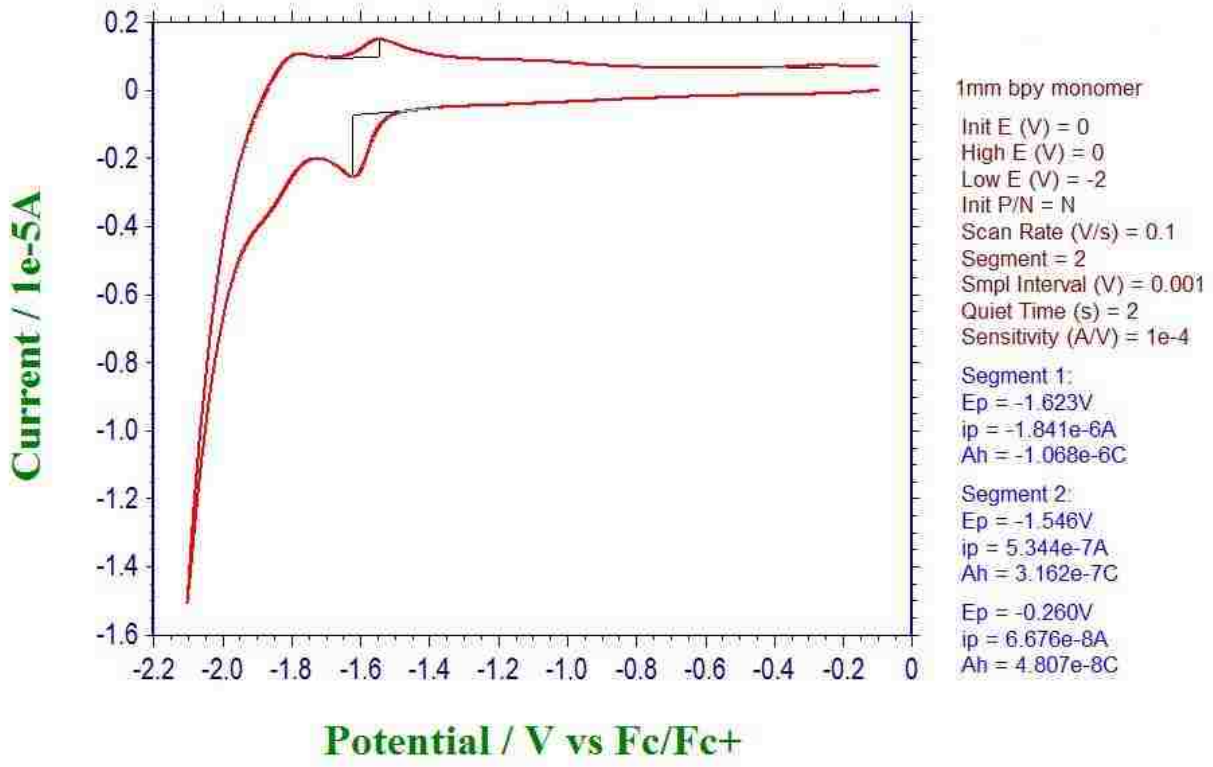
Current / 1e-5A
0.2
0
-0.2
-0.4
-0.6
-0.8
-1.0
-1.2
-1.4
-1.6
-2.2 -2.0 -1.8 -1.6 -1.4 -1.2 -1.0 -0.8 -0.6 -0.4 -0.2 0
Potential / V vs Fc/Fc+
1mm bpy monomer
Init E (V) = 0
High E (V) = 0
Low E (V) = -2
Init P/N = N
Scan Rate (V/s) = 0.1
Segment = 2
Smpl Interval (V) = 0.001
Quiet Time (s) = 2
Sensitivity (A/V) = 1e-4
Segment 1:
Ep = -1.623V
ip = -1.841e-6A
Ah = -1.068e-6C
Segment 2:
Ep = -1.546V
ip = 5.344e-7A
Ah = 3.162e-7C
Ep = -0.260V
ip = 6.676e-8A
Ah = 4.807e-8C

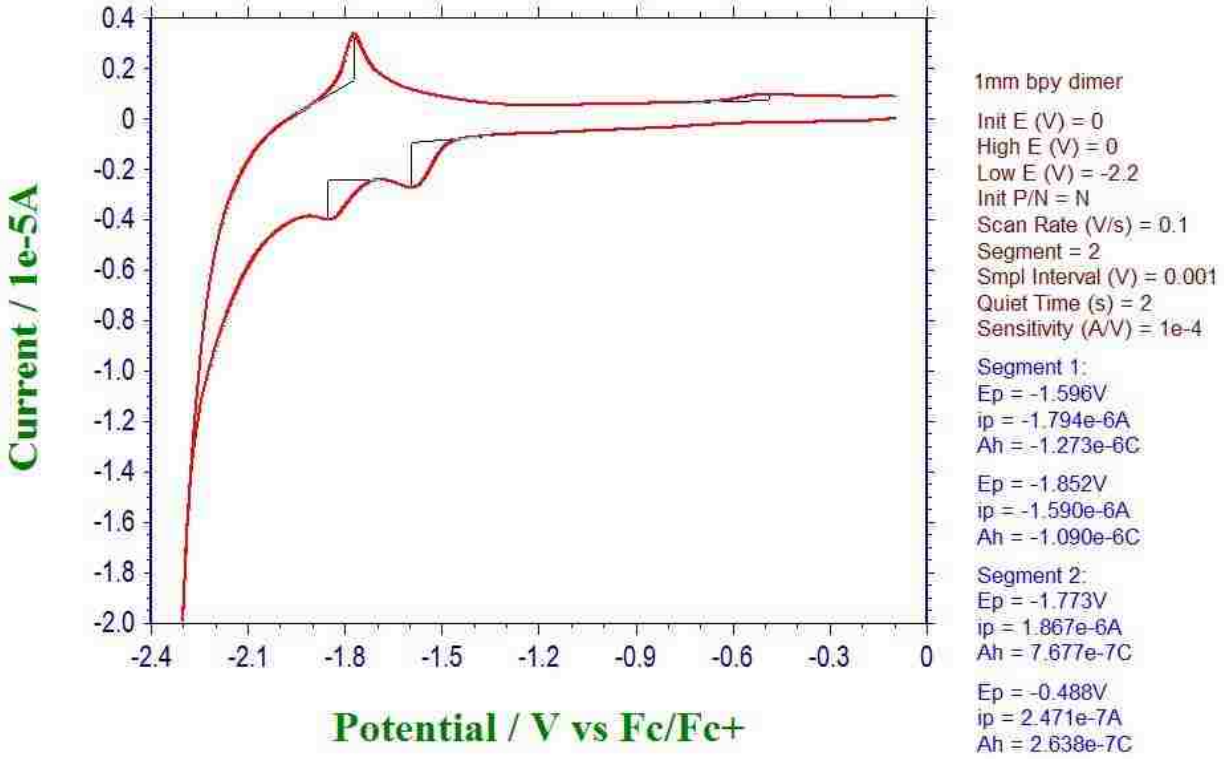
Current / 1e-5A
0.4
0.2
0
-0.2
-0.4
-0.6
-0.8
-1.0
-1.2
-1.4
-1.6
-1.8
-2.0
-2.4 -2.1 -1.8 -1.5 -1.2 -0.9 -0.6 -0.3 0
Potential / V vs Fc/Fc+
1mm bpy dimer
Init E (V) = 0
High E (V) = 0
Low E (V) = -2.2
Init P/N = N
Scan Rate (V/s) = 0.1
Segment = 2
Smpl Interval (V) = 0.001
Quiet Time (s) = 2
Sensitivity (A/V) = 1e-4
Segment 1:
Ep = -1.596V
ip = -1.794e-6A
Ah = -1.273e-6C
Ep = -1.852V
ip = -1.590e-6A
Ah = -1.090e-6C
Segment 2:
Ep = -1.773V
ip = 1.867e-6A
Ah = 7.677e-7C
Ep = -0.488V
ip = 2.471e-7A
Ah = 2.638e-7C

Figure 3.8.12. Cyclic voltammogram of $[Ru(dmbpy)_2diphenRu(dmbpy)_2]^{4+}$ in acetonitrile.

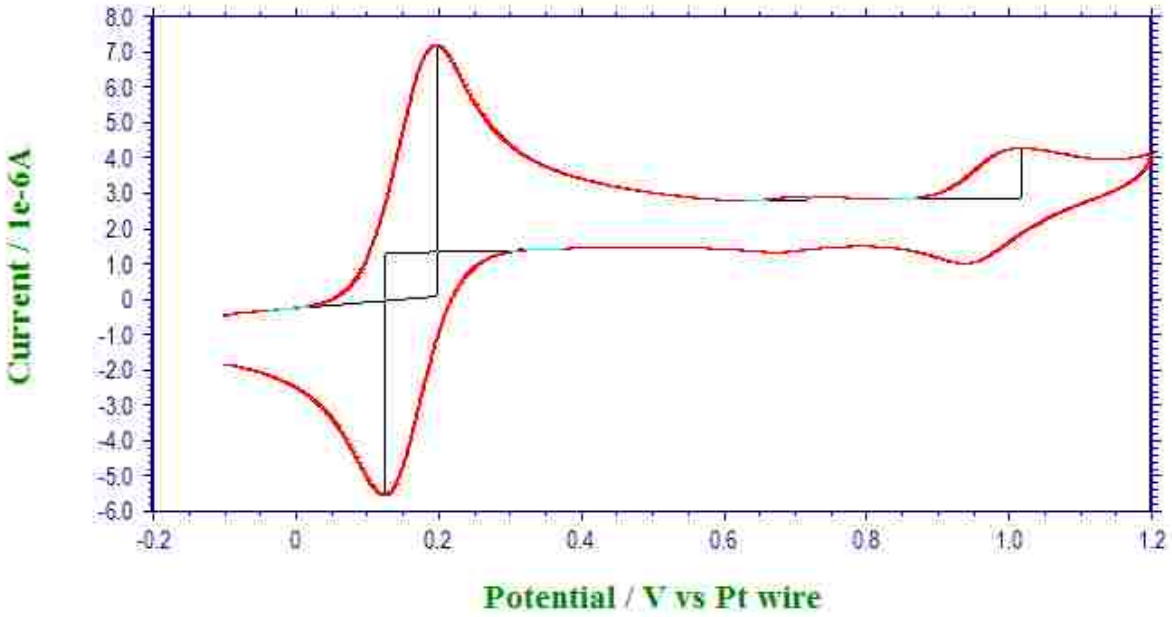
Current / 1e-6A
8.0
7.0
6.0
5.0
4.0
3.0
2.0
1.0
0
-1.0
-2.0
-3.0
-4.0
-5.0
-6.0
-0.2
0
0.2
0.4
0.6
0.8
1.0
1.2
Potential / V vs Pt wire

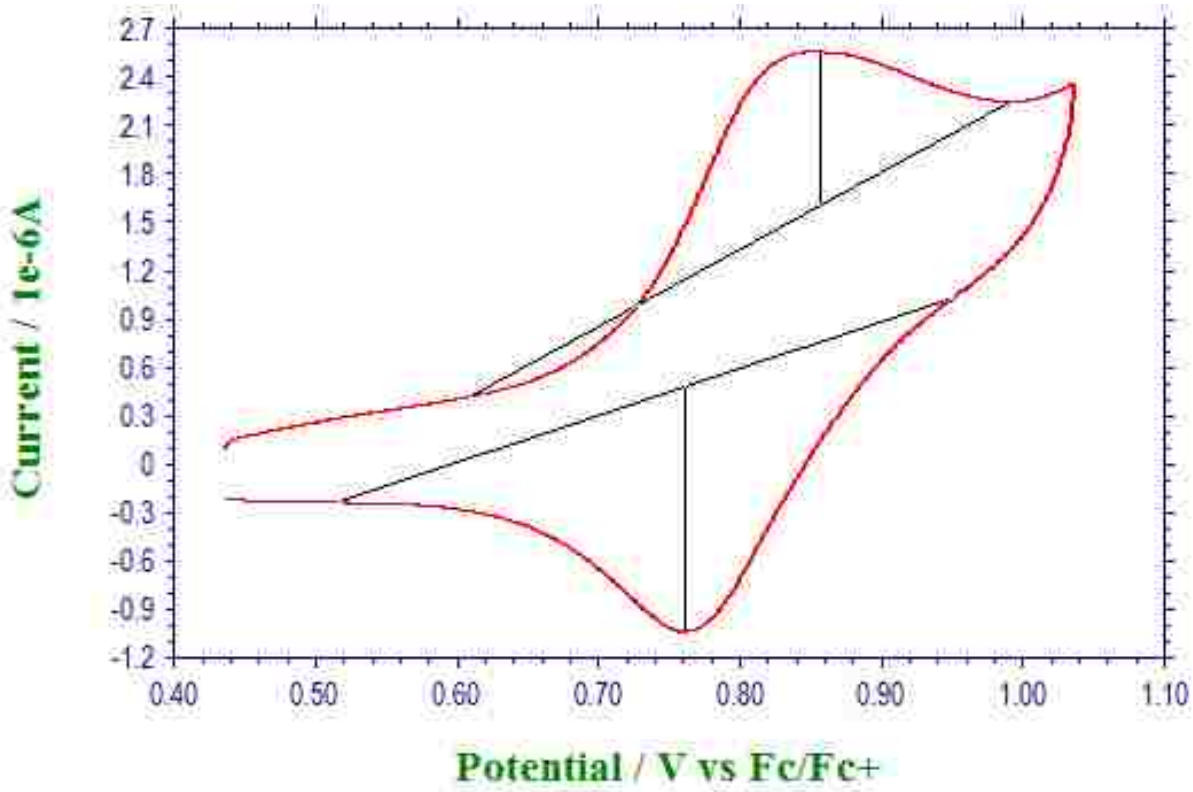
Current / 1e-6A
2.7
2.4
2.1
1.8
1.5
1.2
0.9
0.6
0.3
0
-0.3
-0.6
-0.9
-1.2
0.40
0.50
0.60
0.70
0.80
0.90
1.00
1.10
Potential / V vs Fc/Fc+

Figure 3.8.13. Cyclic Voltammogram of $[Ru(dmbpy)_2diphenRu(bpy)_2]^{4+}$ in acetonitrile.

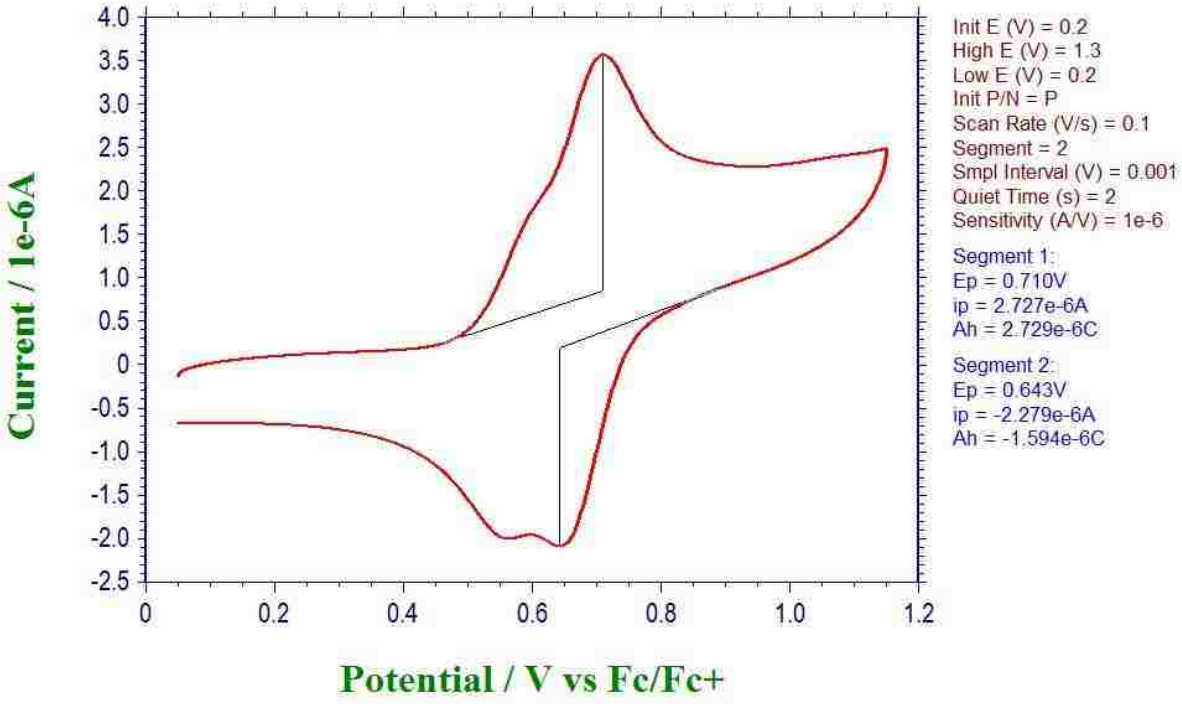
Current / 1e-6A
Potential / V vs Fc/Fc+
4.0
3.5
3.0
2.5
2.0
1.5
1.0
0.5
0
-0.5
-1.0
-1.5
-2.0
-2.5
0
0.2
0.4
0.6
0.8
1.0
1.2
Init E (V) = 0.2
High E (V) = 1.3
Low E (V) = 0.2
Init P/N = P
Scan Rate (V/s) = 0.1
Segment = 2
Smpl Interval (V) = 0.001
Quiet Time (s) = 2
Sensitivity (A/V) = 1e-6
Segment 1:
Ep = 0.710V
ip = 2.727e-6A
Ah = 2.729e-6C
Segment 2:
Ep = 0.643V
ip = -2.279e-6A
Ah = -1.594e-6C

Figure 3.8.14. Cyclic voltammetric scan rate dependence of $[Ru(dmbpy)_2diphen(bpy)_2Ru]^{4+}$ in acetonitrile.

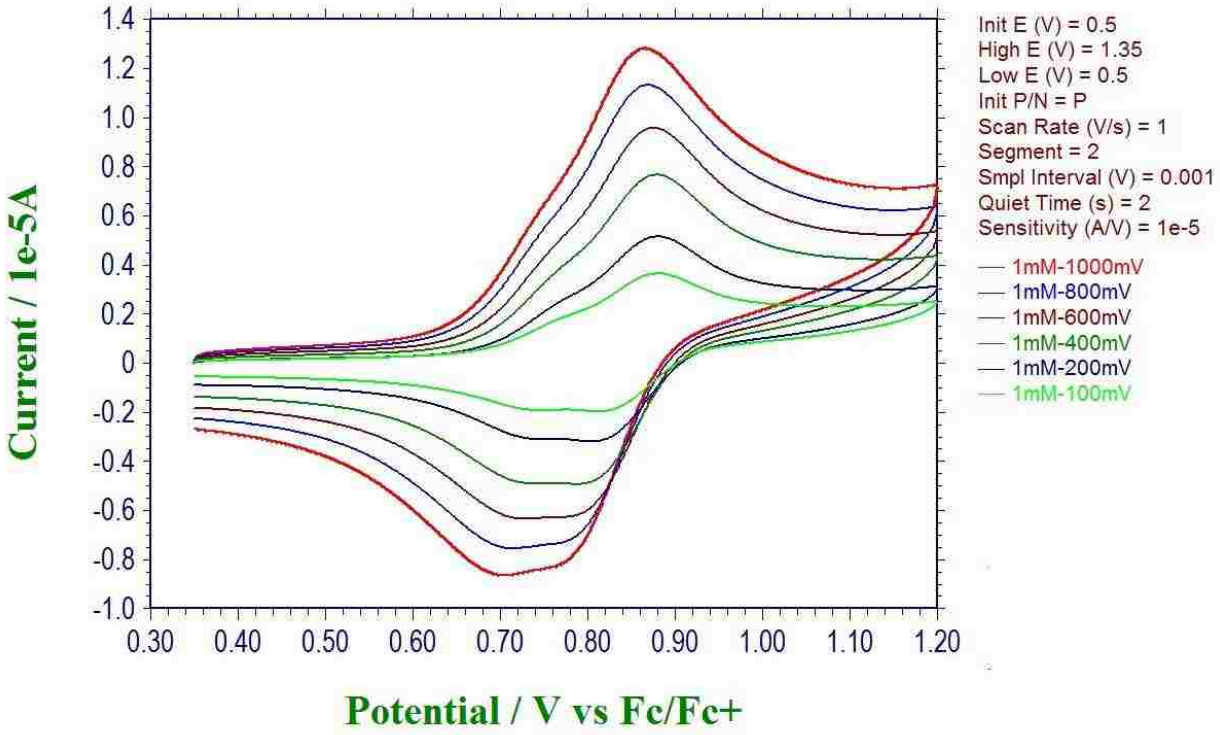
Current / 1e-5A
1.4
1.2
1.0
0.8
0.6
0.4
0.2
0
-0.2
-0.4
-0.6
-0.8
-1.0
0.30
0.40
0.50
0.60
0.70
0.80
0.90
1.00
1.10
1.20
Potential / V vs Fc/Fc+
Init E (V) = 0.5
High E (V) = 1.35
Low E (V) = 0.5
Init P/N = P
Scan Rate (V/s) = 1
Segment = 2
Smpl Interval (V) = 0.001
Quiet Time (s) = 2
Sensitivity (A/V) = 1e-5
1mM-1000mV
1mM-800mV
1mM-600mV
1mM-400mV
1mM-200mV
1mM-100mV

Figure 3.8.15. Cyclic voltammetric concentration studies of $[Ru(dmbpy)_2diphen(bpy)_2Ru]^{4+}$ in acetonitrile.

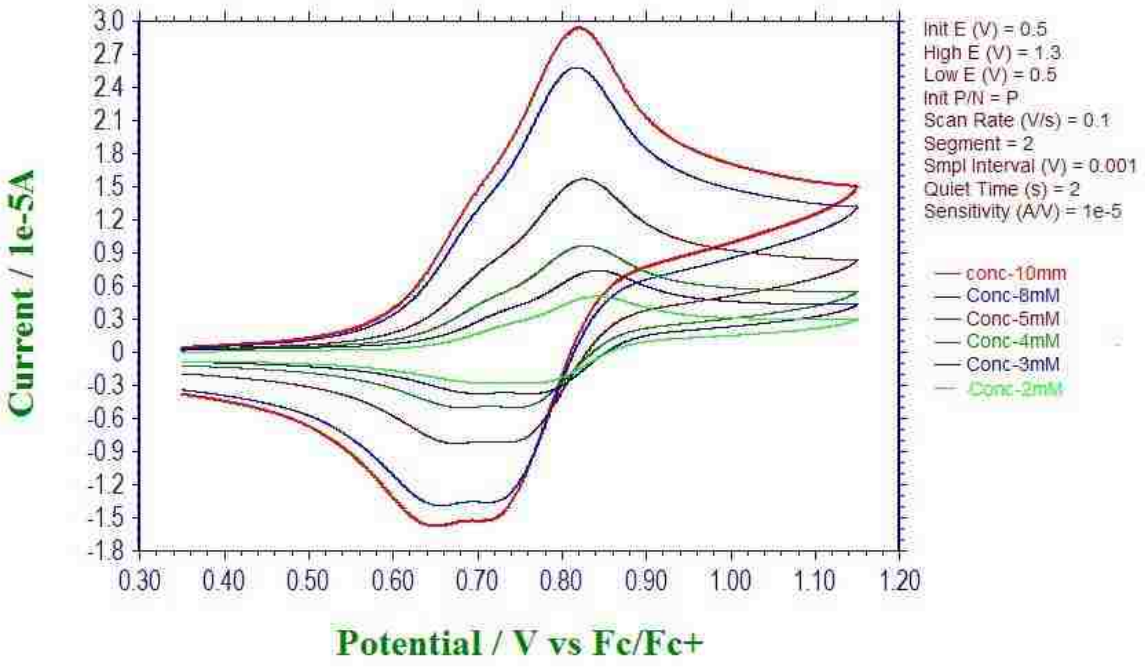
Current / 1e-5A
Potential / V vs Fc/Fc+
Init E (V) = 0.5
High E (V) = 1.3
Low E (V) = 0.5
Init P/N = P
Scan Rate (V/s) = 0.1
Segment = 2
Smpl Interval (V) = 0.001
Quiet Time (s) = 2
Sensitivity (A/V) = 1e-5
conc-10mm
Conc-8mM
Conc-5mM
Conc-4mM
Conc-3mM
Conc-2mM

Figure3.8.16. Cyclic voltammogram of $[(dmbpy)_2RudiphenRu(dmbpy)_2]^{4+}$and

$[Ru(dmbpy)_2diphen]^{2+}$ showing ligand reductions

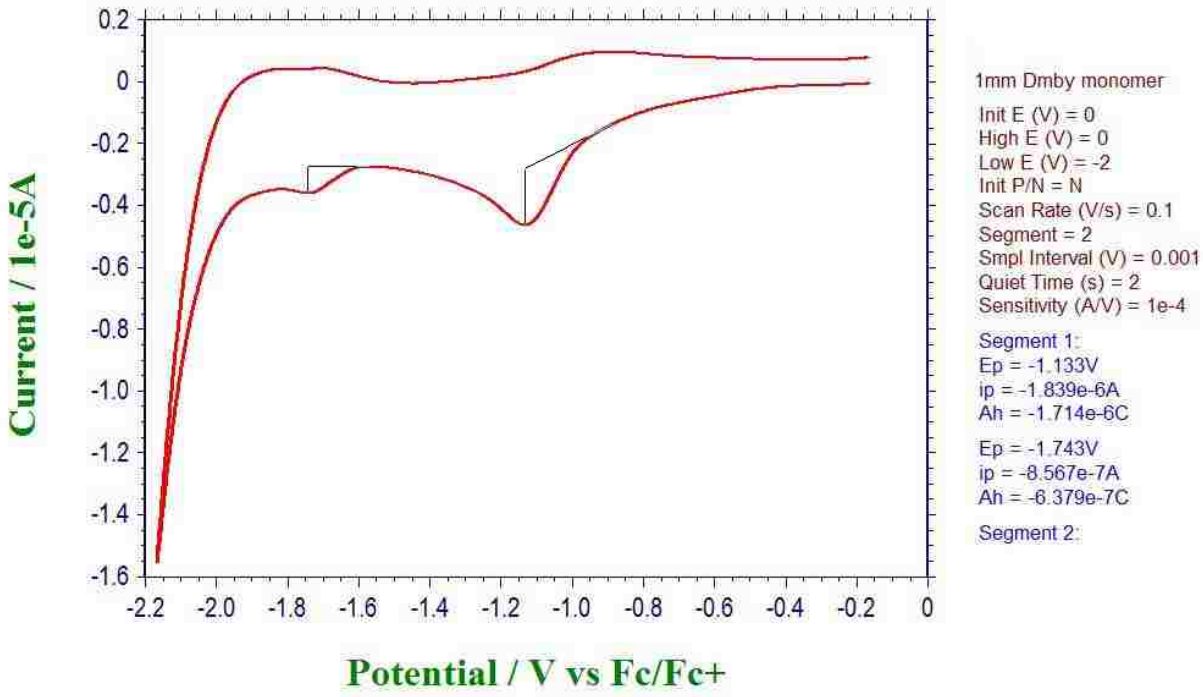
Current / 1e-5A
Potential / V vs Fc/Fc+
1mm Dmby monomer
Init E (V) = 0
High E (V) = 0
Low E (V) = -2
Init P/N = N
Scan Rate (V/s) = 0.1
Segment = 2
Smpl Interval (V) = 0.001
Quiet Time (s) = 2
Sensitivity (A/V) = 1e-4
Segment 1:
Ep = -1.133V
ip = -1.839e-6A
Ah = -1.714e-6C
Ep = -1.743V
ip = -8.567e-7A
Ah = -6.379e-7C
Segment 2:

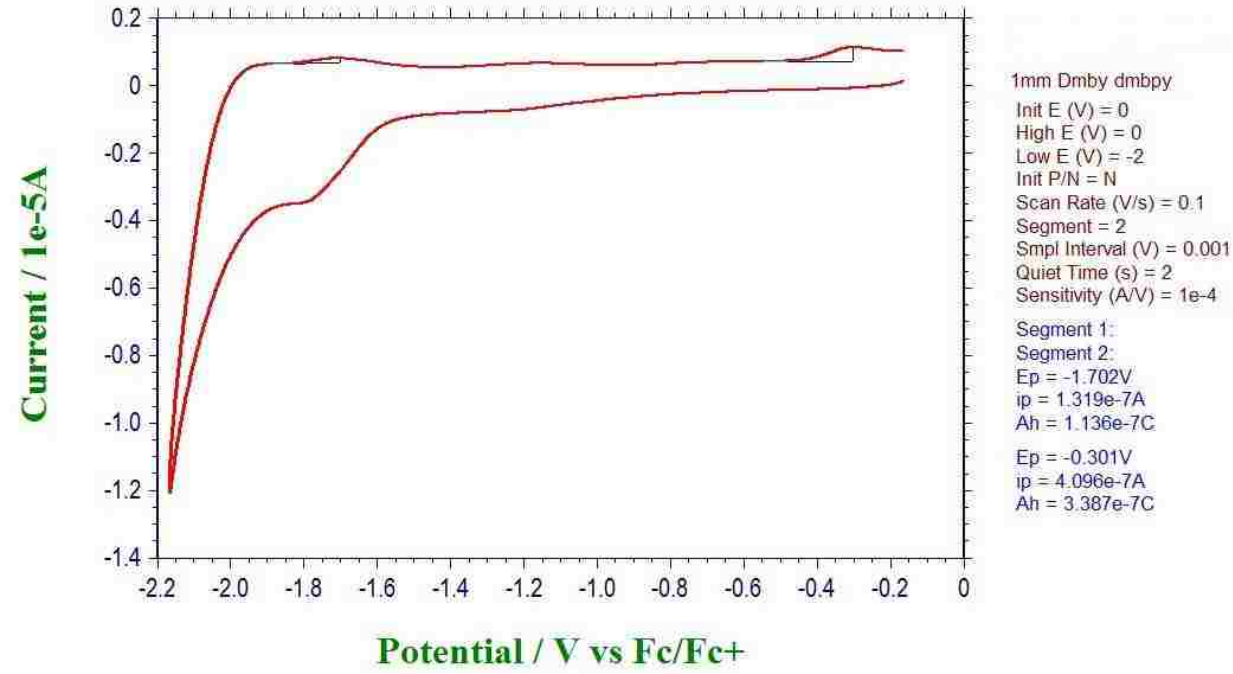
Current / 1e-5A
Potential / V vs Fc/Fc+
1mm Dmby dmbpy
Init E (V) = 0
High E (V) = 0
Low E (V) = -2
Init P/N = N
Scan Rate (V/s) = 0.1
Segment = 2
Smpl Interval (V) = 0.001
Quiet Time (s) = 2
Sensitivity (A/V) = 1e-4
Segment 1:
Segment 2:
Ep = -1.702V
ip = 1.319e-7A
Ah = 1.136e-7C
Ep = -0.301V
ip = 4.096e-7A
Ah = 3.387e-7C

3.9 Ruthenium (II) TAP Dimer Synthesis

In an effort to explore more thoroughly the coupling between the metal centers ligands that result in complexes which much higher oxidation potentials were explored. One in particular was successfully synthesized. The TAP ligand was prepared through a series of Schiff base condensation reactions and a reduction reaction [72].

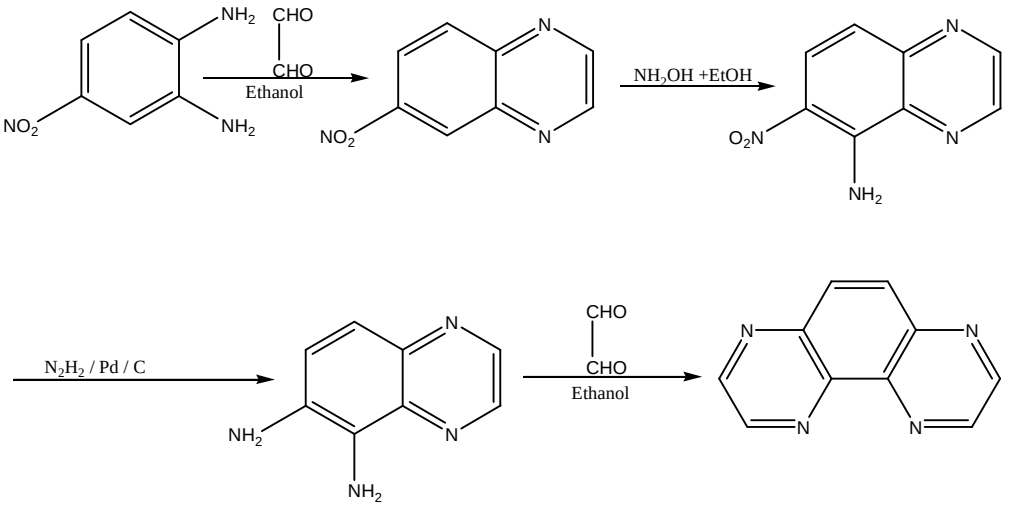

Scheme 3.9.1 Synthesis of TAP Ligand

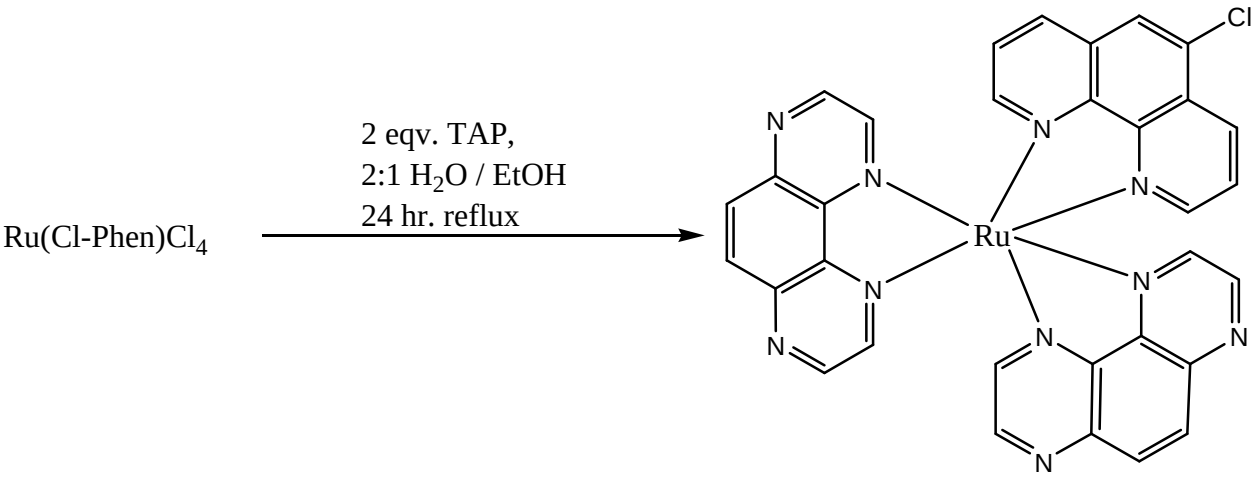

Scheme 3.9.2 Synthesis of TAP Monomer

$$[Ru(CO)_2Cl_2]n + 2n(TAP) \xrightarrow{\text{2-methoxyethanol}} [Ru(CO)_2Cl_2(TAP)_2]$$

$$[Ru(CO)_2Cl_2(TAP)_2] + (\text{Cl-phen}) + 2Me_3NO \xrightarrow{\text{2-methoxyethanol}} [Ru((TAP)_2\text{Cl-phen}]Cl_2 + 2Me_3N + 2CO_2$$

$$[Ru((TAP)_2\text{Cl-phen}]Cl_2 + 2NH_4PF_6 \longrightarrow [Ru((TAP)_2\text{Cl-phen}](PF_6)_2 + 2NH_4Cl$$

Scheme 3.9.3. Synthesis of TAP Monomer via decarbonylation reaction

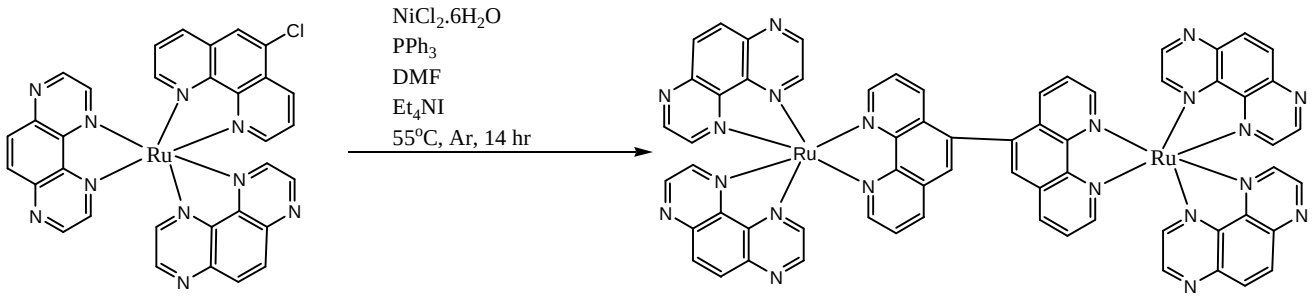

Scheme 3.9.4. Synthesis of TAP Dimer

Scheme 3.9.1 outlines the basic synthesis of the free ligand which was completed with adequate over all yield. The purity of the product was checked with gas chromatography mass spectrometry, illustrated in Figure 3.9.1,which verified that only the expected product was present. The NMR further confirmed the identity of the product and is illustrated in figures 3.9.2 and 3.9.3**.**

The intermediate monomeric complex was also successfully prepared as evidenced by the electrospray mass spectrum illustrated in figure 3.9.4. In this example, the M/Z of the parent ion = 339.9 matches the expected M/Z of 340.0 for the intermediate $[Ru(TAP)_2(\text{Cl-phen})]^{2+}$.

Unfortunately, the preparation of dimer was not completely satisfactory. Although the complex could be prepared it was always produced in the presence of the monomer, $[Ru(TAP)_2phen]^{2+}$. There was an additional, and unexpected complication, which resulted from the mass spectrometer used in the analysis. Figure 3.9.5 shows the spectrum of the mixture of dimer and monomer at three different skimmer voltages. It is clear that the skimmer voltage alters the apparent ratio monomer to dimer. At high skimmer voltages the monomer is dominant. Figure 3.9.6 shows a cleaner picture of the situation at a skimmer voltage of 13 volts.

Figure: 3.9.1 ESI-MS spectra and GC of TAP Ligand.

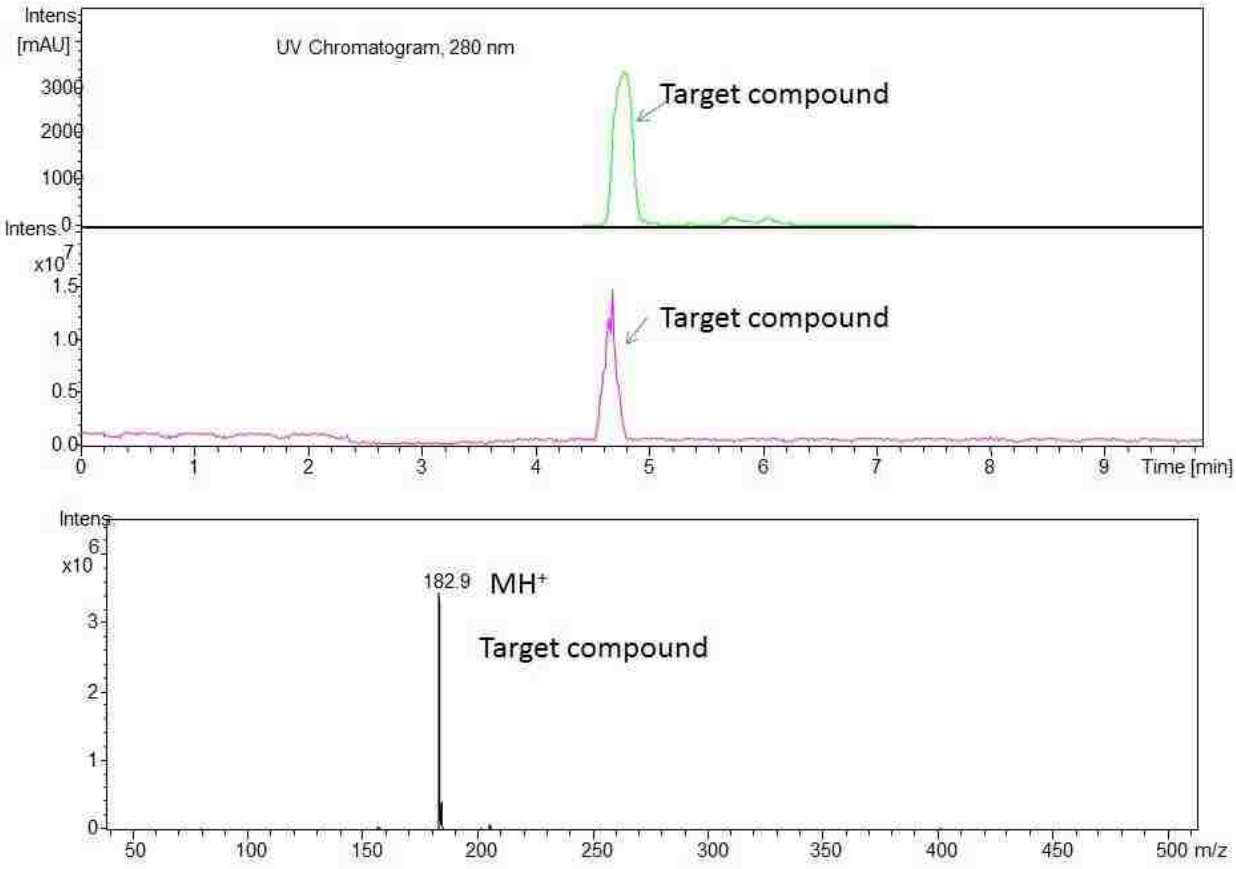
Intens.
[mAU]
UV Chromatogram, 280 nm
Target compound
Intens.
x10^7
Target compound
Time [min]
Intens.
x10^6
182.9 MH+
Target compound
m/z

Figure: 3.9.2. ^{1}H NMR of TAP Ligand in DMSO $d_{6.}$

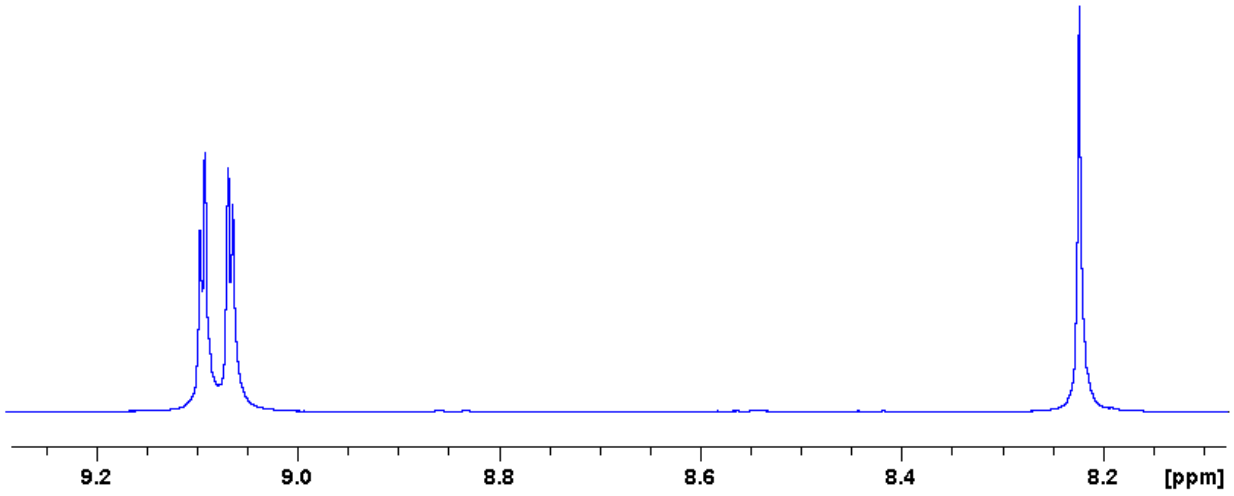
9.2
9.0
8.8
8.6
8.4
8.2
[ppm]

Figure: 3.9.3. ^{13}C NMR of TAP Ligand in DMSO-d_6

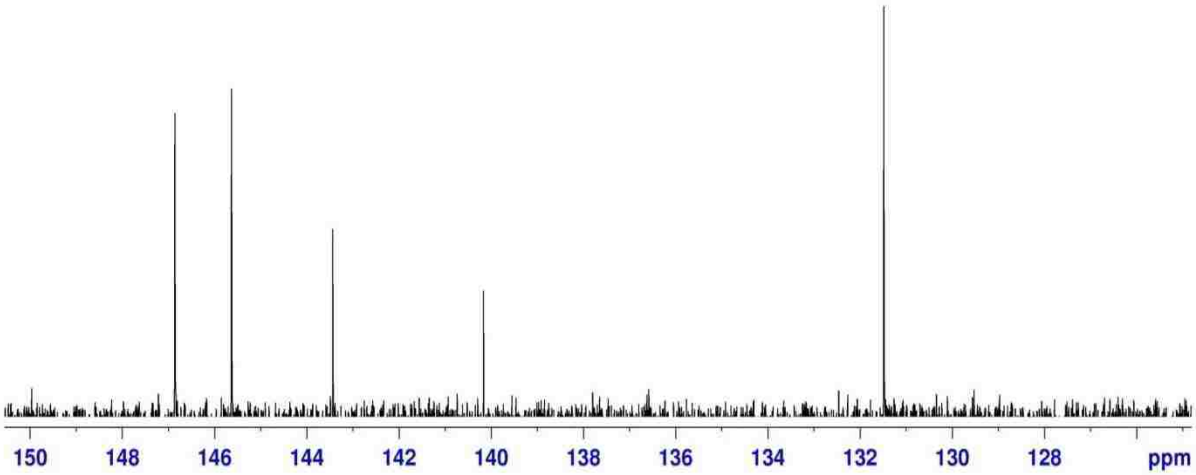
150
148
146
144
142
140
138
136
134
132
130
128
ppm

Figure: 3.9.4. ESI-MS spectra of $[Ru(TAP)_2Cl\text{-}phen]^{2+}$ in $d_3\text{-}CD_3CN$.

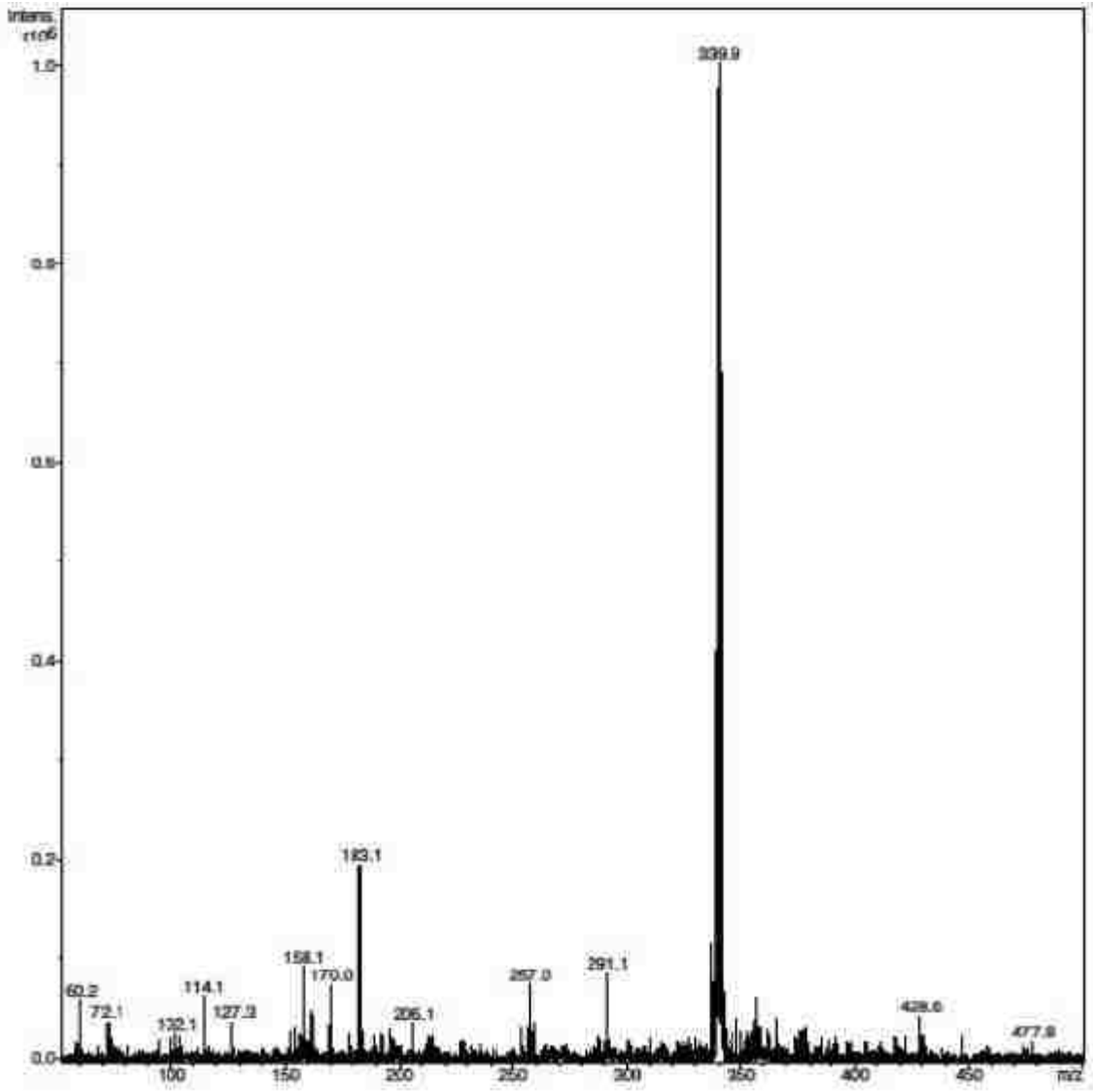
Intens.
x10^6
1.0
0.8
0.6
0.4
0.2
0.0
339.9
183.1
158.1
170.0
114.1
127.2
60.2
72.1
132.1
206.1
257.0
291.1
428.6
477.9
100
150
200
250
300
350
400
450
m/z

Figure: 3.9.5. ESI-MS spectra of $[Ru(TAP)_2diphenRu(TAP)_2]^{4+}$

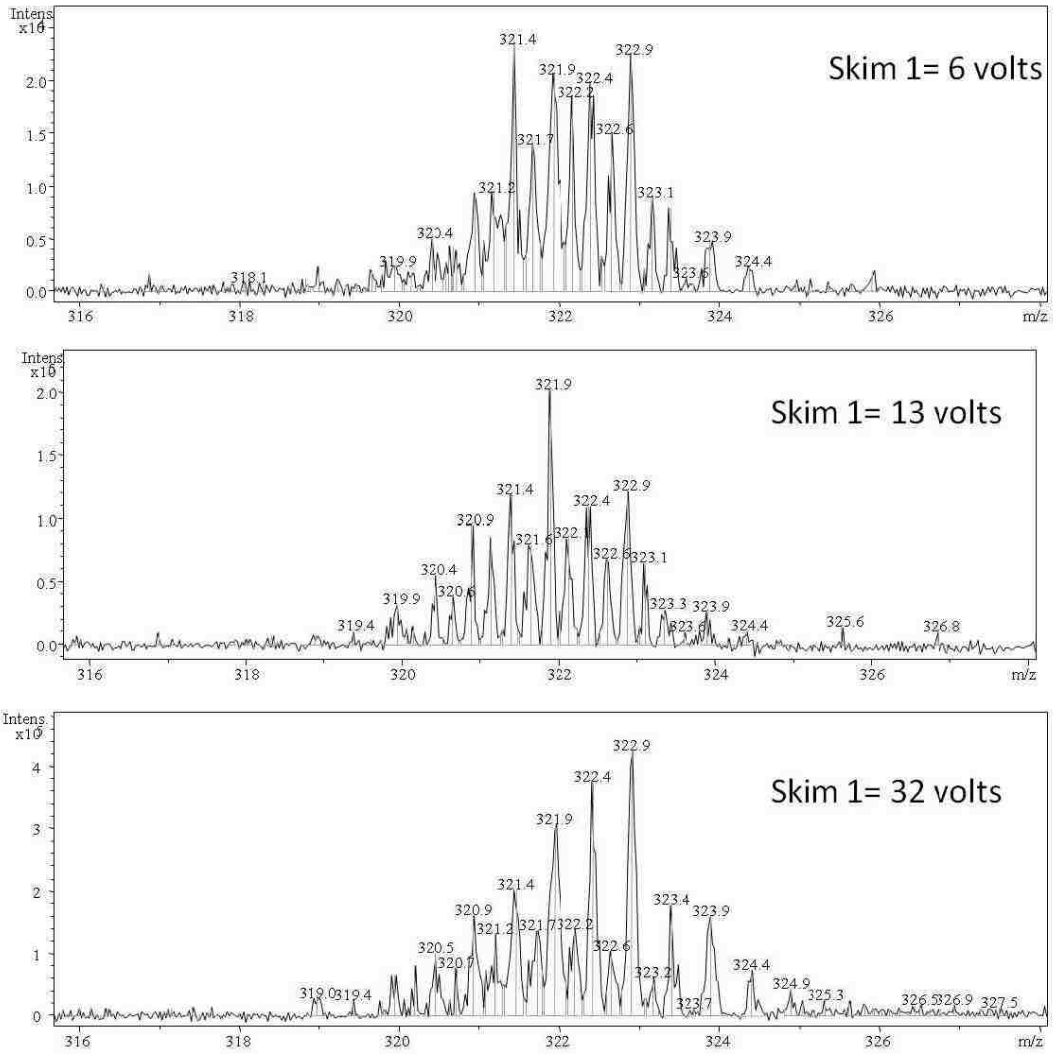

Increasing skim voltage
Increase the monomer

Figure: 3.9.6. Ratio of $[Ru(TAP)_2diphenRu(TAP)_2]^{4+}$ to $[Ru(TAP)_2phen]^{2+}$ from ESI-MS spectra.

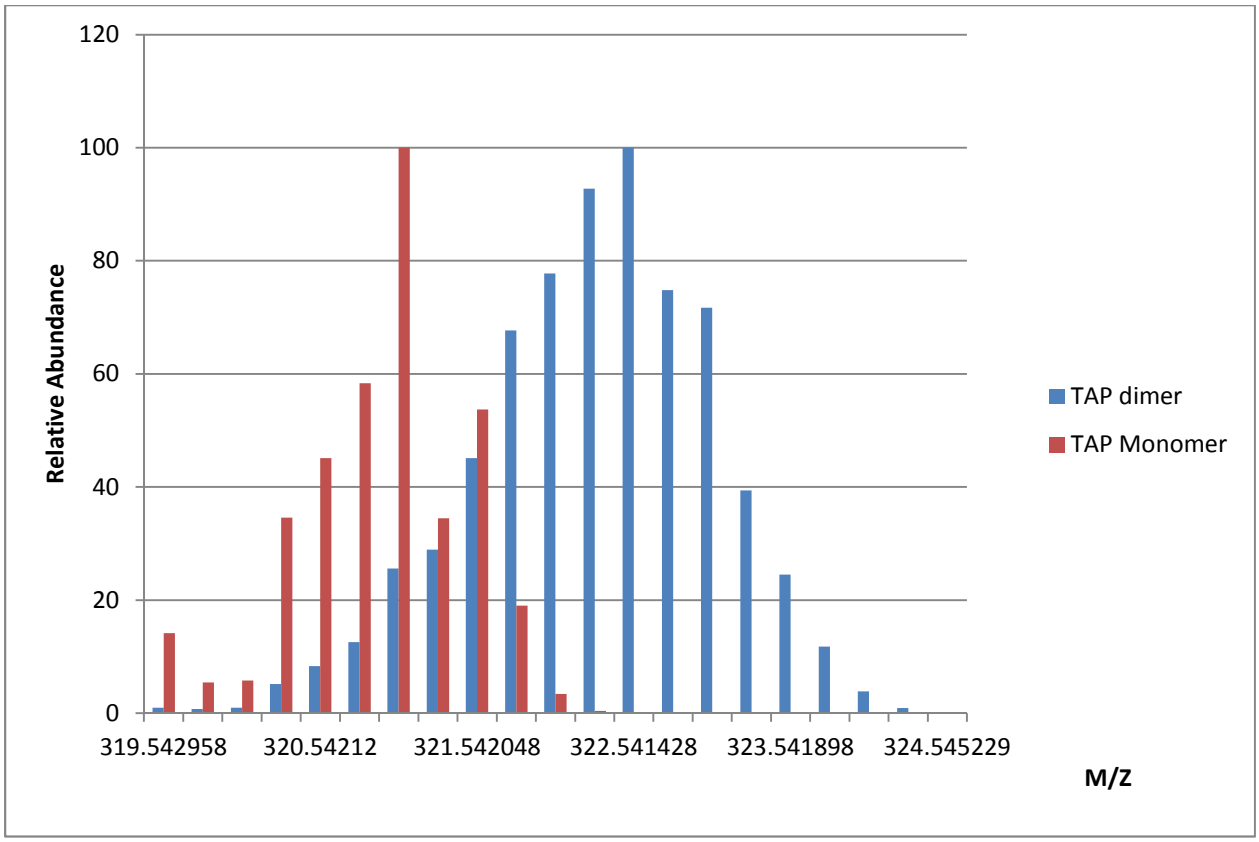
120
100
80
60
40
20
0
Relative Abundance
319.542958
320.54212
321.542048
322.541428
323.541898
324.545229
M/Z
TAP dimer
TAP Monomer

CHAPTER 4: Discussion

4.1 Ruthenium (II) Mixed Dimer Complex

Ruthenium (II) mixed dimer was synthesized by combining $[Ru(dmbpy)_2(CO)_2](PF_6)_2$ (1.0 mmol) and $[Ru(bpy)_2diphen]^{2+}$(1.2 mmol) in the presence of an excess amount of trimethylamine N oxide which served as the decarbonylating agent. The reaction was run for 2hr under a nitrogen atmosphere. This approach is generally used to synthesize a mixed dimer in which the two ligands surrounding the ruthenium metals are different.

In order to enhance the possibility of quenching the excited state of our complex (by drifting electrons from one side to the other), we synthesized a mixed dimer. Also, we can gain insight into the parameters which determine the life time in a mixed dimer by examining the electrochemistry to see how the two metal centers behave. These points are important in the development of solar energy conversion devices and redox catalyst in four electron donors. If the energies of the lowest excited state are different in a dimer, the energy should be trapped in the center with the lowest energy. If this works, multiple centers could be designed in an antenna-like array.

Preliminary results from the Durham's lab have shown that the excited state life time of a dimer is longer than that of a monomer when the experiment was done in an aqueous medium. Unfortunately, what we observed was different from what we had expected. The excited state life time of the monomers and dimers were similar. This might be due to the fact that our experiment was done in acetonitrile instead of water.

Cyclic voltammetry results indicate that our mixed dimer is made up of two metal centers that have no electronic interaction with one another. This is confirmed by the presence of two oxidation and reduction peaks between 0.55 – 0.7 V respectively. This implies the bridging (5,5'-

bis 1,10-phenanthroline) ligand acts an insulator holding the two metal centers together (Class one metal complex) but not allowing electronic interaction between the two centers.

Fluorescence emission result of our mixed dimer in liquid nitrogen also confirms the fact that our mixed dimer is made up of two metal centers with no electronic interaction with each other. The relative emission intensity of the mixed dimer which was approximately 3000 counts per second was roughly equal to that of the bipyridine (bpy) and 4,4'-dimethyl bipyridine (dmbpy) dimer combined together. The lowest excited state energy complex was the dmbpy dimer while the highest energy moiety was the bpy dimer and our mixed dimer was in the middle of these two. The fluorescence emission experiment in air also suggests the same results. From these results, one can also conclude that there is no quenching taking place in the excited state of the mixed dimer. If we had quenching, the emission life time of the mixed dimer would be half that of the symmetric dimers.

Flash photolysis results of our complexes (mixed dimer, symmetrical dimers and monomers) showed that the excited state lifetime of the mixed dimer, dmbpy dimer, bpy dimer, bpy monomer and dmbpy monomer is 125 µs, 118 µs, 134 µs139 µs and 129µs respectively. This result shows that there is no quenching taking place in the excited state of the mixed dimer since the life time values are virtually identical.

Results of the intervalence charge transfer experiment showed that the was no intervalence charge transfer transition. This was evidenced by the lack of a band at 650 nm. The lack of an intervalence charge transfer band could suggest that our complex is a class one complex.

4.2 Ruthenium (II) Dmbpy Dimer Complex

Classical method for the synthesis of symmetric dimers using a nickel catalyzed coupling reaction [70] by Toyota et al did not give us a positive result. To overcome this huddle, we carried out a decarbonylation reaction following the protocol of Thomas et al [69]. Two symmetric dimers namely ruthenium (II) dmbpy and ruthenium (II) bpy dimers were synthesized respectively. These two dimers were chosen because their ligands namely dmbpy and bpy were those present in the mixed dimer. Also we wanted to compare the electrochemistry of the symmetric dimers to that of the asymmetric dimer and see if there is a shift in the reduction potential of the mixed dimer just by attaching various substituents unto it.

Cyclic voltammetry results shows a single oxidation and reduction wave with the maximum oxidation potential and reduction potential at 0.86 V and 0.76 V respectively. The fluorescence emission (in air) result shows that the dmbpy dimer has the lowest excited state energy compared to that of the bpy and mixed dimers respectively. This could be explained by the fact that the dmbpy dimer has an electron donating group (dmbpy) which makes the ruthenium metal center less positively charged and as such giving it a lower reduction potential unlike the bpy dimer which contains a more electron withdrawing ligand (bpy ligand) thus making the ruthenium metal center more positively charged (oxidizing) henceforth giving the bpy dimer a greater redox potential. The redox potential of the dmbpy dimer is about 100 mV lower than that of the bpy dimer. The excited state lifetime of the dmbpy dimer is 118 µs which is basically identical to that of the other dimers (bpy dimer 134 µs. and mixed dimer 125 µs).

4.3 Ruthenium (II) Bpy Dimer

The Bpy ligand is more oxidizing than dmbpy but less oxidizing than TAP with a redox potential of 1.10 eV. The presence of two nitrogen atoms on the bipyridine ring deactivates the ring and as such the bpy dimer can readily accept an electron from a protein molecule. This dimer was synthesized by modifying the proctocol of Toyota et al [70].

The scheme for this synthesis is illustrated below.

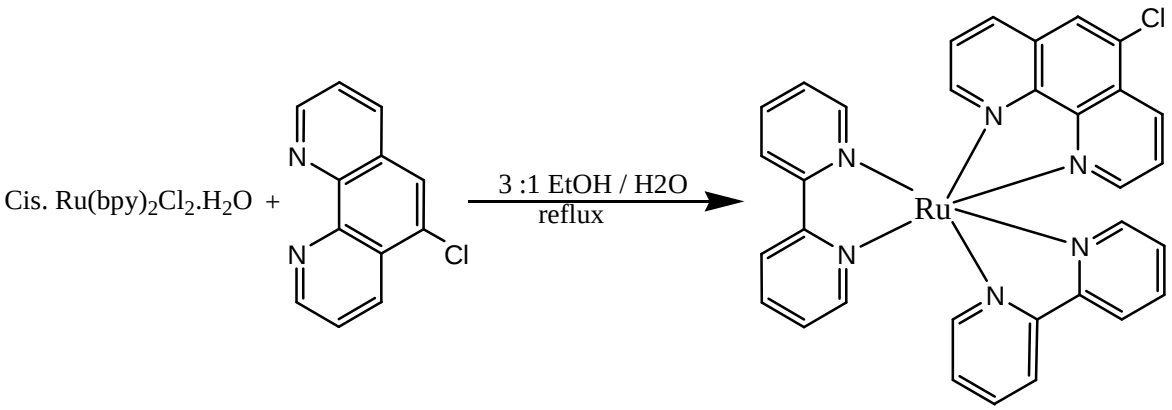

Scheme 3.3.1: Synthesis of bpy monomer

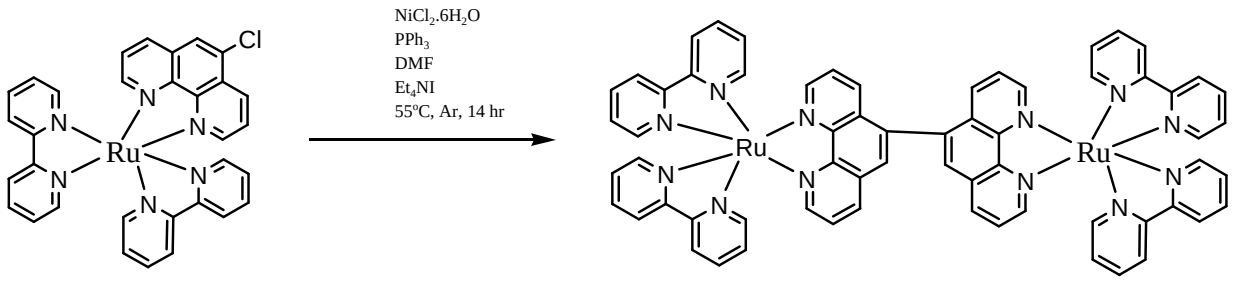

Scheme 3.3.2: Synthesis of bpy dimer

Cyclic voltammetry results shows a single oxidation and reduction wave with the maximum potential of the oxidation and reduction waves at 0.94 and 0.91 V respectively. The maximum absorption of the bpy dimer is at 452 nm compared to that of the bpy monomer which is at 450 nm. Results from the laser flash photolysis suggests that the excited state life time of the bpy dimer is 134 μs. Results from the fluorescence emission experiment done in air suggests that the excited state energy of the bpy dimer is greater than that of the dmbpy and mixed dimers respectively. This is due to the fact that the bpy ligand is a stronger oxidizing agent than the dmbpy hence rendering the ruthenium metal center more positive which accounts for a greater redox potential of this dimer and consequently a greater excited state energy. Flash photolysis results from the temperature dependence measurement of the bpy dimer suggest that the dimer behaves as a monomer. This implies, there is no electronic coupling between the two metal centers in the dimer.

4.4 Ruthenium (II) TAP Dimer Complex

The Tap ligand is a strong oxidizing ligand with a redox potential of 1.93 eV. The TAP ligand was prepared through a series of Schiff base (condensation reactions and a reduction reaction [72].When this ligand was attached to a ruthenium complex, it formed a monomer. This dimer is synthesized by a nickel catalyzed coupling reaction of the monomer. This protocol is a classical method for the synthesis of ruthenium (II) dimers by nickel catalyzed coupling first done by [70]. The main drawback of this reaction is that the nickel (0) complex which acts as a catalyst in this reaction is air sensitive and as such care should be taken so that it does not die while the reaction is taking place.

This Ru (II) dimer can be covalently bonded to a protein molecule to form Ru(II)-Fe(III) species. This species when excited by a laser to form Ru(II)*-Fe (III) species The Ru(II)* can then react with a quencher species in solution to form Ru(I)-Fe(III) which can further be reduced to Ru(II)-Fe(III). This reduced form of the protein can then react with another protein in solution. These reactions generally involve a large amount of proteins resulting to a very high yield of photochemical products. Preliminary results from the Durham's group have shown that increasing the redox potentials of the complex increases the yield of the desired product. Highest yields of photochemical products have been obtained with strong oxidizing dimer which led us to synthesize and characterize the ruthenium (II) TAP dimers.

4.5 Electrochemical study of Ru (II) Dimers

Electrochemical studies were done by preparing various concentrations of our complexes and dissolving each in 0.1M $TBAPF_6$ in acetonitrile (which acted as the supporting electrolyte). The reference and counter electrodes were made up of a platinum wire (pseudo reference) and the working electrode was made up of a platinum disc. The area of the reference electrode was 0.785 mm^2. Since we were using a pseudo reference electrode, we had to calibrate our result by adding some ferrocene in our solution and by subtracting the potential of the analyte in ferrocene from that without the ferrocene to get the actual potential of our analyte.

Electrochemical experiments were done in order to determine the reversibility of our complexes. One can conclude from these results that our symmetric dimers and monomers were reversible with one oxidation and one reduction wave respectively. The mixed dimer complexes were also reversible but unlike the symmetric dimers, they had two oxidation and two reduction peaks respectively. This result suggests that our symmetric dimers is made up of one metal center linked together by a 5,5'-bis-1,10-phenanthroline (diphen) bridging ligand. The asymmetric (mixed) dimer on the other hand was made up of two metal centers with no electronic coupling between the two metal centers (class one complex). The diphen bridging ligand acts as an electronic insulator prohibiting any kind of electronic interaction.

References

(1) Douce, R.; Brouquisse, R.; Journet, E. In *In Electron transfer and oxidative phosphorylation in plant mitochondria;* Academic: 1987; Vol. 11, pp 177-211.

(2) HATEFI, Y.; HAAVIK, A.; GRIFFITHS, D. Studies on Electron Transfer System .41. Reduced Coenzyme Q (Qh2)-Cytochrome C Reductase. *J. Biol. Chem.* **1962**, *237*, 1681-&.

(3) HATEFI, Y.; GRIFFITHS, D.; HAAVIK, A. Reconstitution of Electron Transport System .1. Preparation and Properties of Interacting Enzyme Complexes. *Biochem. Biophys. Res. Commun.* **1961**, *4*, 441-&.

(4) LEUNG, K.; HINKLE, P. Reconstitution of Ion-Transport and Respiratory Control in Vesicles Formed from Reduced Coenzyme Q Cytochrome-C Reductase and Phospholipids. *J. Biol. Chem.* **1975**, *250*, 8467-8471.

(5) Huttemann, M.; Lee, I.; Pecinova, A.; Pecina, P.; Przyklenk, K.; Doan, J. W. Regulation of oxidative phosphorylation, the mitochondrial membrane potential, and their role in human disease. *J. Bioenerg. Biomembr.* **2008**, *40*.

(6) HATEFI, Y. The Mitochondrial Electron-Transport and Oxidative-Phosphorylation System. *Annu. Rev. Biochem.* **1985**, *54*, 1015-1069.

(7) PAN, L.; DURHAM, B.; WOLINSKA, J.; MILLETT, F. Preparation and Characterization of Singly Labeled Ruthenium Polypyridine Cytochrome-C Derivatives. *Biochemistry (N. Y.)* **1988**, *27*, 7180-7184.

(8) LIU, R.; GEREN, L.; ANDERSON, P.; FAIRRIS, J.; PEFFER, N.; MCKEE, A.; DURHAM, B.; MILLETT, F. Design of Ruthenium-Cytochrome-C Derivatives to Measure Electron-Transfer to Cytochrome-C Peroxidase. *Biochimie* **1995**, *77*, 549-561.

(9) DURHAM, B.; PAN, L.; LONG, J.; MILLETT, F. Photoinduced Electron-Transfer Kinetics of Singly Labeled Ruthenium Bis(bipyridine) Dicarboxybipyridine Cytochrome-C Derivatives. *Biochemistry (N. Y.)* **1989**, *28*, 8659-8665.

(10) Zaslavsky, D.; Sadoski, R.; Rajagukguk, S.; Geren, L.; Millett, F.; Durham, B.; Gennis, R. Direct measurement of proton release by cytochrome c oxidase in solution during the F -> O transition. *Proc. Natl. Acad. Sci. U. S. A.* **2004**, *101*, 10544-10547.

(11) GEREN, L.; BEASLEY, J.; FINE, B.; SAUNDERS, A.; HIBDON, S.; PIELAK, G.; DURHAM, B.; MILLETT, F. Design of a Ruthenium Cytochrome-C Derivative to Measure Electron-Transfer to the Initial Acceptor in Cytochrome-C-Oxidase. *J. Biol. Chem.* **1995**, *270*, 2466-2472.

(12) PAN, L.; HIBDON, S.; LIU, R.; DURHAM, B.; MILLETT, F. Intracomplex Electron-Transfer between Ruthenium-Cytochrome-C Derivatives and Cytochrome-C-Oxidase. *Biochemistry (N. Y.)* **1993**, *32*, 8492-8498.

(13) WILLIE, A.; STAYTON, P.; SLIGAR, S.; DURHAM, B.; MILLETT, F. Genetic-Engineering of Redox Donor Sites - Measurement of Intracomplex Electron-Transfer between Ruthenium-65 Cytochrome-B5 and Cytochrome-C. *Biochemistry (N. Y.)* **1992**, *31*, 7237-7242.

(14) Wang, K.; Mei, H.; Geren, L.; Miller, M.; Saunders, A.; Wang, X.; Waldner, J.; Pielak, G.; Durham, B.; Millett, F. Design of a ruthenium-cytochrome c derivative to measure electron transfer to the radical cation and oxyferryl heme in cytochrome c peroxidase. *Biochemistry (N. Y.)* **1996**, *35*, 15107-15119.

(15) GEREN, L.; HAHM, S.; DURHAM, B.; MILLETT, F. Photoinduced Electron-Transfer between Cytochrome-C Peroxidase and Yeast Cytochrome-C Labeled at Cys-102 with (4-Bromomethyl-4'-Methylbipyridine)[bis(bipyridine)]ruthenium2+. *Biochemistry (N. Y.)* **1991**, *30*, 9450-9457.

(16) NILSSON, T. Photoinduced Electron-Transfer from Tris(2,2'-Bipyridyl)ruthenium to Cytochrome-C-Oxidase. *Proc. Natl. Acad. Sci. U. S. A.* **1992**, *89*, 6497-6501.

(17) Roundhill, D. M. *Photochemistry and Photophysics of Metal Complexes;* Plenum press: New York, 1994; .

(18) BOLLETTA, F.; JURIS, A.; MAESTRI, M.; SANDRINI, D. Quantum Yield of Formation of the Lowest Excited-State of Ru(bpy)3(2+) and Ru(phen)3(2+). *Inorganica Chimica Acta-Letters* **1980**, *44*, L175-L176.

(19) DALLINGER, R.; WOODRUFF, W. Time-Resolved Resonance Raman Study of the Lowest (D-Pi-Star, 3ct) Excited-State of Tris(2,2'-Bipyridine)ruthenium(ii). *J. Am. Chem. Soc.* **1979**, *101*, 4391-4393.

(20) CARLIN, C.; DEARMOND, M. Evidence for Symmetry Reduction in Excited-States of [Ru(bpy)3]2+ and Related-Compounds. *Chemical Physics Letters* **1982**, *89*, 297-302.

(21) FELIX, F.; FERGUSON, J.; GUDEL, H.; LUDI, A. Electronic-Spectra of M(bipy)2+3 Complex-Ions (M=fe, Ru and Os). *Chemical Physics Letters* **1979**, *62*, 153-157.

(22) Kober, E. M.; Sullivan, B. P.; Meyer, T. J. Solvent dependence of metal-to-ligand charge-transfer transitions. Evidence for initial electron localization in MLCT excited states of 2,2'-bipyridine complexes of ruthenium(II) and osmium(II). *Inorg. Chem.* **1984**, *23*, 2098-2104.

(23) VANHOUTEN, J.; WATTS, R. Temperature-Dependence of Photophysical and Photochemical Properties of Tris(2,2'-Bipyridyl)ruthenium(ii) Ion in Aqueous-Solution. *J. Am. Chem. Soc.* **1976**, *98*, 4853-4858.

(24) HAGER, G.; CROSBY, G. Charge-Transfer Excited-States of Ruthenium(ii) Complexes .1. Quantum Yield and Decay Measurements. *J. Am. Chem. Soc.* **1975**, *97*, 7031-7037.

(25) HAGER, G.; WATTS, R.; CROSBY, G. Charge-Transfer Excited-States of Ruthenium(ii) Complexes .2. Relationship of Level Parameters to Molecular-Structure. *J. Am. Chem. Soc.* **1975**, *97*, 7037-7042.

(26) HIPPS, K.; CROSBY, G. Charge-Transfer Excited-States of Ruthenium(ii) Complexes .3. Electron-Ion Coupling Model for Dpi-] Configurations. *J. Am. Chem. Soc.* **1975**, *97*, 7042-7048.

(27) ELFRING, W.; CROSBY, G. Excited-States of Mixed-Ligand Chelates of Ruthenium(ii) - Quantum Yield and Decay Time Measurements. *J. Am. Chem. Soc.* **1981**, *103*, 2683-2687.

(28) VANHOUTEN, J.; WATTS, R. Temperature-Dependence of Photophysical and Photochemical Properties of Tris(2,2'-Bipyridyl)ruthenium(ii) Ion in Aqueous-Solution. *J. Am. Chem. Soc.* **1976**, *98*, 4853-4858.

(29) HAGER, G.; WATTS, R.; CROSBY, G. Charge-Transfer Excited-States of Ruthenium(ii) Complexes .2. Relationship of Level Parameters to Molecular-Structure. *J. Am. Chem. Soc.* **1975**, *97*, 7037-7042.

(30) GIORDANO, P.; FREDERICKS, S.; WRIGHTON, M.; MORSE, D. Simultaneous Multiple Emissions from Fac-Xre(co)3(3-Benzoylpyridine)2-N-Pi-Star Intraligand and Charge-Transfer Emission at Low-Temperature. *J. Am. Chem. Soc.* **1978**, *100*, 2257-2259.

(31) FERGUSON, J.; KRAUSZ, E.; MAEDER, M. Charge Localization in the Luminescent States of Ru(bpy)3(2+) in Fluid Solutions. *J. Phys. Chem.* **1985**, *89*, 1852-1854.

(32) FERGUSON, J.; HERREN, F. A Model for the Interpretation of the Electronic-Spectra of the Complex-Ions M(bpy)2+3 (M=fe,ru,os) in D3 and C2 Sites. *Chem. Phys.* **1983**, *76*, 45-59.

(33) FERGUSON, J.; KRAUSZ, E. Time-Resolved Luminescence and Mcpl of Ru(bpy)3(2+) in Glassy Solvents at the Fluid Glass-Transition. *Chemical Physics Letters* **1986**, *127*, 551-556.

(34) FERGUSON, J.; HERREN, F. The Electronic-Structure of the Metal-To-Ligand Charge-Transfer States of M(bpy)32+(m=fe,ru,os). *Chemical Physics Letters* **1982**, *89*, 371-375.

(35) CROSBY, G. Spectroscopic Investigations of Excited-States of Transition-Metal Complexes. *Acc. Chem. Res.* **1975**, *8*, 231-238.

(36) MEYER, T. Photochemistry of Metal Coordination-Complexes - Metal to Ligand Charge-Transfer Excited-States. *Pure and Applied Chemistry* **1986**, *58*, 1193-1206.

(37) DeArmond, M. K.; Carlin, C. M. Multiple state emission and related phenomena in transition metal complexes. *Coord. Chem. Rev.* **1981**, *36*, 325-355.

(38) DAY, P.; SANDERS, N. Spectra of Complexes of Conjugated Ligands .I. Charge-Transfer in Phenanthroline Complexes - Energy Shifts on Substitution. *Journal of the Chemical Society a -Inorganic Physical Theoretical* **1967**, 1530-&.

(39) CEULEMANS, A.; VANQUICKENBORNE, L. On the Charge-Transfer Spectra of Iron(ii)-Tris(2,2'-Bipyridyl) and Ruthenium(ii)-Tris(2,2'-Bipyridyl) Complexes. *J. Am. Chem. Soc.* **1981**, *103*, 2238-2241.

(40) DAUL, C.; WEBER, J. The Electronic-Structure and Low-Lying Excited-States of the Ruthenium(ii)tris(diimine) Complex. *Chemical Physics Letters* **1981**, *77*, 593-600.

(41) BRATERMAN, P.; HEATH, G.; YELLOWLEES, L. Absorption and Emission in Tris(2,2'-Bipyridyl)ruthenium(ii) - Effects of Excited-State Asymmetry. *Journal of the Chemical Society-Dalton Transactions* **1985**, 1081-1086.

(42) JURIS, A.; BALZANI, V.; BARIGELLETTI, F.; CAMPAGNA, S.; BELSER, P.; VONZELEWSKY, A. Ru(ii) Polypyridine Complexes - Photophysics, Photochemistry, Electrochemistry, and Chemi-Luminescence Rid D-3322-2009. *Coord. Chem. Rev.* **1988**, *84*, 85-277.

(43) Kalyanasundaram, K. *Photochemistry of Polypyridine and Porphyrin complexes;* Academic Press INC: San Diego, 1992; .

(44) TOKELTAK.NE; HEMINGWA.RE; BARD, A. Electrogenerated Chemiluminescence .13. Electrochemical and Electrogenerated Chemiluminescence Studies of Ruthenium Chelates. *J. Am. Chem. Soc.* **1973**, *95*, 6582-6589.

(45) Vlcek, A. A. Ligand-based redox series. *Coord. Chem. Rev.* **1982**, *43*, 39-62.

(46) SAJI, T.; AOYAGUI, S. Polarographic Studies on Bipyridine Complexes .1. Correlation between Reduction Potentials of Iron(ii), Ruthenium(ii) and Osmium(ii) Complexes and those of Free Ligands. *J Electroanal Chem* **1975**, *58*, 401-410.

(47) CREUTZ, C.; TAUBE, H. A Direct Approach to Measuring Franck-Condon Barrier to Electron Transfer between Metal Ions. *J. Am. Chem. Soc.* **1969**, *91*, 3988-&.

(48) Browne, W.; Hage, R.; Vos, J. Tuning interaction in dinuclear ruthenium complexes: HOMO versus LUMO mediated superexchange through azole and azine bridges. *Coord. Chem. Rev.* **2006**, *250*, 1653-1668.

(49) PETROV, V.; HUPP, J.; MOTTLEY, C.; MANN, L. Resonance Raman Studies in the Extended Near-Infrared Region - Experimental-Verification of a 3-Site Mixing Mechanism

for Valence Delocalization in the Creutz-Taube Ion. *J. Am. Chem. Soc.* **1994**, *116*, 2171-2172.

(50) PIEPHO, S. Vibronic Coupling Model for the Calculation of Mixed-Valence Line-Shapes - a New Look at the Creutz Taube Ion. *J. Am. Chem. Soc.* **1990**, *112*, 4197-4206.

(51) HUPP, J. Solvent Control of Orbital Mixing and Electronic Coupling in Ligand-Bridged Mixed-Valence Complexes - Evidence for an Intervalence Hole-Transfer Pathway. *J. Am. Chem. Soc.* **1990**, *112*, 1563-1565.

(52) Demadis, K.; Hartshorn, C.; Meyer, T. The localized-to-delocalized transition in mixed-valence chemistry. *Chem. Rev.* **2001**, *101*, 2655-2685.

(53) Brunschwig, B.; Creutz, C.; Sutin, N. Optical transitions of symmetrical mixed-valence systems in the Class II-III transition regime. *Chem. Soc. Rev.* **2002**, *31*, 168-184.

(54) Chen, P.; Meyer, T. Medium effects on charge transfer in metal complexes. *Chem. Rev.* **1998**, *98*, 1439-1477.

(55) Braun-Sand, S.; Wiest, O. Theoretical studies of mixed-valence transition metal complexes for molecular computing. *Journal of Physical Chemistry a* **2003**, *107*, 285-291.

(56) Londergan, C.; Kubiak, C. Vibronic participation of the bridging ligand in electron transfer and delocalization: New application of a three-state model in pyrazine-bridged mixed-valence complexes of trinuclear ruthenium clusters. *Journal of Physical Chemistry a* **2003**, *107*, 9301-9311.

(57) CALLAHAN, R.; BROWN, G.; MEYER, T. Effects of Weak Metal-Metal Interactions in Ligand-Bridged Complexes of Ruthenium - Dimeric Complexes Containing Ruthenium Ions in Different Coordination Environments. *Inorg. Chem.* **1975**, *14*, 1443-1453.

(58) CALLAHAN, R.; BROWN, G.; MEYER, T. Intervalence Transfer in Unsymmetrical, Ligand-Bridged Dimeric Complexes of Ruthenium. *J. Am. Chem. Soc.* **1974**, *96*, 7829-7830.

(59) TOM, G.; CREUTZ, C.; TAUBE, H. Mixed-Valence Complexes of Ruthenium Ammines with 4,4'-Bipyridine as Bridging Ligand. *J. Am. Chem. Soc.* **1974**, *96*, 7827-7829.

(60) POWERS, M.; MEYER, T. Intervalence Transfer in Pyrimidine-Bridged Dimer [(Bpy)2ciru(pym)rucl(bpy)2]3+. *Inorg. Chem.* **1978**, *17*, 2955-2958.

(61) Demadis, K.; Neyhart, G.; Kober, E.; White, P.; Meyer, T. Intervalence transfer at the localized-to-delocalized, mixed-valence transition in osmium polypyridyl complexes. *Inorg. Chem.* **1999**, *38*, 5948-5959.

(62) POWERS, M.; MEYER, T. Medium and Distance Effects in Optical and Thermal Electron-Transfer. *J. Am. Chem. Soc.* **1980**, *102*, 1289-1297.

(63) CALLAHAN, R.; KEENE, F.; MEYER, T.; SALMON, D. Intervalence Transfer and Electron-Transfer in Mixed-Valence Ion [(Bpy)2clru(pyz)rucl(bpy)2]3+. *J. Am. Chem. Soc.* **1977**, *99*, 1064-1073.

(64) Crutchley, R. J. Intervalence charge transfer and electron exchange studies of dinuclear ruthenium complexes. *Adv. Inorg. Chem.* **1994**, *41*, 273-325.

(65) Allen, G. C.; Hush, N. S. Intervalence-transfer absorption. I. Qualitative evidence for intervalence-transfer absorption in inorganic systems in solution and in the solid state. *Prog. Inorg. Chem.* **1967**, *8*, 357-389.

(66) Robin, M. B.; Day, P. Mixed valence chemistry. A survey and classification. *Advan. Inorg. Chem. Radiochem.* **1967**, *10*, 247-422.

(67) MARCUS, R.; SUTIN, N. Electron Transfers in Chemistry and Biology. *Biochim. Biophys. Acta* **1985**, *811*, 265-322.

(68) Vos, J. G.; Kelly, J. M. Ruthenium polypyridyl chemistry; from basic research to applications and back again. *Dalton Transactions* **2006**, 4869-4883.

(69) Thomas, N. C.; Deacon, G. B. Tris(bidentate)ruthenium(II) bis[hexafluorophosphate] complexes. *Inorg. Synth.* **1989**, *25*, 107-110.

(70) Toyota, S.; Goto, A.; Kaneko, K.; Umetani, T. Syntheses, spectroscopic properties, and CU(I) complexes of all possible symmetric BI-1,10-phenanthrolines. *Heterocycles* **2005**, *65*, 551-562.

(71) Aguirre, P.; Sariego, R.; Moya, S. Ruthenium (II) complexes in catalytic oxidation. *Journal of Coordination Chemistry* **2001**, *54*, 401-413.

(72) Nasielski-Hinkens, R.; Benedek-Vamos, M. Synthesis of di- and tetrasubstituted 1,4,5,8-tetraazaphenanthrenes (pyrazino[2,3-f]quinoxalines). *J. Chem. Soc. , Perkin Trans. 1* **1975**, 1229.

(73) KELLY, J.; OCONNELL, C.; VOS, J. Preparation, Spectroscopic Characterization, Electrochemical and Photochemical Properties of Cis-Bis(2,2'-Bipyridyl)carbonylruthenium(ii) Complexes. *Journal of the Chemical Society-Dalton Transactions* **1986**, 253-258.

(74) Strouse, G. F.; Anderson, P. A.; Schoonover, J. R.; Meyer, T. J.; Keene, F. R. Synthesis of polypyridyl complexes of ruthenium(II) containing three different bidentate ligands. *Inorg. Chem.* **1992**, *31*, 3004-3006.

(75) Johnson, E. C.; Sullivan, B. P.; Salmon, D. J.; Adeyemi, S. A.; Meyer, T. J. Synthesis and properties of the chloro-bridged dimer [(bpy)2RuCl]22+ and its transient 3+ mixed-valence ion. *Inorg. Chem.* **1978**, *17*, 2211-2215.

(76) Sullivan, B. P.; Salmon, D. J.; Meyer, T. J. Mixed phosphine 2,2'-bipyridine complexes of ruthenium. *Inorg. Chem.* **1978**, *17*, 3334-3341.

(77) Lay, P. A.; Sargeson, A. M.; Taube, H. Cis- and trans-bis(1,2-ethanediamine)iridium(III) complexes. *Inorg. Synth.* **1986**, *24*, 287-291.

(78) COOPER, G.; RICKARD, R. Improved Procedure for Oxidation of 5-Nitro-2-Methylpyridine to 5-Nitropyridine-2-Carboxylic Acid (5-Nitro-Alpha-Picolinic Acid). *Synthesis-International Journal of Methods in Synthetic Organic Chemistry* **1971**, 31-&.

(79) Gillaizeau-Gauthier, I.; Odobel, F.; Alebbi, M.; Argazzi, R.; Costa, E.; Bignozzi, C.; Qu, P.; Meyer, G. Phosphonate-based bipyridine dyes for stable photovoltaic devices. *Inorg. Chem.* **2001**, *40*, 6073-6079.

(80) RILLEMA, D.; ALLEN, G.; MEYER, T.; CONRAD, D. Redox Properties of Ruthenium(ii) Tris Chelate Complexes Containing the Ligands 2,2'-Bipyrazine, 2,2'-Bipyridine, and 2,2'-Bipyrimidine. *Inorg. Chem.* **1983**, *22*, 1617-1622.

(81) KRAUSE, R. Synthesis of Mixed Complexes of Ruthenium(ii) with 2,2'-Dipyridyl. *Inorg. Chim. Acta* **1977**, *22*, 209-213.